Study of Mechanical Properties and Cyclic Stretching-induced Remodeling of Cellular Primary Cilia

細胞一次繊毛の力学特性と繰り返し引張刺激に伴うリモデリングに関する研究

Doctoral dissertation

DO Tien Dung

Division of Human Mechanical Systems and Design

Graduate School of Engineering, Hokkaido University

2022

Abstract

The primary cilia are solitary, immotile organelles that project from the surface of almost every cell in human body. They function as mechanosensors, which help cells to sense surrounding mechanical signals such as fluid flow shear stress, and then adapt to the change of mechanical stimulation. Understanding the mechanical properties of primary cilia provides better insight into how primary cilia respond to applied mechanical signals. However, the mechanical properties of primary cilium are still not well-understood, especially the elastic and viscoelastic properties. Moreover, although the responses of primary cilia to fluid flow have been well studied, the remodeling of primary cilia in response to indirect stimulation such as substrate stretching is a mystery. In this dissertation, the mechanical properties of primary cilia were elucidated, such as Young's modulus and viscoelastic properties, together with the remodeling of primary cilia in response to cyclic substrate stretching. In addition, the microstructures of primary cilia were studied to get a better understanding of cilia mechanical responses and mechanotransduction function. A primary cilium model, including the major mechanical components, was also simulated.

In Chapter 1, the fundamentals of cells and primary cilia (their structures and functions in cell life) were reviewed. The prior studies of measurement of mechanical properties of cilia and remodeling function in response to mechanical forces were described. This chapter also reviewed the methodologies of mechanical testing and mechanical loading applied to biological materials.

In Chapter 2, the in-house micro-tensile experiment set-up and related components supporting the investigation of mechanical properties of primary cilia were introduced. The primary cilia were isolated from cells and executed by the micro-tensile experiments to obtain the Young's modulus at different strain rates. The viscoelastic models of primary cilia were mathematically built up and the global fitting with experimental data was run to induce viscoelastic properties of primary cilia. As far as we know, this study is the first direct measurement of Young's modulus and viscoelasticity of primary cilia. Moreover, together with global Young's modulus, the distribution of local Young's

modulus on the primary cilia by the Atomic Force Microscope (AFM) was provided for comparison.

In Chapter 3, the remodeling function of primary cilia in response to the cyclic substrate stretching and the microstructures of primary cilia contributing to their mechanics was investigated. While the direct stimulation of fluid flow to primary cilia is well-known, the indirect stimulation of cyclic substrate stretching to primary cilia is still not characterized. It was revealed that primary cilia may adapt and remodel their behaviours (length, incidence, orientation) in response to cyclic substrate stretching. Our first tests suggested biologically that the actin cytoskeleton network contributes to transmit the mechanical signal from the substrate to the primary cilium.

Chapter 4 showed the microstructure components of primary cilia using Transmission Electron Microscopy (TEM), which provides a better understanding of responses of primary cilia to mechanical signals. The TEM images showed visually the connection of the base of primary cilia to the actin filaments supporting the hypothesis in Chapter 3 that actin network is an intermediate factor transmitting mechanical signals from the substrate to cilia. In addition, the numerical results in this chapter illustrate for the first time a primary cilium model, including the main mechanical components of cilia: microtubules and cross-linking structure. Most of the previous studies assumed the primary cilium as a homogenous and elastic beam; this model may help further cilia simulation to obtain a better understanding of cilia mechanics.

Chapter 5 summarized the works in the dissertation and offers the prospective studies that can be investigated in this research field.

Acknowledgements

This dissertation would not have been possible without the support of many people and this is an accomplishment that I share with them.

Above all, I would like to express my sincere gratitude to my supervisor Prof. Toshiro Ohashi for his valuable guidance, support, and patience to me. Although we had the difficult times in doing research, he was always besides and support me until these ending moments. I am very grateful for his tolerance for my mistakes and his commitment to complete my research. He taught me not only doing research, but also completing my personality. I learned many things from him and I am really appreciated what he has done for me.

I also greatly acknowledge Prof. Teruo Sone and Mr. Phyo Han Thwin in Laboratory of Applied Molecular Microbiology, Graduate School of Agriculture, Hokkaido University for their enthusiastic help of isolating primary cilia. I also thank Mr. Toshiaki Ito in Electron Microscope Laboratory, Research Faculty of Agriculture, Hokkaido University for a technical support in TEM technique, Dr. Kentaro Kobayashi at Nikon Imaging Center at Hokkaido University for being very helpful with image acquisition.

I would like to send my gratitude to Mrs. Naoe Konno, a secretary in our laboratory, for her works and support. She helped me and other lab members a lot. She is very kind to us, and I am always happy when talking to her.

I am pleased to extend my thankful to all e3 staff, some persons have already left the office but some are still working. Since the first day I came to Hokkaido University, they are all very enthusiastic to their works and really care for international students. For international students like us, it is extremely helpful and meaningful.

My life in Hokkaido University cannot complete without my laboratory members. They are always beside me when I was ups and downs. We shared many good memories together, a lot times filled with laughs. They are part of my beautiful memories in Hokkaido University. I cannot say enough my feelings to them. I would like to express

my special acknowledge to my closest friend, Mazlee Bin Mazalan. Many thanks to Katsushi Tamai, Satoshi Matsuo, Katsuyoshi Jimuro, Brice Venayre, Cai Haonan, Li Jiazhen, Ma Ming, Gu Yanming, Lan Yanan, Li Jingyi, Otgon Baasansuren, Nour Chebbi, Lyu Yan, Chen Yu, Lee Sung Kil, Lai Mun Kit, Ryota Toyohara. Dindi Guzon, Ryan Oliver Regis, Silvia Marino I will not forget them and memories we shared together.

Finally, I want to send my deeply gratitude to my family. They were my courage every time I faced to difficulty times. They gave me more strength to continue and reach these moments.

Thank you everyone!

Abbreviations

ADPKD: Autosomal Dominant PKD

ARPKD: Autosomal Recessive PKD

AFM: Atomic Force Microscope

BAOEC: Bovine Aorta Endothelial Cells

BSA: Bovine Serum Albumin

CSI: Cell Shape Index

CCP: Clathrin-Coated Pits

CCV: Clathrin-Coated Vesicles

CSM: Compressible Sphere Model

DMEM: Dulbecco’s Modified Eagle Medium

DNA: Deoxyribonucleic Acid

PBS: Phosphate Buffered Saline

ICT: Intraciliary Transport

IFT: Intraflagellar Transport

ICSM: Incompressible Sphere Model

MDCK: Madin-Darby Canine Kidney

HSM: Half-Space Model

PKD: Polycystic Kidney Disease

PDGFR: Platelet-Derived Growth Factor Receptors

PDMS: Polydimethylsiloxane

QPD: Quadrant Photodetector

TEM: Transmission Electron Microscope

TGF-β: Transforming Growth Factor Beta

SLS: Standard Linear Solid

SBT: Slender-Body Theory

Shh: Sonic hedgehog

Table of Contents

List of Figures

List of Tables

Chapter 1

Introduction

1.1 Background

Cellular mechanosensation is the ability of cells to sense and respond to mechanical signals. The dysfunction in mechanosensing can lead to a variety of diseases, including atherosclerosis, osteoporosis, and cancer. Primary cilia are solitary linear cellular extensions that extend from the surface of cells. For decades, the biological function of these enigmatic structures was elusive; however, recent evidences have suggested an emerging picture in which the primary cilium functions as a complex nexus that senses and responds to physical and chemical extracellular signals. The deletion or defect of primary cilia leads to mechanosensing effects, which results in proliferation, differentiation, and migration defection.

Due to the small size of the cilium (approximately 5 - 10 μm in length, 0.2 μm in diameter and 1/30,000 of the total cellular volume) (Delling et al., 2013), it is difficult to investigate the mechanical properties of primary cilia and therefore to understand their mechanotransduction mechanism. This dissertation, in order to provide more insight into pictures of primary cilia mechanics, revealed mechanical properties of isolated primary cilia such as Young's modulus and viscoelastic properties, which had not been studied so far, and the remodeling function of primary cilia in response to mechanical signals. The microstructure of primary cilia is also investigated to clarify the reasons of mechanical behaviour of primary cilia in response to surrounding mechanical signals. Moreover, for the first time, a primary cilium model including major mechanical components is simulated; this may help to understand appropriately cilia mechanics in further numerical studies.

This chapter is organized to overview the literature on the first concepts of cells and mechanotransduction, which is one of the important mechanisms of cells. Next, it introduces primary cilia, their structure, and their functions. Prior studies of the measurement of mechanical properties of cilia are also reviewed. Different mechanical tests applying to biological materials, as well as different mechanical loadings applied to cells or tissues, are mentioned.

1.2 Cell - Fundamental unit of life

Cells were first discovered by a British scientist Robert Hooke in 1665 by looking at slices of corks (Fig. 1.1). He discovered that they were formed of many chambers arranged like a honeycomb, and he coined the term “cells” for these chambers. Later, in 1674, Van Leeuwenhoek, with the help of the developed microscope, discovered the free living cells in pond water.

After these discoveries, the cell theory, which was proposed by Schleiden (1838) and Schwann (1839), stated that all plants and animals are composed of cells and the cell is the basic unit of life. There are two kinds of organisms:

Unicellular organisms consist of one independently functioning cell whose activities occur within one cell. Bacteria are known as unicellular organisms. Multicellular organisms consist of many cells. The human body, for example, comprises approximately 60 trillion diverse cells arising from just one fertilized cell. The individual organism grows not just by cell division, but also by an increase in its volume. Furthermore, the cells diversify into groups and every group of cells becomes adapted for various functions. The specialization is called cell differentiation. Groups of cells having the same form and function are called tissues, and different functional groups of tissues form an organ, which focuses on a specific set of tasks within the organism (Fig. 1.2).

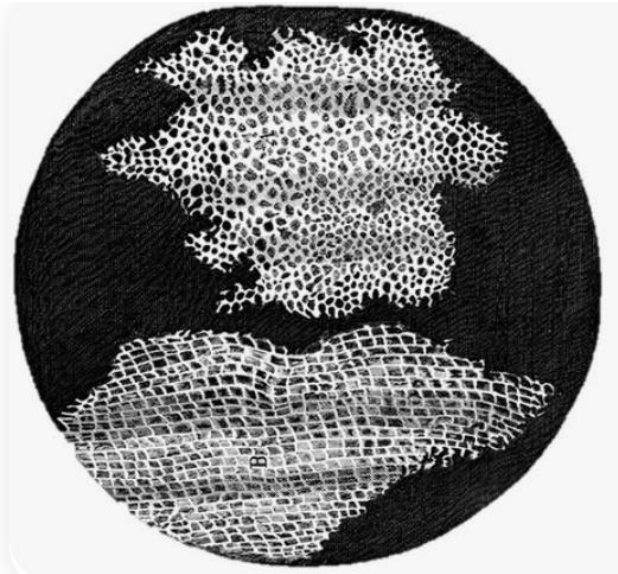

Fig. 1.1: Cork cells observed by Robert Hooke (1665).

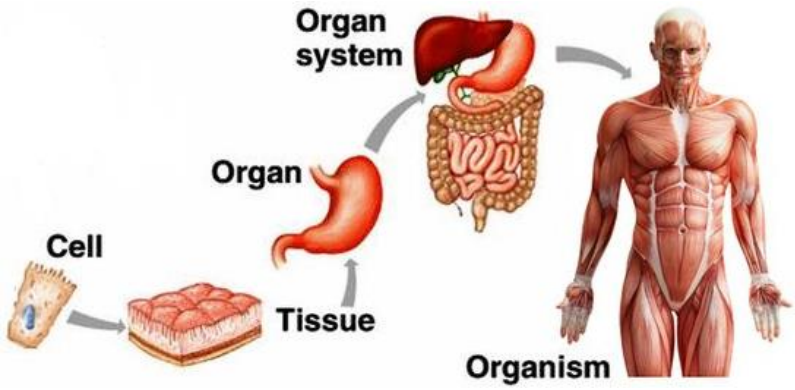

Fig. 1.2: Multicellular system
(https://www.blendspace.com/lessons/d86pmZGZhZJaAg/organ-system).

1.3 Mechanotransduction

Living cells are constantly exposed to mechanical stimuli. The mechanical forces may come from heart pumping, muscle contractions or compressive force from the body weight. The process which supports cells in sensing these signals is termed mechanosensing. Mechanotransduction is an important intracellular process; to adapt to changes in the extracellular environment cells convert surrounding physical signals, such as fluid flow shear stress or stretching, into biological responses inside cells.

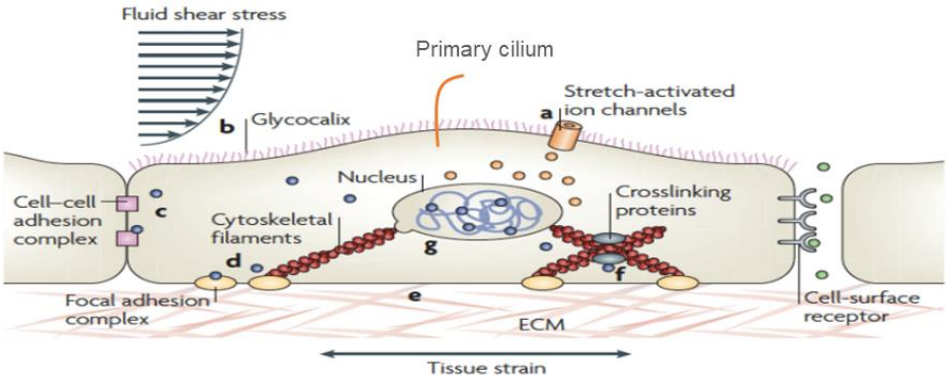

Fig. 1.3: Mechanotransduction mechanism (modified from Jaalouk et al. 2009).

At the organismal level, mechanosensing helps the cardiovascular system to maintain and regulate blood pressure and the auditory system to detect sound waves. At the cellular level, mechanosensing can direct differentiation, proliferation, migration and apoptosis. In order to support the mechanosensing mechanism, cells have a series of mechanosensors such as primary cilia, stretch-activated ion channels, glycocalyx (Fig. 1.3).

1.4 Primary cilia structures and their functions

Primary cilia are singular, non-motile extensions of the cells that protrude into the extracellular environment (Fig. 1.4). They have been found in almost all cell types (Table 1.1) such as kidney (Praetorius and Spring, 2001), cartilage (McGlashan et al., 2010), tendon (Rowson et al., 2018) and bone (Hoey et al., 2012). This structure is formed when the cell is in G0 or G1 phase, and disappears during S/G2 phase (Plotnikova et al., 2009) (Fig. 1.5). By observing the process of resorption in a mammalian cell type, Rieder et al. (1979) showed that a cell with a primary cilium has entered into mitosis, arguing with a model in which primary cilia interfere with mitosis and prevent a cell from going through the cell division.

The development of TEM has helped to obtain a clear characterization of the primary cilium. The axoneme of primary cilia growing from the basal body (centriole) has the microtubule structure constructed by polymerization of alpha and beta tubulin with the already polymerized + end at the ciliary tip. In primary cilia, nine microtubule doublets are arranged radially with no central pairs of microtubules (9 + 0 structure) (Satir, 2017),

which distinguishes them from the motile cilia having a 9 + 2 microtubule configuration. Normally, non-motile primary cilia do not have the molecular motors and dynein which contribute to ciliary motion. The entire axoneme is enclosed by a membrane that is continuous with the plasma membrane of the cell (Fig. 1.6).

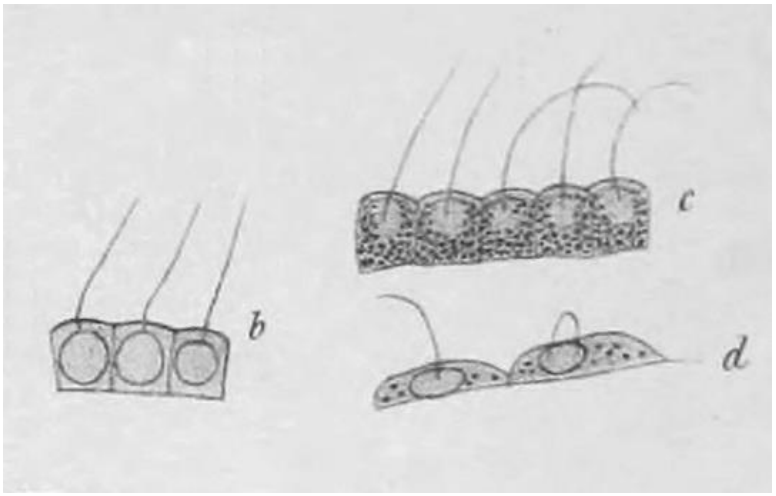

Fig. 1.4: Primary cilia on the liver (b), the hindgut (c) and the ovary (d) of adult *Amphioxus lanceolatus* (Bloodgood., 2009).

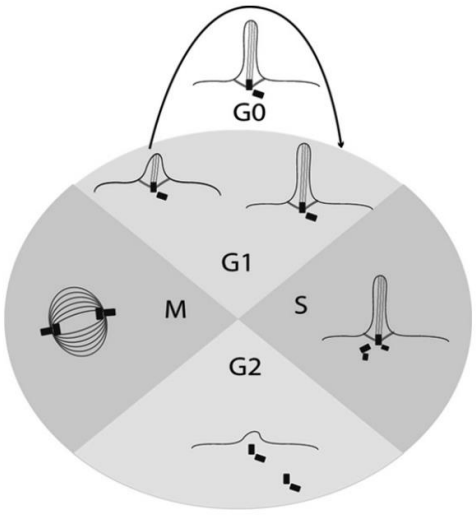

Fig. 1.5: Ciliogenesis and the cell cycle (Plotnikova et al., 2009).

Table 1.1: Expression of primary cilia in various mammalian tissues and cells (Deepak et al., 2017).

Mammalian tissues and cells with primary cilia	
Connective tissues	Oral tissues
Fibroblasts	Gingiva
Chondrocytes	Oral mucosa
Synovial cells	Ameloblasts
Tenocytes	Odontoblasts
Pancreas	Epidermis
Exocrine pancreatic ductal epithelium	Basal cells
Endocrine pancreatic ductal epithelium	Keratinocytes
Islet cells	Melanocytes
Liver	Vascular endothelium
Fat-storing cells	Heart myocardium
Perisinusoidal cells	Aorta
Intrahepatic bile duct	Arteries
Cholangiocytes	Capillaries
Spleen	Airway
Reticular cells	Respiratory epithelium
Muscles	Bone
Smooth muscle cells	Osteocytes
Skeletal muscle cells	Osteoblasts
Sensory organ cells	Kidney
Photoreceptors	Epithelium of renal tubules
Cornea	Podocytes
Taste buds	Bowman capsule
Olfactory epithelium	Mesangial/endothelial cells
Middle and inner ear	Interstitium
Central nervous system and brain	Male reproductive organ
Neuroepithelial cells	Rete testis
Schwann cells	Prostrate
Ventricles	Ductuli efferentes
Ependymal cells	Peritubular myoid cells
Choroid plexus	Interstitial testes cells
Central and peripheral nervous system neurons	Seminal vesicles
Glands	Female reproductive organ
Adrenal gland	Follicular cells (ovary)
Thyroid gland	Germinal epithelium (ovary)
Parathyroid gland	Stromal cells (ovary)
Mammary gland	Theca interna (ovary)
Thymus	Oviduct epithelium
Pituitary gland	Uterus (endometrium)
Myoepithelial cells	Vagina (stratified epithelium)
Stem cells and tissues during embryogenesis and fetal development. Primary cilia are generally present in cell types as described in the above two columns Stem cells and tissues during embryogenesis and fetal development (other cell types may include)	
Inner mass cells (blastocysts)	Fetal epidermis
Outer mass cells (blastocysts)	Fetal epithelium
Primordial erythroblasts	Fetal endothelium
Embryonic node	Mesenchyme

At the base of the primary cilium, where the plasma membrane is depressed, the existence of a ciliary pocket was confirmed (Fig. 1.6). In the cilia body (axoneme) the microtubule structures do not connect to the cilium membrane, while in the ciliary pocket they are anchored to the cilium membrane by the transition fibers (Wheway et al., 2018). The transition fibers include vesicle docking and Intraflagellar Transport (IFT). The vesicles carry ciliary proteins and transmembrane proteins going inside the cilium, while IFT is the process by which all proteins are transported along the cilium from base to tip (anterograde IFT) and from tip to base (retrograde IFT). Along the membrane of cilia, there are many receptors, which are responsible for the signaling pathway. The new proteins are synthesized or created within growing or steady-state axoneme should be transported to the base and then travel to the intracellular matrix for further chemical cascades. IFT is responsible for this transportation. The region where the microtubule triplet at the basal body transforms into the microtubule doublet at the axoneme is called the transition zone. This zone is characterized by Y-shaped links that connect the axonemal microtubules to the cilium membrane. The transition fibers and transition zone combine to form the ciliary gate, which controls the permeability of cilium proteins and lipids.

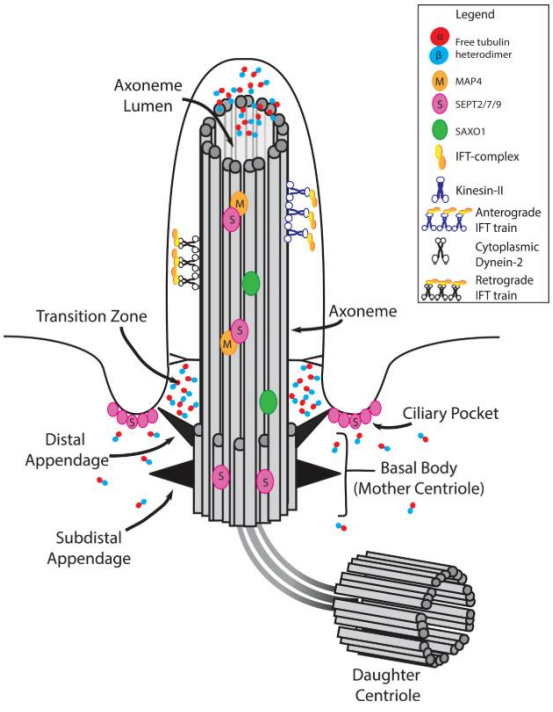

Fig. 1.6: Structure of the primary cilium (Mirvis et al., 2018).

Despite being discovered over a century ago, the function of primary cilia is still a mystery. It is clear now that the primary cilium is a multifunctional antenna, sensing both mechanical (fluid flow, pressure, vibration) and chemical (specific ligand, growth factor, hormone or morphogen) changes in the extracellular environment. In some specialized cases, primary cilia can also respond to light or temperature. Figure 1.7 shows the typical mechanotransduction function of the primary cilium, with calcium flowing into the cells in response to the cilia bending due to fluid flow. Different fluid flow rates produce various bending degrees of primary cilia and different stresses on the cilia membrane. Stresses lead to channel opening and then calcium goes inside the intracellular environment. It was observed that the intracellular calcium concentration does not increase when removing the cilia from cells. The calcium signaling of primary cilia was also examined in the case of cilia attached to cells and of calcium ions extracted from the extracellular matrix, leading to no intracellular calcium elevation inside cells.

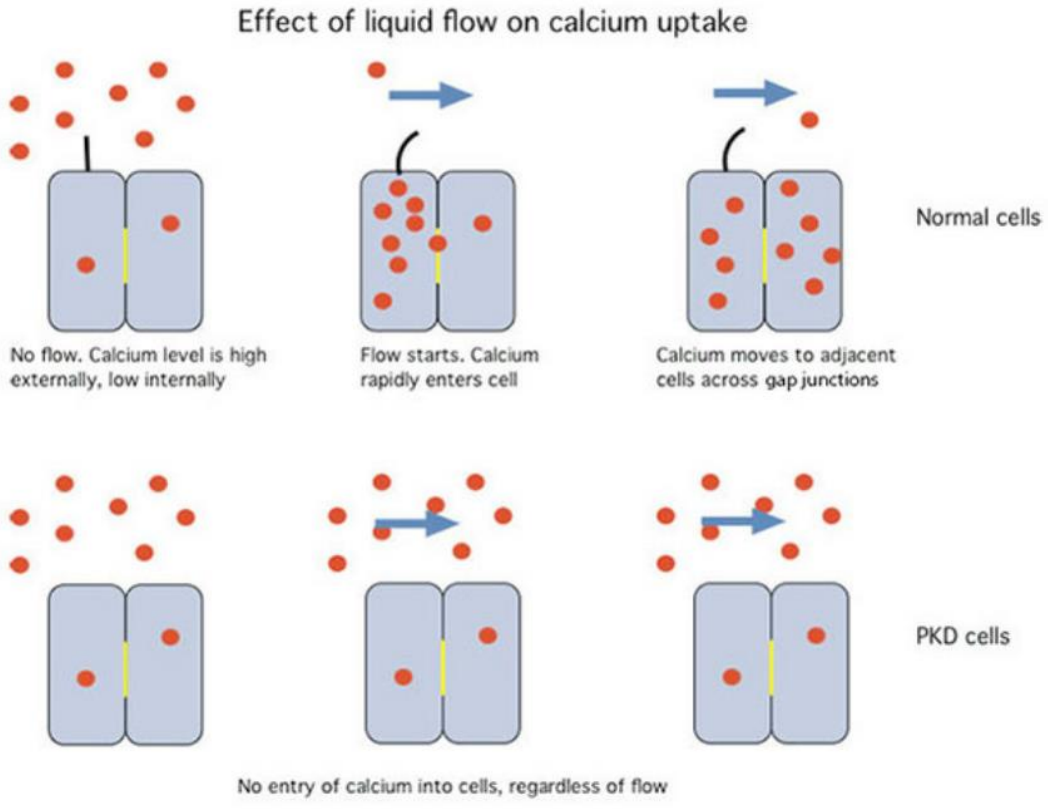

Fig. 1.7: Effect of fluid flow on the uptake calcium in normal and PKD kidney cells (https://www.nature.com/scitable/content/the-effect-of-fluid-flow-on-the-14372683/).

Due to the important role of cilia in mechanotransduction, the disruption or the dysfunction of cilia structure results in significant diseases termed “ciliopathies”, such as polycystic kidney disease, blindness and syndromic developmental disorders (Satir, 2017; Kowal et al., 2015).

Among the disease caused by the dysfunction of primary cilia, Polycystic Kidney Disease (PKD) is the most common inherited disease in humans (Fig. 1.8). The disease comes in two major forms: autosomal dominant and autosomal recessive. Autosomal Dominant PKD (ADPKD) affects mostly adults and has an incidence of at least 1 in 1000. Autosomal Recessive PKD (ARPKD) occurs in neonates and children; it affects up to 1 in 6000 live births. This disease comes from the exaggerated proliferation of epithelial cells lining in the ducts and tubules of kidney; they form cysts that later expand. The massive enlargement of the kidneys leads to end-stage renal failure. Polycystin-1 and polycystin-2 are two receptors on the primary cilia membrane, and the disruption of these two proteins is directly linked to PKD (Brown et al., 2014). Other ciliopathies are summarized in Table 1.2 (Ware et al., 2011).

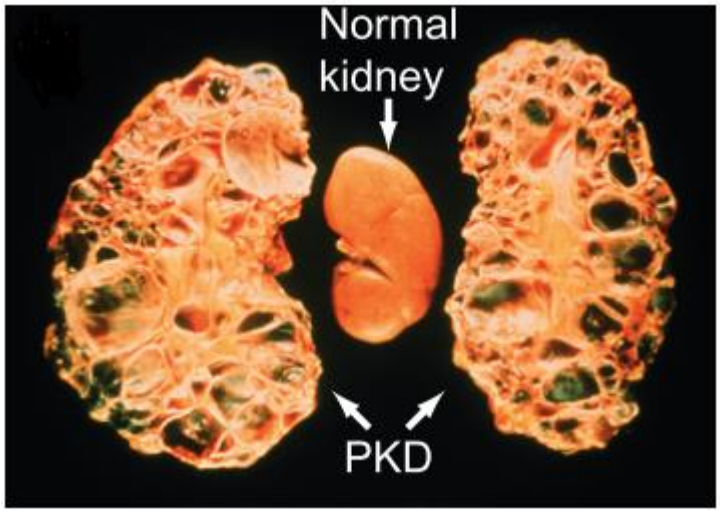

Fig. 1.8: Polycystic kidney disease (Brown et al., 2014).

Table 1.2: Summary of ciliopathies (Ware et al., 2011).

Ciliopathy	Features	Gene(s)	Pulmonary involvement
Primary ciliary dyskinesia	Bronchiectasis, sinusitis, otitis media, infertility, situs defects	DNAI1, DNAH5, DNAH11, DNAI2, KTU, TXNDC3, RPGR, RSPH4A, RSPH9, LRRC50, CCDC40, CCDC39	Prominent
Polycystic kidney disease	Renal cysts; hepatic fibrosis; autosomal dominant and recessive forms	PKHD1, PKD1, PKD2	Reported: bronchiectasis
Nephronophthisis	Renal cysts with or without extra-renal symptoms	NPHP1-4, IQCB1, CEP290, GLIS2, RPGRIP1L, NEK8, SDCCAG8, TMEM67, TTC21B	Reported in conjunction with allelic syndromes
Senior-Loken syndrome	Juvenile nephronophthisis, Leber amaurosis	NPHP1-6, SDCCAG8	Not reported
Leber congenital amaurosis	Visual impairment in first year of life; pigmentary retinopathy	GUCY2D, RPE65, LCA3-14 (including LCA10, CEP290)	Reported: abnormal respiratory cilia
Meckel-Gruber syndrome	Renal cysts, CNS anomalies (encephalocele), polydactyly, congenital heart defects	MKS1, TMEM216, TMEM67, CEP290, RPGRIP1L, CC2D2A	Not reported
Meckel-Gruber syndrome	Renal cysts, CNS anomalies (encephalocele), polydactyly, congenital heart defects	MKS1, TMEM216, TMEM67, CEP290, RPGRIP1L, CC2D2A	Not reported
Joubert and related syndromes	hypoplasia of the cerebellar vermis (molar tooth sign), dysregulated breathing pattern, retinal dystrophy, renal anomalies	JBTS1, TMEM216, AHI1, NPHP1, CEP290, TMEM67, RPGRIP1L, ARL13B, CC2D2A,	Not reported: episodic tachypnea ± apnea described as central in origin
Bardet-Biedl syndrome	Obesity, polydactyly, retinitis pigmentosa, anosmia, congenital heart defects	BBS1, 2, ARL6, BBS4,5, MKKS, BBS7, TTC8, BBS9, 10, TRIM32, BBS12, MKS1, CEP290, C2ORF86; modifiers MKS1, MKS3, CCDC28B	Not reported, but evidence for airway ciliary dysfunction in animal models
Oral-facial-digital syndrome type I	Oral cavity, face, and digit anomalies; CNS abnormalities; cystic kidney disease; X-linked with male lethality	OFD1	Reported: PCD phenotype
Alstrom syndrome	Dilated cardiomyopathy, obesity, sensorineural hearing loss, retinitis pigmentosa, endocrine abnormalities, renal and hepatic disease	ALMS1	Frequent: pneumonia, COPD, moderate to severe interstitial fibrosis

1.5 Mechanical properties of primary cilia

Despite being discovered a long time ago, in the last 10 years, accumulative findings of cilia's importance in cellular function have made primary cilia become more attractive biologically and mechanically for researchers.

Measuring the essential mechanical properties of the cilia can support the mechanosensation hypothesis and provide an improved understanding of their signaling role in the cells. Several methods were studied so far to investigate the mechanical properties of primary cilia and evaluate how primary cilia convert mechanical stimuli to biological signals (Fig. 1.9). For instance, the primary cilia were exposed to micropipette, magnetic beads in the magnetic field or fluid shear stress, and then the mechanotransduction process in terms of intracellular calcium elevation was observed.

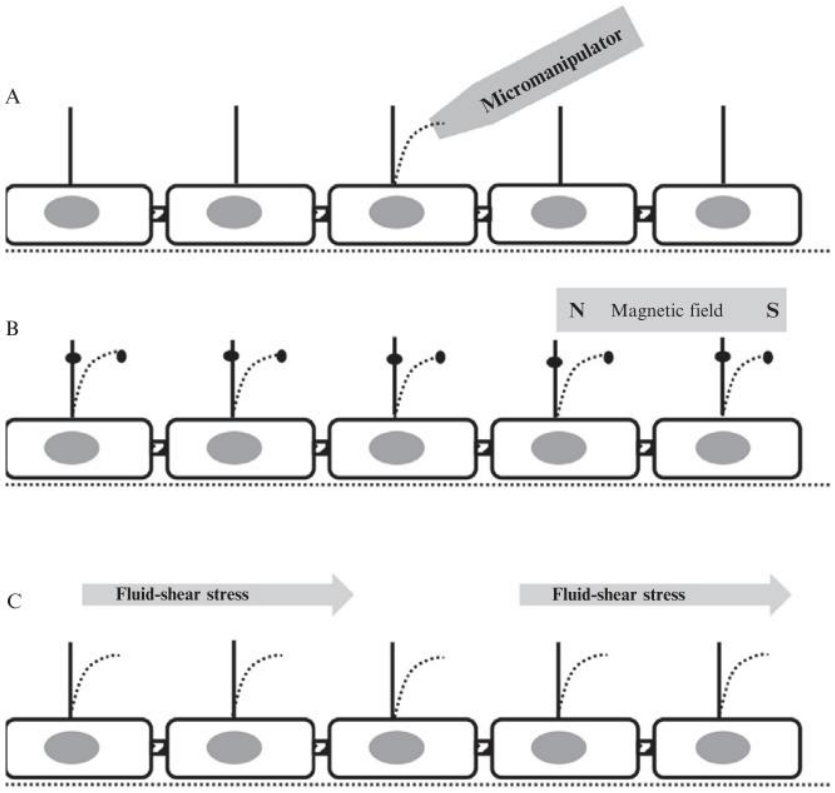

Fig. 1.9: Approaches to study mechanosensory function of cilia. (A): Bending cilium by applying negative pressure at the tip of a micropipette. (B): Attaching micro/nano beads to the primary cilia and then pull by magnetic field. (C): Applying the fluid shear stress on the top of the cells (Nauli et al., 2013).

In Table 1.3, the mechanical properties of primary cilia are summarized. The previous studies on the mechanical properties of primary cilia and microtubules will be reviewed. It could be noticed that most of the measured mechanical properties of primary cilia are flexural rigidities. The only Young's modulus of primary cilia that was reported so far is the converted result from the flexural rigidity by Rydholm et al. (2010), which is not an experimental result. Some measured mechanical properties of microtubules are also reported and they might be helpful for the result evaluation in our discussion.

In 1997, Schwartz et al. (1997) first analyzed and modelled the primary cilium bending in response to fluid flow (Fig. 1.10). They used the light microscope to quantify the deflections of kidney epithelial cell primary cilia in response to laminar fluid flow *in vitro*. To model the cilia bending behavior in response to the fluid flow, the cilium was modeled as a uniformly rigid, cylindrical cantilevered beam of varied length. The flow was simulated as a constant perpendicular drag force applied to the entire length of the cilia. The flexural rigidity of the cilium was iteratively updated until the simulated beam deflections matched the observed deflections (Schwartz et al., 1997). However, this model was limited by the assumption of a constant velocity and drag profile along the primary cilia. The flexural rigidity was calculated to be approximately 3.1 x 10^{-23} Nm^2.

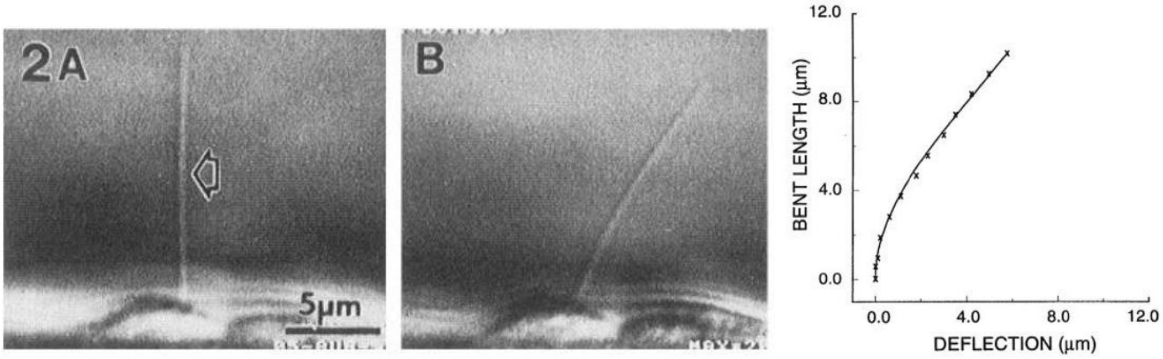

Fig. 1.10: Primary cilia bending in response to fluid shear. Left panel: the cilium passively bent under low level of shear. Middle panel: The degree of bending increased as the flow increased. Right panel: The bending prediction of numerical model of primary cilia, the 'x' is experimental data, solid line is the model (Schwartz et al., 1997).

Table 1.3: The summarized results of mechanical properties of primary cilia and microtubules.

	Author, year	Flexural rigidity [Nm^2]	Young's modulus [kPa]	Experimental method
Primary cilia	Schwartz et al., 1997	3.1×10^{-23}	-	Fluid flow
	Rydholm et al., 2010	-	178 (converted)	Fluid flow
	Young et al., 2012	$1 - 5 \times 10^{-23}$	-	Fluid flow
	Downs et al., 2014	31×10^{-23}	-	Fluid flow
	Battle et al., 2014	2.5×10^{-23}	-	Optical trap
	Resnick, 2016	1.7×10^{-23}	-	Optical trap
	Flaherty et al, 2018	1×10^{-24} - 1×10^{-20}	-	Optical trap
Microtubules	Tuszyński et al., 2005	-	1.32×10^{6}	Tensile test
	Gittes et al., 1993	2.2×10^{-23}	-	Thermal bending
	Kikumoto et al., 2006	7×10^{-23}	-	Optical trap

Rydholm et al. (2010) used FEM with the structural mechanics module in Comsol Multiphysics to construct a three-dimensional, structural, mechanical model of the apical part of the cell, including the linear elastic microtubule core of primary cilium, with Young's modulus of the primary cilium being 178 kPa, and viscoelastic properties of cilia membrane and apical cell membrane. The stiffness damping of the membrane was set to 10 s. The model showed that the peak stress occurred at the base of the cilium, which is in agreement with Young et al. (2012). Interestingly, they indicated that the delay in calcium response is caused by the membrane stress at the ciliary base.

Young et al. (2012) later developed a more precise model of fluid flow profile around primary cilia and conducted quantitative comparison of cilium bending between experiments and modeling to obtain the flexural rigidity (Fig. 1.11). The statistics of the bending rigidity of primary cilia fall in the range of 1 - 5 x 10^{-23} Nm^2. They calculated and found that the maximum tension is at the junction of primary cilium, which suggested that the stressed-active ion channels on the axoneme near to the base are more likely to be opened during the bending of cilium. By estimating the recovery time of cilia after stopping the flow, they also revealed the relaxation time of the cilium.

In the Young's model, because of the slenderness of primary cilium $\beta \ll 1$, the slender-body theory (SBT) is used to obtain the approximation of the Stokes flow around primary cilia. Combining it with the elastic beam model of primary cilia, the equilibrium profile of cilium is determined when the cilia basal body responds to the hydrodynamic load from the fluid flow. By observing the base angle from the experiment, the equilibrium cilium is fitted to estimate the cilia flexural rigidity *EI*.

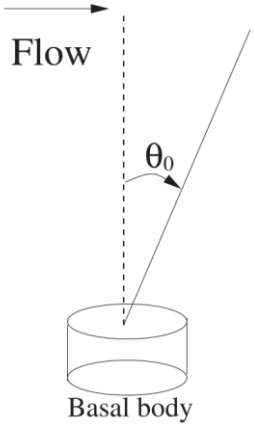

Fig. 1.11: The model of cilium axoneme coupled to a rotational spring at the cilium base. The basal body supports the cilium bending under flow (Young et al., 2012).

Downs et al. (2014) developed primary cilium model exploiting advances in both imaging and computational method. A coupled fluid-structure interaction model, which combines 3D fluid dynamics with a large rotation of anchorage of primary cilia (Fig. 1.12), provided a significantly different flexural rigidity value than the previous studies. The flexural rigidity of primary cilia was reported to be roughly 2 x 10^{-22} Nm^2. The order of magnitude of this value is 10 times higher than that of previous results. This difference may be explained by both their advances in imaging method and computational models and the experimental conditions, since their shear stress is two orders of magnitude higher than Schwart et al. (1997). As interesting finding they reported that primary cilia may experience plastic deformation. By observing the behavior of cilia after stopping the flow, two cilia returned to the initial position, while other two cilia exhibited a new position 2 min after the stop and kept this position for at least 20 min. As far as I know, this is the first study reporting this mechanics of primary cilia. Ciliated cells under laminar flow were imaged using laser scanning confocal microscopy (Fig. 1.13). Another interesting observation is the kinked deflection of primary cilia. This deflected form is possibly caused by the lower part of cilia protected by the glycocalyx layer, which results in the deflection at the upper part only. The lower portion of cilia could contribute to the greater flexural rigidity *EI* value at the base of cilia.

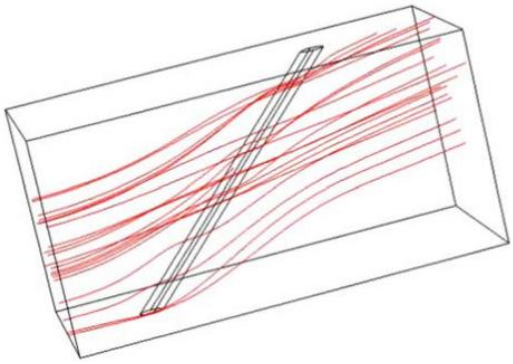

Fig. 1.12: The Comsol finite element model showed the cilium exposed by fluid streamlines (Downs et al., 2014).

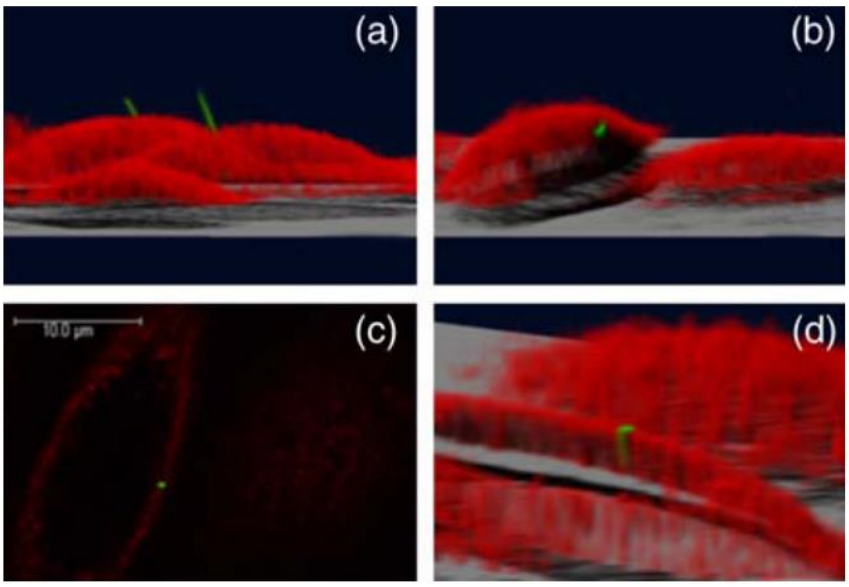

Fig. 1.13: 3D reconstruction images of cell and primary cilia (Downs et al., 2014).

In 2015, the flexural rigidity of primary cilia was also measured using an optical trap exciting the resonant oscillation (Resnick, 2015). In this study, the single dynamic measurement by resonant oscillation could have reliable results as multiple independent experiments. An improved feature in this model is the nonlinear rotational spring of the cilia base model. It was concluded that the physical structure at the base of cilia plays an important role in mechanosensing mechanism. This conclusion was in agreement with Battle et al. (2015). Not like Resnick, Battle et al. (2015) used the optical trap to do single application to bend the cilia and observe their mechanical responses (Fig. 1.14). The flexural rigidity was around 2.5 x 10^{-23} Nm^2. They found the correlated fluctuation of the

cilium and the basal body, which suggests that the mechanical responses of the axoneme is transmitted from the basal body structure. Figure 1.14 shows the deflection of the primary cilium in optical trap control (left panel), and the relaxation time of cilia at different lengths after releasing the bending.

In 2018, for the first time, by measuring the fluctuating position of an optically trapped cilium tip, Flaherty et al. (2018) reported the dependence of flexural rigidity on the cilia length (Fig. 1.15).

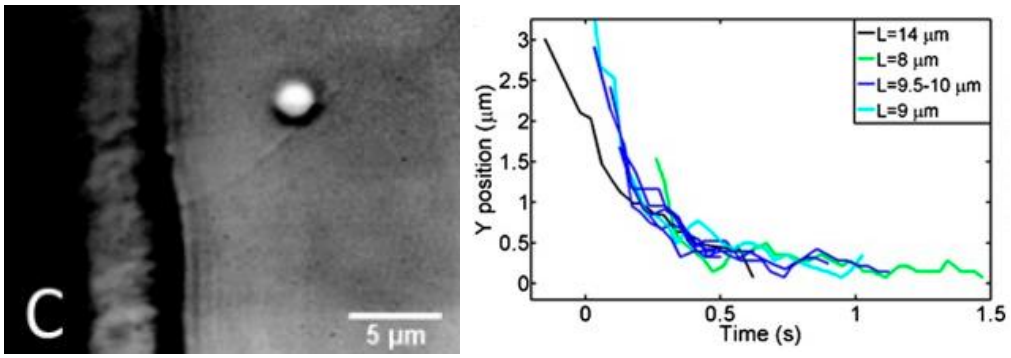

Fig. 1.14: Primary cilia bending by optical tweezer (Battle et al., 2015). Left panel: The deflected primary cilium is controlled by the optical trap. Right panel: The relaxation curve of primary cilia of different lengths.

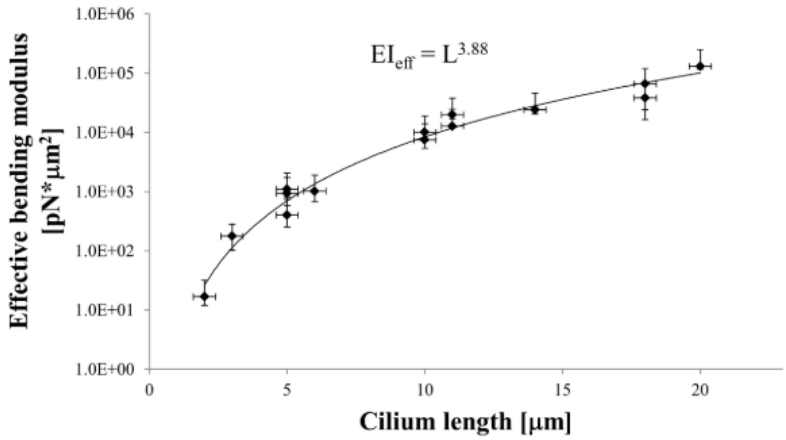

Fig. 1.15: The dependence of bending modulus on cilium length (Flaherty et al., 2018).

Primary cilia are composed of nine microtubule doublets arranged radically, so knowing mechanical properties of microtubules is also necessary to evaluate overall mechanical properties of primary cilia. So far some studies investigated the mechanical properties of microtubules. Gittes et al. (1993) measured flexural rigidity of microtubules by analysing thermal fluctuation of single filaments of microtubules. Owing to the size of microtubules, it is technically difficult to apply a tiny mechanical force and measure the deflection, therefore the authors measured the bending of microtubules by thermal forces. They reported the flexural rigidity of microtubules being 2.2 x 10^{-23} Nm^2. In 2006, Kikumoto et al. (2006) developed another method to determine the flexural rigidity of a single microtubule. They used two optical traps to measure the buckling force and then calculated the average microtubule rigidity. Their measured value was approximately 7 x 10^{-23} Nm^2 (Fig. 1.16)

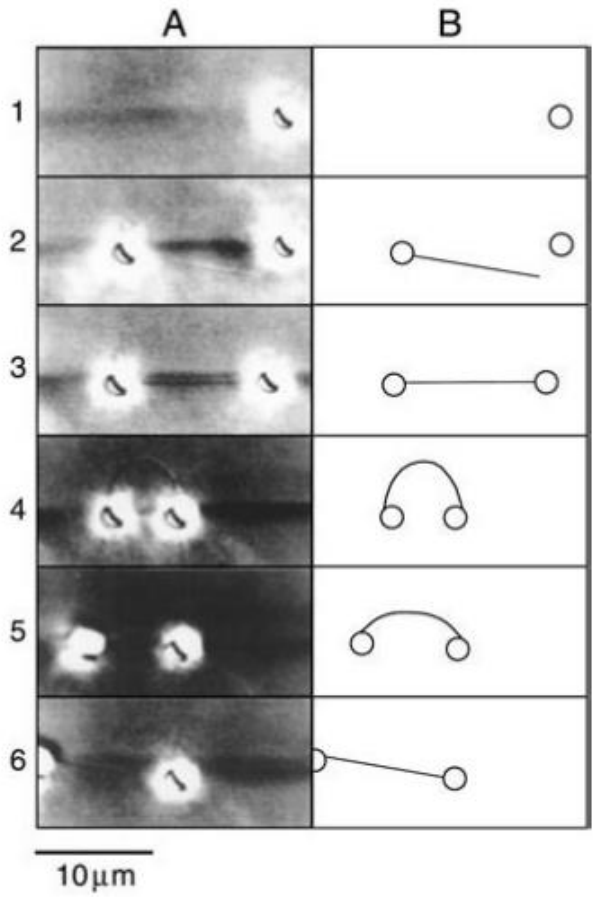

Fig. 1.16: The example of single-microtubule capturing, buckling, and releasing in optical traps (Kikumoto et al., 2006).

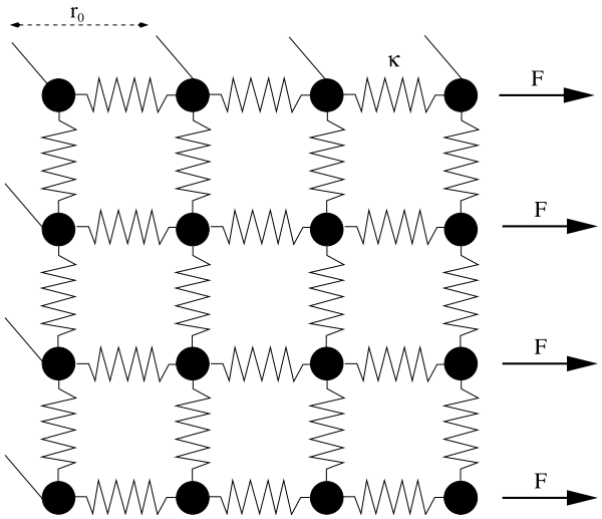

Fig. 1.17: The simple model of internal geometry of the microtubule (Tuszyński et al., 2005).

Tuszyński et al. (2005) estimated the elastic properties of single microtubules by modulating the microtubule structure and applying molecular forces between dimers (Fig. 1.17); their estimate was about 1.32 x 10^6 kPa. The Young's modulus of primary cilia is in the order of hundred kPa, while that of microtubule is in the order of GPa. The difference between these two values might be explained by other possible components that contribute to determine the elastic modulus of primary cilia.

1.6 Remodeling of primary cilia in response to mechanical signals

It is well-known that cells are constant exposed to mechanical stimuli from the surrounding extracellular matrix (such as flow for endothelial cells or kidney cells, 3D collagen for bone cells, tendon cells …). To adapt to the dynamic change of extracellular environment, cells may change their morphology and functions through their mechanosensors such as primary cilia. Many researchers elucidated the primary cilium bending mechanics in response to mechanical stimuli, together with the mutual connection between the bending and biological adaption inside intracellular matrix. However, how primary cilia change their behaviors such as morphology, incidence and orientation in response to mechanical signals is not well understood and there are not many studies working on this topic.

Espinha et al. (2014) explored that compared to kidney cells in control condition, cells exposed to fluid shear had more microtubules at the ciliary base, or the increase of

microtubule acetylation, which increases binding of microtubule-associated and consequently microtubule stiffness (Geiger et al., 2009). Characteristics of primary cilia, such as axoneme length, can be manipulated to recover or adjust the mechano-sensitivity (Marshall et al., 2001). Iomini et al. (2004) also reported that prolonged exposure of high fluid shear stress would induce primary cilia disassembly. These studies suggested the remodeling function of primary cilia in response to adapt the changes of fluid flow. There are only few studies so far investigated the remodeling of primary cilia in response to mechanical stimulation, which is summarized in Table 1.4.

McGlashan et al. (2010) studied how the chondrocytes of articular cartilage can sense their mechanical environment. They developed a 3D agarose culture model to culture chondrocyte and executed the compressive strain on chondrocyte. They found that the chondrocyte cilia elongate over the time of 24 h cyclic compression, and then shorten, resorb after 48 h (Fig. 1.18). Interestingly, if those cells were put in the free-swelling condition for 72 h, the number of ciliated cells and the cilia length increase again. They believed that it is the adaptive mechanism to adjust chondrocyte sensitivity to the local biomechanical environment.

Table 1.4: Summary of cilia remodeling under stretching conditions.

Author, year (ref)	Studied object	Cilia remodeling
McGlashan et al., 2010	Chondrocyte primary cilia in 3D cultured model	Cilia length elongated under compressive condition
Gardner et al., 2011	Tendon primary cilia *in situ*	Cilia length elongated under stretching condition

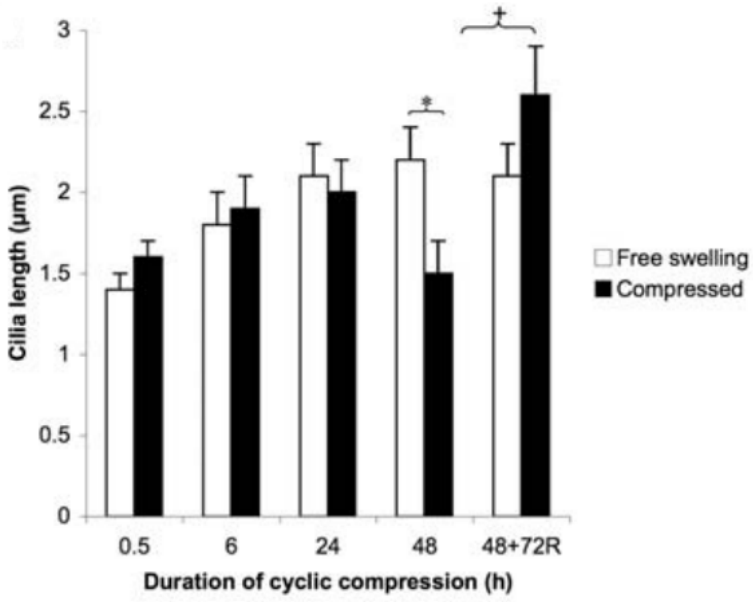

Fig. 1.18: Changes of chondrocyte cilia length in compressive loading condition (McGlashan et al., 2010).

In this study, the physical parameters such as the incidence and the length were examined. It still needs to do further studies to find out the mechanism of changing chondrocyte cilia length in mechanical loading conditions. Gardner et al. (2011) examined the effect of loading conditions on the length of primary cilia in tendon cells *in situ.* They suggested that primary cilia, which were exposed to fluid shear stress, can be remodeled through the change of length. The results also showed that the tendon cell's primary cilia experience a significant elongation after 24 h of stress-deprivation, and they reach the steady state at 48 h (Fig. 1.19 & 1.20). The reason of this lengthening of tendon cell cilia is not clearly understood, but it might be explained that the cilia lengthen their length to increase the ability to receive the weak mechanotransduction signal in the case of physical stimulation absence. The cyclic loading conditions help tendon cell cilia to maintain their length.

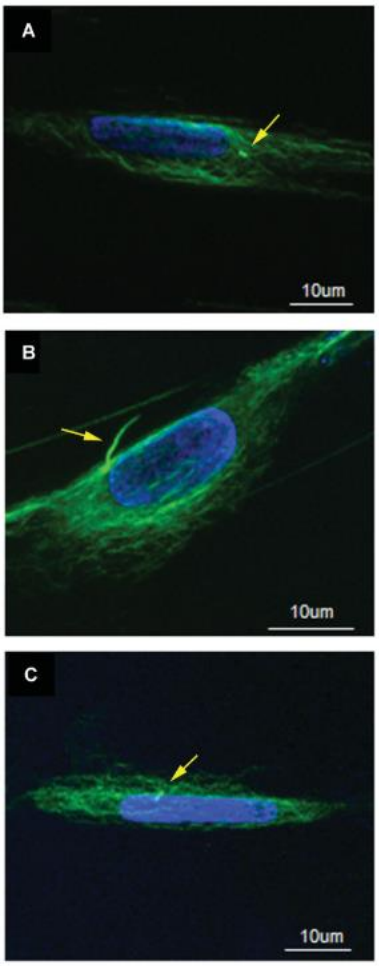

Fig. 1.19: Representative photomicrograph images of cilia (arrows) on rat tail tendon cells. (A) Fresh control. (B): 24 h stress-deprived. (C): 24 h cyclically loaded (Gardner et al., 2011).

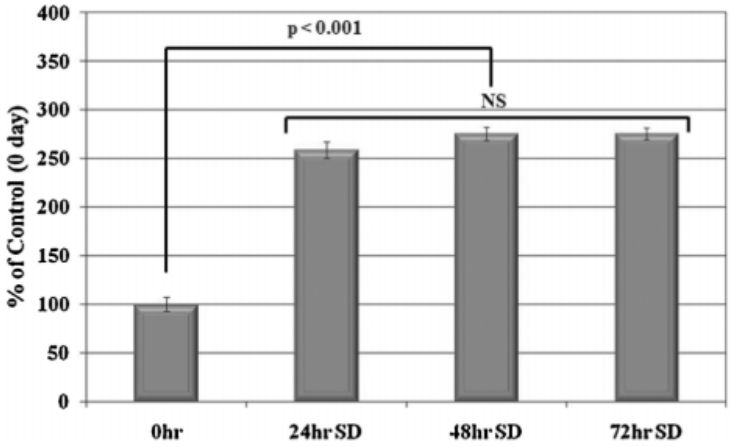

Fig. 1.20: Relative change in length of primary cilia following various time periods of stress deprivation (Gardner et al., 2011).

1.7 Methodology of mechanical testing

The responses of cells and biological materials depend not only on the mechanical force applied to them, but also on the mechanical properties of cells and those materials. Therefore, it is necessary to evaluate the mechanical properties of tissues, cells or organelles to understand better the cellular behavior. Depending on the objectives and purpose of studies, such as investigating global mechanical properties or local mechanical properties of biological materials, different techniques can be applied. The summary of mechanical tests can be briefly shown in Table 1.5.

Tensile and compressive tests are commonly used to measure global mechanical properties. These are the traditional tests, but are still useful for biological materials. The elastic, or Young's modulus, of the sample is generally obtained from the slope of the stress-strain curve. The viscoelastic properties can also be studied through these methods. To measure the local mechanical properties, the probe-based technique of AFM is often used. The cantilever tip is indented to the sample surface to obtain the experimental force-indentation, then the mechanical properties of the sample are determined according to the models of force-indentation curves. The range of well-defined forces, which AFM is able to apply, is around pico-Newtons to nano-Newtons. The beads-related techniques such as optical tweezers and magnetic tweezers were also utilized. The sample can be trapped in the focused light, or by magnetic beads; and then the force is transduced to sample by controlled optical beads or magnetic field.

Table 1.5: Summary of the mechanical testing methods.

Mechanical testing	Tested objective	Mechanical properties	Author, year
Tensile test	Actin filaments	Elastic modulus	Kojima et al., 1994
	Actin stress fibers	Tensile modulus	Deguchi et al., 2006
	Actin stress fibers	Viscoelasticity	Matsui et al., 2009
AFM	Human platelets	elastic modulus	Radmacher et al., 1996
	Bone section of cow tibia	Rigidity modulus	Tao et al., 1992
	Endothelial cells	Elastic modulus	Ohashi et al., 2002
Micropipette Aspiration	Arteries	Elastic modulus	Ohashi et al., 2005
	Chondrocytes	Elastic modulus	Li et al., 2019
Optical tweezer	Primary cilia	Flexural modulus	Resnick, 2016
	Collagen	Molecular force of single collagen	Rezaei et al., 2011
Magnetic tweezer	Nucleic acids	Bending, stretching, twisting properties	Kriegel et al., 2017

1.7.1 Micro tensile test

Using the tensile test to measure the Young's modulus is a very well-known and traditional method to measure the mechanical properties of materials. In this section, it just briefly introduces this method and some applications in biological materials. Although the biological materials have some limitations such as the tiny size (micrometers), tiny applied force (nanoNewtons or picoNewtons) and tiny deflection (micrometers), this method was still used in some cases.

The elastic behaviour can be easily understood by imaging the spring under the action of a force. In principle, when the tensile force applied to a material, the tensile modulus, or the Young's modulus (E), the material property, is quantified between the stress (force per unit area) and the strain (the change in length divided by the original length) in the linear elastic region of a material and is determined by Eq. 1.1,

$$\sigma = E \times \varepsilon \qquad (1.1)$$

where E is the Young's modulus of materials, σ the tensile stress, and ε the tensile strain.

To measure Young's modulus of biological materials, traditionally, the samples had been tested using constant strain-rate experiments where a sample is deformed at a constant rate in the linear region or until failure. Several groups applied this method to measure the mechanical properties of cells organelles such actin filaments and stress fibers.

In 1994, Kojima et al. (1994) was one of the first people applied tensile test to study the mechanical properties of biological materials. He applied this method to measure the stiffness of single actin filament (Fig. 1.21). Basically, the single actin filament were held by microneedles (the stiff and soft ones) which were manipulated by hydraulic manipulators. The force was driven by piezo actuators and the nanometer-range displacement was displaced by the soft microneedle. The whole setup was built on an inverted fluorescence microscope to record the changes during the stretching process. As far as we know, this is one of the first studies applied the traditional tensile test to biological specimens.

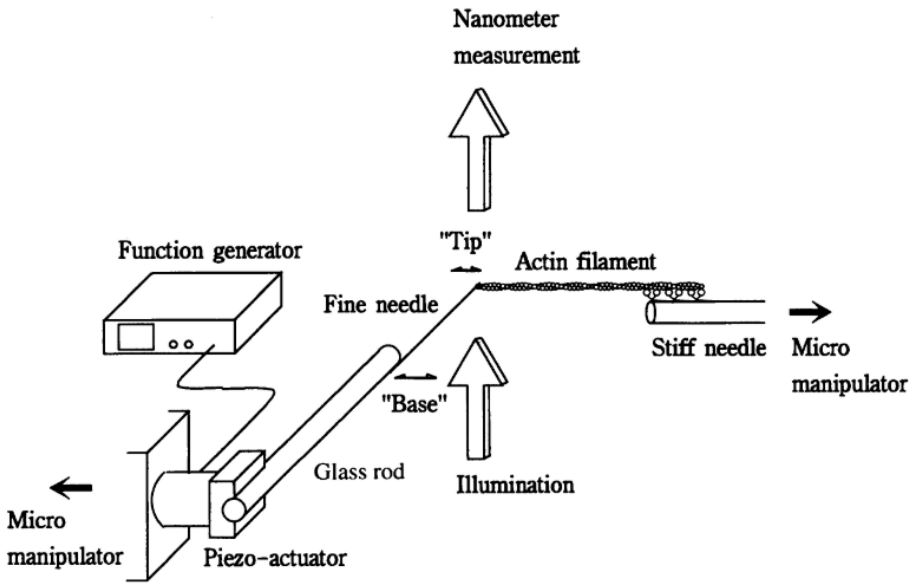

Fig. 1.21: Schematic diagram of the actin microtensile test (Kojima et al., 1994).

In 2006, Deguchi et al. (2006) used the tensile test to measure the mechanical properties of isolated stress fibers. Stress fibers are contractile bundle of actin filament and play a main role in mechanotransduction of cells. At the time of this research, the mechanical properties of stress fibers are poorly understood, and by measuring their mechanical properties, this study provided useful information on the force transmission inside cells (Fig. 1.22). In 2009, using the same configuration of Deguchi et al. (2006), Matsui et al. (2009) developed the system to investigate the viscoelastic properties of stress fibers through creep and relaxation tests.

Compared to other advanced techniques to measure the Young's modulus of biological materials such as magnetic resonance elastography, optical coherence elastography, ultrasound elastography …, this traditional tensile loading is more difficult to handle due to the tiny size of biomaterials and time consuming. That is why not many people choose this method for measuring mechanical properties of biological materials. However, because of the direct stretching, the traditional tensile test is more reliable.

In our study, this method was chosen to measure the global Young's modulus of isolated primary cilia.

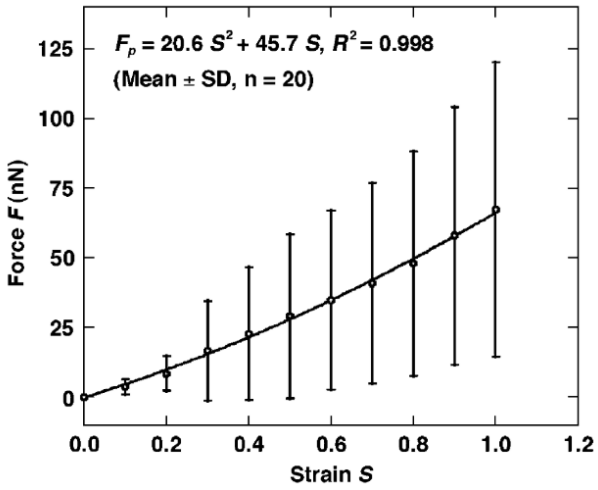

Fig. 1.22: Force-strain data in the physiological strain range of 0.0 - 1.0 of stress fibers (Deguchi et al., 2006).

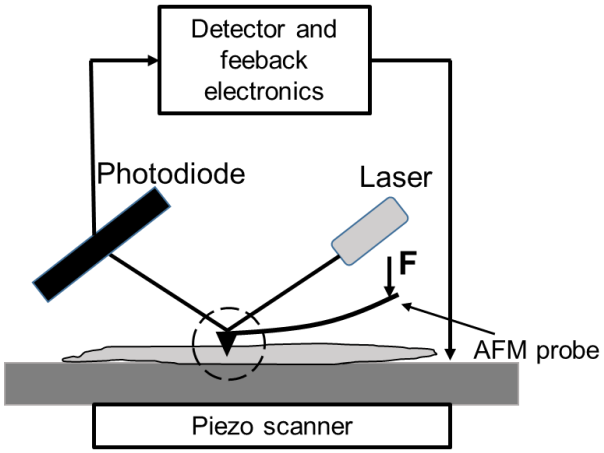

Fig. 1.23: Typical configuration of an AFM.

1.7.2 Atomic force microscopy

The AFM, invented in 1986 (Binnig et al., 1986), is the useful and popular technique for imaging biological specimens such as cells, organelles, proteins and DNA without any specific treatment. The schematic of AFM is shown in Fig. 1.23. The measurement of local mechanical properties of materieals is also possible with the AFM using the force modulation. The wide range of biological specimens' elastic properties has been determined

by AFM such as cells (BAEC cells, MDCK cells, myocytes ….), bone, organelles (platelets, gelatin …), etc.

To measure mechanical properties, the force spectroscopy is used. The cantilever comes to contact with the sample's surface, and then retract, while the interaction between the tip and sample is measured. This process can be repeated in different locations to build up a full map of the surface's properties, or can be repeated at the same point to have the properties of one local location. AFM was chosen to measure the local Young's modulus of primary cilia.

In 2002, Ohashi et al. (2002) applied AFM to measure the elastic modulus of sheared endothelial cells. It is well known that after exposure to fluid shear stress, endothelial cells elongate and orient in the flow direction, but the elastic modulus was not estimated experimentally. In their research, they had determined the elastic properties of sheared endothelial cells at different locations along the main axis of cells (Fig. 1.24) (number 4 is at the cell center location, and number 1 and 7 is at the periphery of cells), which induce to change of stiffness of cytoskeleton.

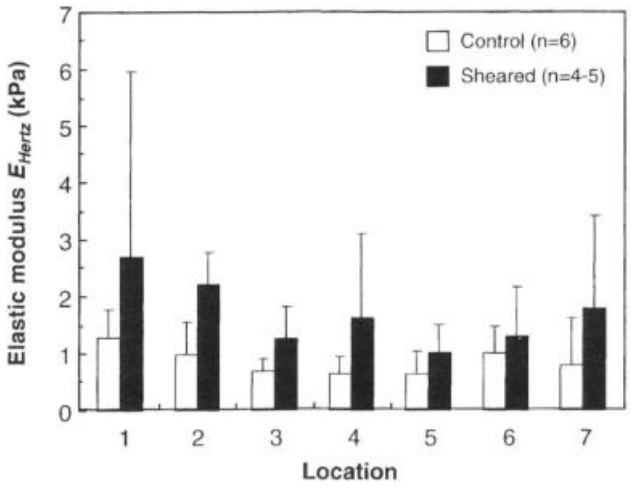

Fig. 1.24: : The increase of elastic modulus of sheared endothelial cells at different locations (Ohashi et al., 2002).

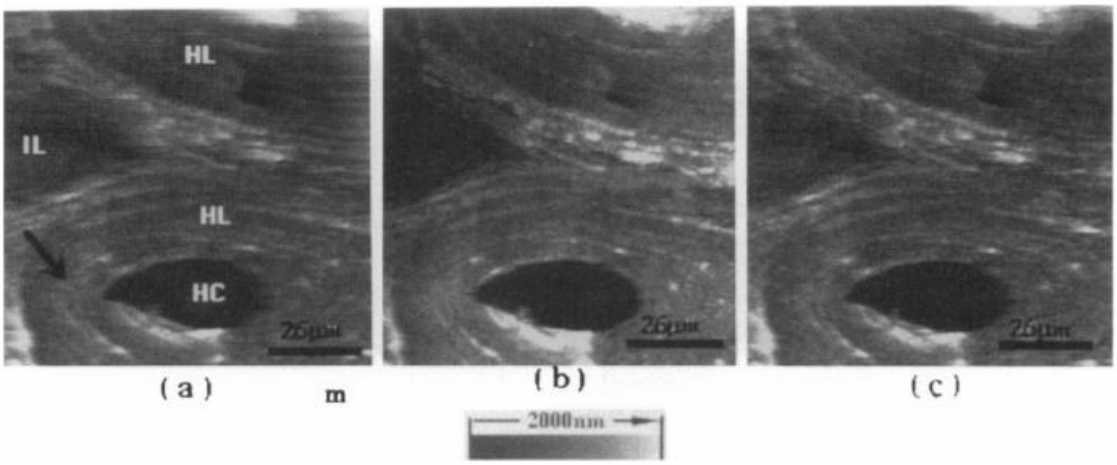

Fig. 1.25: AFM images of cow tibia. The osteonal lamellae, Harversian canal and interstitial lamellae are indicated as HL, HC and IL (Tao et al., 1992).

Tao et al. (1992) had used AFM to measure the local rigidity modulus on the surface of the section of cow tibia. Under the limited scan range of AFM, the authors can obtain the different parts of the cow tibia' section such osteonal lamellae, Harversian canal and interstitial lamellae (Fig. 1.25) and calculate the equivalent rigidity modulus. They found that the osteonal lamellae appears to be more rigid than the interstitial lamellae.

In 1996, Radmacher et al. (1996) determined the elastic modulus of human platelet using AFM. The topographic and elastic property map of platelet was obtained by the force mapping. The different parts of the platelet show the distributed stiffness (Fig. 1.26). The pseudonucleus (P) is the softest area (1.5 to 4 kPa). Going to edge area, the stiffness increases, the inner web (I) has the stiffness of 4 kPa, the outer web (O) ranges around 10 - 40 kPa, and the cortex is stiffest (50 kPa).

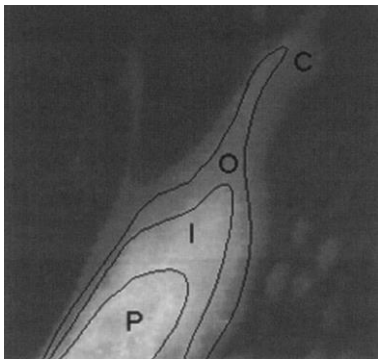

Fig. 1.26: Topography and the elastic modulus of platelet at different locations (Radmacher et al., 1996).

1.7.3 Micropipette aspiration

Micropipette aspiration was also developed to measure the local mechanical properties of samples such as the cell membrane. Based on the applied negative pressure and the deformation of the sample, the elastic modulus can be determined (Fig. 1.27).

Li et al. (2019) investigated the mechanical properties of chondrocyte from different mechanical models of micropipette aspiration. Three models they considered were Half-Space Model (HSM), Incompressible Sphere Model (ICSM) and Compressible Sphere Model (CSM). They concluded that the elastic moduli and viscoelastic parameters of chondrocytes for the ICSM and CSM are significantly higher than those of HSM. Their results are indicated in Table 1.6.

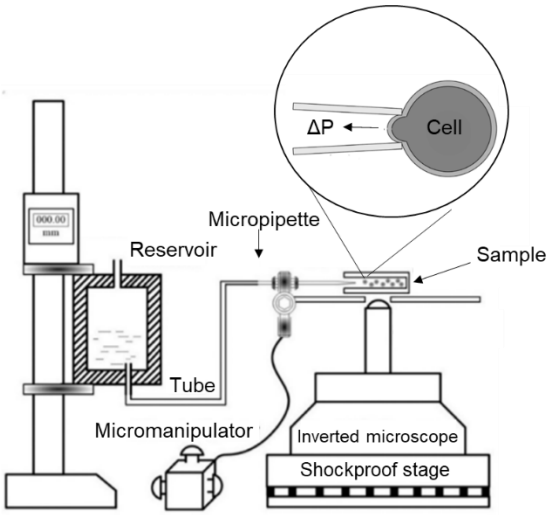

Fig. 1.27: Schematic diagram of micropipette aspiration (modified from Li et al., 2019).

Table 1.6: Elastic and Viscoelastic properties of Chondrocyte measured by different models (Li et al., 2019).

	MPA (Current Study)		
	ICSM	CSM0.38	CSM0.26
E (kPa)	0.84 ± 0.66	0.99 ± 0.87	1.12 ± 0.75
E_0 (kPa)	0.91 ± 0.14	1.75 ± 0.35	2.25 ± 0.44
E_∞ (kPa)	0.51 ± 0.09	0.75 ± 0.06	0.93 ± 0.11
μ (kPa•s)	8.84 ± 1.52	17.26 ± 2.52	25.43 ± 4.25

Previously, Ohashi et al. (2005) utilized the micropipette aspiration to measure the mechanical properties of arteries under biaxial stretching. They found that the elastic modulus of arteries has no significant difference with the cases of circumferential stretch ratio below 1.3 and an axial stretch ratio of 1.0, 1.1 and 1.2.

1.7.4 Optical tweezer

The schematic of the optical tweezer technique is illustrated in Fig. 1.28. A high-power laser generator emits the laser beam; after going through several lenses (T1, steering mirror SM, T2, and OBJ), the trapping beam is focused into the sample. The maximum force and the trap stiffness depend mostly on the laser power. The position and force are detected by QPD. The disadvantages of optical tweezers could be photodamaging or heating.

Resnick (2015) applied this technique to investigate the mechanical properties of primary cilia. An optical trapping captured the primary cilia, and then the force was applied to study the flexural rigidity of primary cilia.

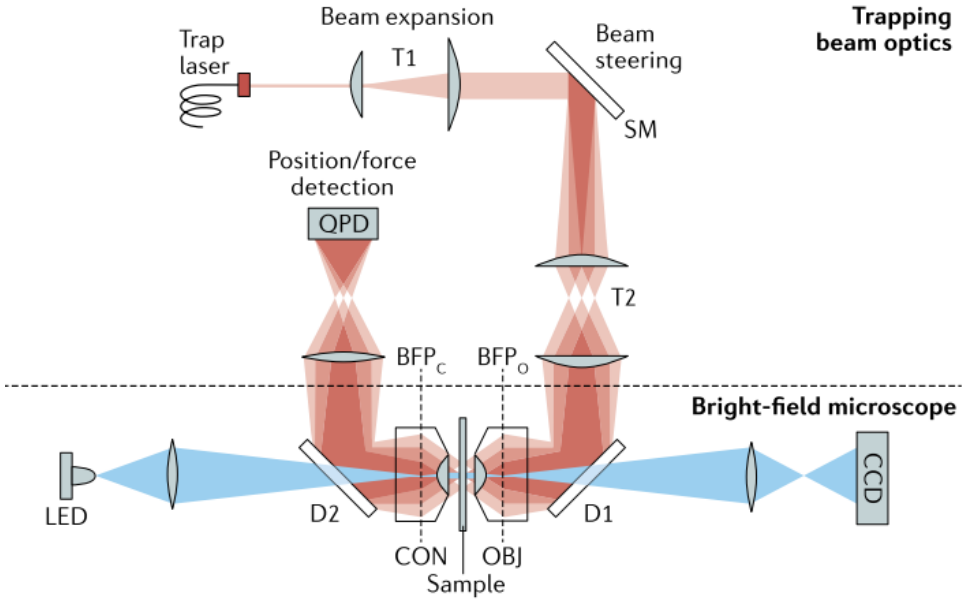

Fig. 1.28: Schematic diagram of optical tweezer (Bustamante et al., 2021).

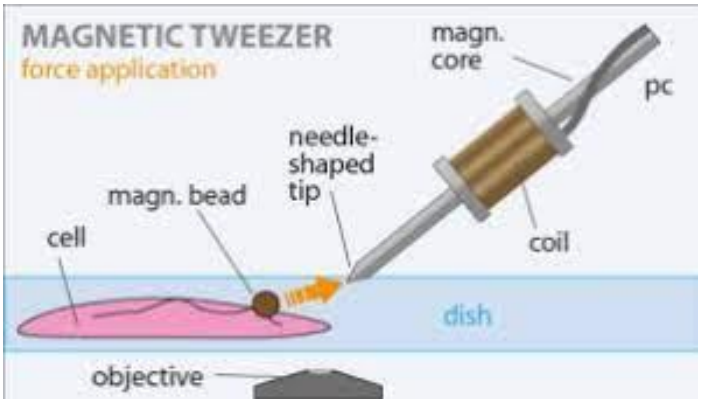

Fig. 1.29: Magnetic tweezer (https://bio.physik.fau.de/methods/magnetic-tweezer/).

1.7.5 Magnetic tweezer

Similar mechanism as the optical tweezer, a magnetic bead is approached and attached to the desired specimen, then the bead is manipulated by external magnets (Fig. 1.29). The most challenging of magnetic tweezers is the calibration and handling the beads in magnetic fields.

1.8 Methodology of mechanical loading

To sustain the human body alive and function, it is necessary to understand the physical, and biochemical functions of organisms, organ systems, individual organs, tissues and cells. In particular, mechanically, the analysis of mechanical loading exposed to human body has always been a crucial topic in biomechanical research. Mechanical stimulations influence cell behaviors. Different mechanical forces exposed to cells, different cell responses are regulated. Cells may sense the mechanical environment through receptors or sensors called mechanosensors. They adapt to the stimuli by altering, mechanically, their morphology, stiffness, orientation or alignment, and biologically, adhesion, proliferation, differentiation, gene and protein expression, apoptosis. Many mechanical loadings have been researched to cells *in vitro*, including tension, compression, shear, centrifugation, and vibration to understand more deeply cells mechanisms. The most well-known mechanical loadings exposed to cells are fluid shear stress and stretching.The summarized mechanical loadings is shown in Table 1.7.

In this study, it is desired to examine the remodeling of primary cilia in response to mechanical loadings. The primary cilia are mechanosensors of cells and locate at the top

Table 1.7: Summary of mechanical loading methods to biological materials.

Mechanical loading	Tested objective	Author, year
Stretching model	Endothelial cells	Ambrosi et al., 2002
	Tenocytes	Maeda et al., 2013
	Endothelial cells	Ohashi et al., 2007
Fluid flow	Tenocytes	Maeda et al., 2013
	Primary cilia	Schwartz et al., 1997
	Bone cells	Vaughan et al., 2014
Pressure	human Bone Marrow Stem Cell (hBMSC)	Stavenschi et al., 2018

surface of cells. Due to that position, it is obvious that fluid shear stress directly expose to the cilia, and the primary cilia may sense changes of shear stress. However, so far there is no study of how the primary cilia respond to indirect mechanical loadings of substrate stretching at the bottom of cells. It is hypothesized that the actin cytoskeleton, which is the mediate connector between the focal adhesions and the base of primary cilia, can transmit the changes of substrate stretching to primary cilia.

1.8.1 Stretching model

The concept of stretching devices is to generate strain on cultured cells. With that concept, the cell monolayer is usually cultured on the surface of elastic membranes, typically Polydimethylsiloxane (PDMS) substrates (Fig. 1.30). By applying cyclic stretching to the elastic membranes, the cells cultured on them can be stretched (Fig. 1.31).

Various approaches for cell stretching devices, commonly including motor-driven, indentation, pneumatic, magnetic and electromagnetic actuation, have been developed to induce mechanical deformation of the elastic membrane. Different parameters can be varied in stretch mode (uniaxial, biaxial, and equiaxial), stretch waveform (static, sinusoidal and square), strain magnitude, frequency to provide various conditions of cells' living environment for researchers. It is noticed that some systems have the maximum strain at the center of the substrate, while the peripheral substrate areas have the minimal strain.

Unlike the plastic or glass dishes where the surface of plastic or glass is charged and cells can attach to them without any specific chemical treatment, the PDMS chambers or substrates are hydrophobic and cells have difficulty attaching to it. Therefore, the chamber surface should be coated with an extra-cellular matrix like fibronectin, collagen, laminin, or gelatine before cultivation.

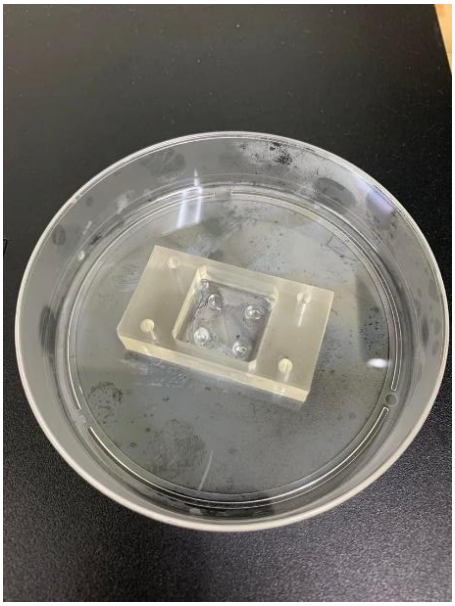

Fig. 1.30: An example of PDMS substrate.

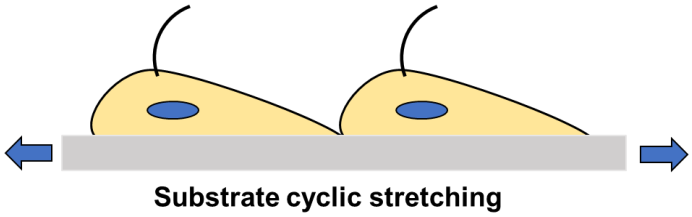

Fig. 1.31: The schematic mechanism of stretching model.33

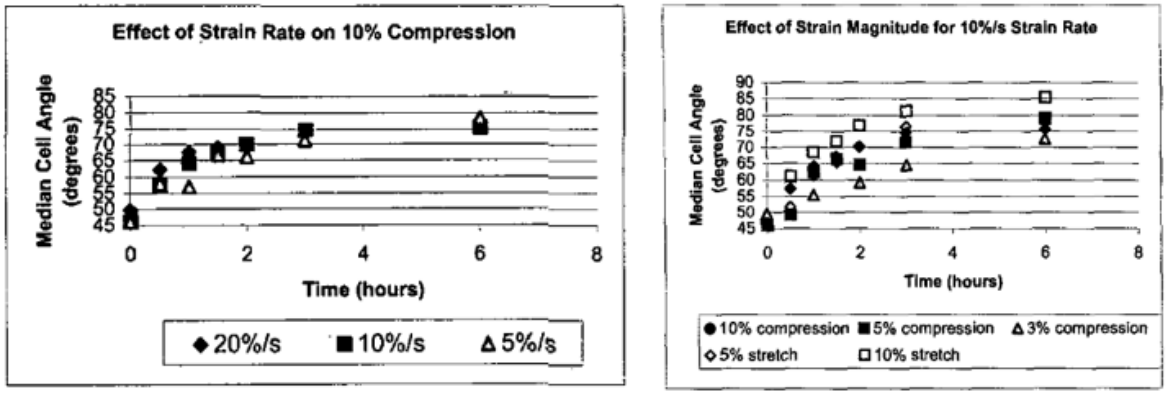

Fig. 1.32: The effect of strain rate on compression (left) and effect of strain magnitude on compression and stretching (Ambrosi et al., 2002).

In 2002, Ambrosi et al. (2002) examined the reorientation response of endothelial cells to cyclic compression and stretching. They found that the cell reorientation during cyclic stretching and compression depends on the magnitude, not the strain rate. However, the reorientation of cells under cyclic compression is slower than that of cells under cyclic stretch (Fig. 1.32). It could be explained by the less pronounced disruption of actin stress fibers in the compression, compared to stretching.

In 2013, Maeda et al. (2013) applied simultaneously the cyclic tensile strain and fluid shear stress on tenocytes in the microgroove structure to maintain the best *in situ* tenocyte conditions in terms of morphology and working environment. This was the advance studied since, for the first time, a combined stimulation of cyclic tensile strain and fluid shear stress had been investigated on tenocytes. The distinct results showed the significant increase in the percentage of tenocytes exhibiting Ca^{2+} responses, compared to the solo stimulation (Fig. 1.33).

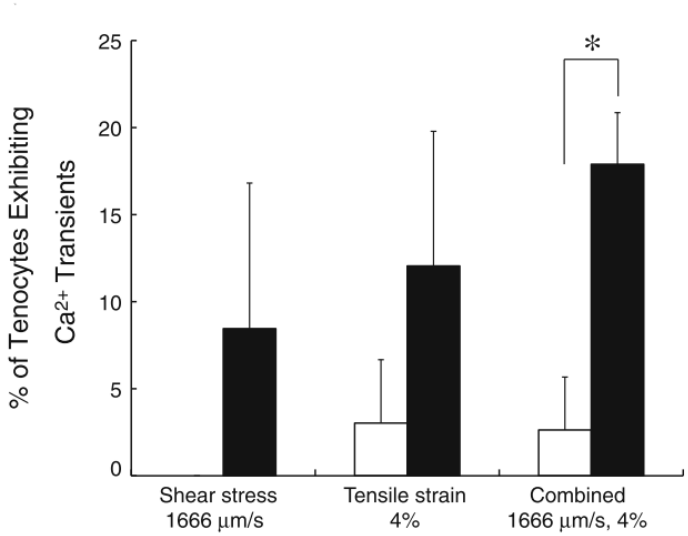

Fig. 1.33: Percentage of tenocyte exhibiting Ca^{2+} over 5 min period. Open bars represent data of pre-stimulation controls and filled bars represent data of stimulated cells (Maeda et al., 2013).

1.8.2 Fluid flow

Fluid flow shear stress may affect cells. For instance, endothelial cells are highly subjected to shear stress from the blood in the vessels, and the range of shear stress depending on vessel size, blood flow. *In vitro*, the medium is pumped into circulation, and the shear stress is controlled by the flow rate, which is controlled by the roller pump (Fig. 1.34). The most typical mechanical response of cells regulated by shear stress is the cell alignment parallel to the flow direction and the integrity increases.

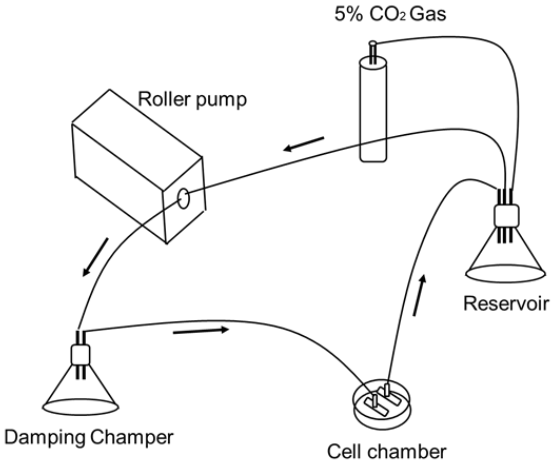

Fig. 1.34: Schematic diagram of fluid flow experiment.

The fluid flow test is one of the most basic mechanical loadings when researchers study about endothelial cells, epithelial cells and bone cells. Most of the studies that were reviewed on measuring mechanical properties of primary cilia in section 1.5 used fluid flow test to observe the bending of primary cilia (Schwartz et al., 1997; Young et al., 2012; Downs et al., 2012; Rydholm et al., 2010). In the stretching model, Maeda et al. (2013) applied simultaneously fluid flow and stretching to tenocytes.

1.9 Research purposes

As mentioned in the literature review, most of the previous studies of mechanical properties of primary cilia are flexural rigidity, which basically is not the material property. Moreover, the results of measured flexural rigidity had a big discrepancy due to the use of different mathematical models to determine the parameters. One of the aims of this research is to clarify the mechanical properties of primary cilia such Young's modulus and viscoelasticity. The experimental elastic modulus may provide an important information of mechanical properties of primary cilia, which may help for further investigation to understand appropriately the mechanics of primary cilia. In all previous numerical studies of primary cilia mechanics, the elastic component was neglected, one reason is its small effect compared to the bending components in response to fluid flow and another reason is the lack of confidence value of elastic properties. The elastic and viscoelastic properties in this study will give valuable information for further understanding of cilia mechanics.

As being mechanosensors of cells and continuously exposed to external mechanical signals in the extracellular matrix, it would be natural to question what happened to primary cilia under those stimulations. Among mechanical signals exposed to cilia, fluid flow shear stress is an obvious stimulus to change cilia's behaviours because of their direct contact, but the cyclic substrate stretching is not well investigated and understood due to their indirect connection. It motivated us to find out what's happening to primary cilia under this stimulus.

Above two research aims are pretty new in the research field of primary cilia, in term of mechanical properties and mechanical responses of primary cilia. Regarding another research topic in this dissertation, it is not really new to discover the microstructure of

primary cilia using TEM. However, this topic may be useful for us, firstly in confirming the diameter of primary cilia, which provides for the calculation of the Young's modulus of primary cilia, and secondly obtained the overall microstructure components of primary cilia to get a better understanding of mechanical responses of cilia. In sake of providing better understanding of cilia mechanics for further numerical work, this study, for the first time, provides a model of the primary cilium with the main mechanical structures. The model also revealed a mechanical properties of cross-linking components between microtubule doublets, which is never reported so far.

1.10 Thesis outline

This thesis is outlined to 5 chapters. The content of each chapter can be summarized as follows:

Chapter 1 introduces the basics of cells, and the primary cilium (its structures, and functions in cell life). The literature reviews of mechanical properties of primary cilia and the remodeling of primary cilia in response to mechanical signals are presented. Moreover, the knowledge of mechanical testing methods and mechanical loadings to biological materials are reviewed in this chapter.

Chapter 2 introduces our measurement of Young's modulus of isolated primary cilia. The mathematical model of primary cilia is also built up to deduce their viscoelastic parameters. The in-house micro-tensile test is constructed by ourselves for the sake of measuring of mechanical properties of cilia. The isolated primary cilia are used for mechanical testing, so the isolation method is also introduced.

Chapter 3 examines the remodeling of primary cilia in response to the cyclic substrate stretching. The remodeling of primary cilia in response to the fluid flow is quite obvious because of their direct contact. In this chapter, it is hypothesized that primary cilia can be remodelled under the substrate stretching condition through the cytoskeleton network. This is one of the first study questions and clarifies this issue. Different strain levels were applied, and the remodeling of cilia, i.e cilia length, and cilia incidence are tested. The inhibition of actin myosin, which inhibits the change of actin network during stretching, is also examined to see whether it affects cilia responses.

Chapter 4 discovers the microstructure of primary cilia using TEM. The diameter of cilia can be confirmed to determine the elastic modulus in Chapter 2. The microstructures of primary cilia are identified through TEM images to clarify the structure of primary cilium and the relative connection to other cellular organelles, which explain the mechanical behaviour of cilia in response to extracellular mechanical signals. Collectively from previous TEM images of the primary cilium, the simulation was performed to model properly a primary cilium with main mechanical components. The simulation confirmed the dependence of mechanical properties of primary cilia on the cross-linking component between microtubules. It also found the range of elastic moduli of this cross-linking component.

Chapter 5 summarizes all the results obtained in this study and provide some prospects for future researches in this field.

Chapter 2

Measurement of mechanical properties of isolated primary cilia from cells

2.1 Introduction

Primary cilia are long, thin, microtubule-based organelles protruding from the apical cellular surface (Lim et al., 2015). They are found in multiple types of cells and have been implicated as mechanosensors to sense changes in the surrounding mechanical environment and as a chemosensor to detect ligand, growth factors, and hormones. For instance, kidney epithelial cells may use primary cilia to sense urine flow and respond by greatly increasing intracellular calcium (Praetorius and Spring, 2001). It is also reported that endothelial primary cilia may bend in response to blood flow, release calcium, and synthesize nitric oxide (Hierck et al., 2008; Van der Heiden et al., 2008). Furthermore, the lack of primary cilia or their dysfunction may lead to a variety of diseases such as polycystic kidney disease (PKD), blindness, and developmental disorders (Brown et al., 2014; Kowal et al., 2015; Satir et al., 2010).

To understand mechanical and biochemical responses of primary cilia to mechanical stimuli such as fluid flow, many studies have so far been conducted. Schwartz et al. (1997) first modeled a microtubule-based elastic structure of primary cilia to study their bending behaviour in response to fluid flow and determine the flexural rigidity. However, their model was limited by the assumption of a constant flow velocity and drag profile along primary cilia. Young et al. (2012) later developed a more precise model of fluid flow profile around primary cilia and conducted a quantitative comparison of cilium bending between experiments and modeling to obtain the flexural rigidity. Downs et al. (2014) used a coupled fluid-structure interaction model, which combines 3D fluid dynamics with a large rotation of anchorage of primary cilia, and provided a significantly different flexural rigidity value compared to the previous studies. In addition to flow experiments, other experimental approaches have been employed to study cilia bending characteristics. The flexural rigidity of primary cilia was measured by an optical trap (Resnick, 2015; Battle et al., 2015; Resnick, 2016), which showed that the flexural rigidity of the ciliary axoneme is length-dependent.

Rydholm et al. (2010) structured a finite element model for the apical part of cells, including the primary cilium membrane to provide flexural rigidity. As for biochemical responses, they also indicated that the delay in calcium response upon bending was

caused by the membrane stress at the ciliary base, where the ciliary membrane was modeled continuously with the viscoelastic plasma membrane. In the simulation, the results were strongly influenced by viscoelastic properties of primary cilia and plasma membranes, however, viscoelastic properties of primary cilia have never been experimentally studied. As primary cilium axoneme mainly consists of nine radially arranged microtubule doublets, it is speculated that primary cilia possess viscoelastic properties similar to microtubules (Lin et al., 2007).

As aforementioned, most previous researchers studied the flexural rigidity of primary cilia and their results had big discrepancies due to the use of different mathematical models to determine the parameters. However, the material properties of primary cilia such as Young's modulus and viscoelasticity are still not investigated. For a better understanding of primary cilia mechanics, Young's modulus as well as viscoelastic properties are directly and precisely measured in this study. Recent advances in ultrastructural observation using TEM have revealed the variations of axoneme configuration from the base to the tip of primary cilia, which has the reduction in the number of microtubule doublets to less than nine pairs (Gluenz et al., 2010; Sun et al., 2019; Jensen et al., 2004). Moreover, the TEM observation has also revealed that the microtubule doublets exist around a few 10 nm deep from the cilia surface. These changes in structure configuration along the primary cilia suggest the change of mechanical properties along the length of cilia and the need for measurement of local Young's modulus. The AFM utilized to explicit the local mechanical properties of primary cilia was used to compare with the measured global Young's modulus by the micro-tensile test.

In this study, Young's modulus of isolated primary cilia was for the first time measured by an in-house micro-tensile test (Deguchi et al., 2006; Kojima et al., 1994). Viscoelastic properties of isolated primary cilia were also firstly evaluated by changing the stretching strain rates.

2.2 Materials and methods

2.2.1 Cell preparation

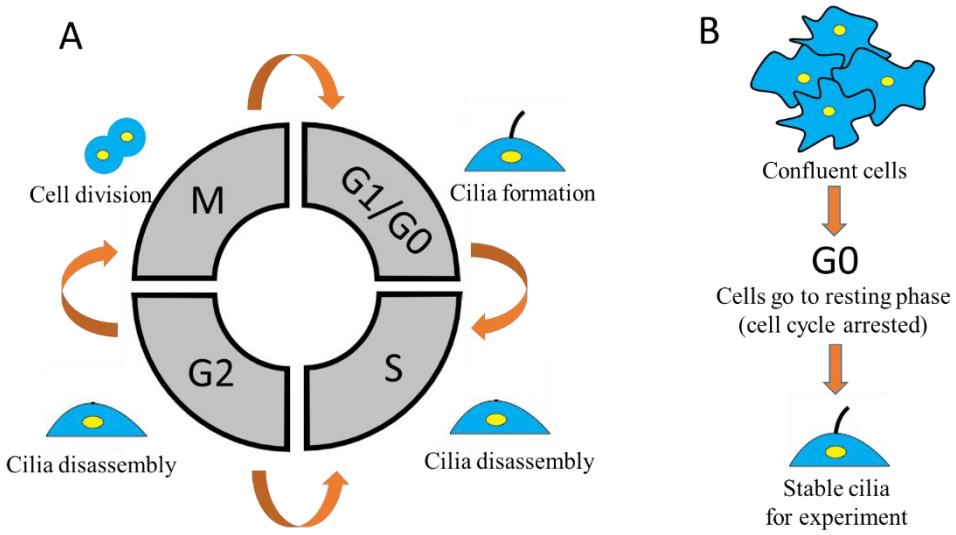

Fig. 2.1: The cilia formation in cell cycle (A) and cell confluent condition (B).

Madin-Darby Canine Kidney (MDCK) cells were used for experiments. Cell culture medium consists of Dulbecco's Modified Eagle Medium (DMEM) supplemented with 10% fetal bovine serum, 1% penicillin and 1% streptomycin. Cells were cultured under a humidified atmosphere of 5% CO_2 at 37°C up to passage 5 - 10. In order to carry out the isolation of primary cilia, cells must be confluent and quiescent (Fig. 2.1), as primary cilia are formed during interphase and reabsorbed during mitosis (Mitchell, 2013).

2.2.2 Isolation of primary cilia and immunofluorescence staining

For the tensile test, primary cilia were isolated from the cell body using the shear force of rotary shaking (Huang et al., 2006). The isolated cilia were centrifuged at 1,000 x g for 10 min at 4ºC. The supernatant was transferred to an ultracentrifuge tube and then centrifuged at 40,000 x g for 30 min at 4ºC.

2.2.2.1 Staining isolated primary cilia

The immunofluorescence staining of isolated primary cilia was processed as follows. In order to maintain the mechanical properties of primary cilia in the micro-tensile test, the fixation step is not proceeded with isolated primary cilia. Isolated primary cilia were

treated with 0.2% (vol/vol) Triton X – 100 (Sigma-Aldrich, USA) for 5 min and then washed with PBS for 10 min. Next, the first antibody (acetylated α-tubulin, Santa Cruz Biotechnology, USA) diluted with 1% BSA (1:1000, Sigma-Aldrich, USA) was added to stain primary cilia for 1 h at 37ºC. Finally, the secondary antibody (Human ads-Alexa Fluor® 488, Southern Biotech, USA) diluted with 1% BSA (1:1000) was treated for 1 h at 4ºC. After each antibody staining step, the solution was centrifuged at 40,000 x g for 30 min at 4ºC. The pellet containing primary cilia was transferred to a glass dish which allows to observe under 60 x lens microscope for the stretching tests.

2.2.2.2 Staining primary cilia on cells, actin filaments and nuclei

Primary cilia attached on cells still need to be confirmed under fluorescence microscope. The staining process is same as staining isolated primary cilia as described above, except the fixation step. The fixation steps of 4% paraformaldehyde is added for staining primary cilia on cells. The process is describe as follows. Cells were fixed in with 4% paraformaldehyde for 10 min at room temperature, then treated with 0.2% (vol/vol) Triton X – 100 (Sigma-Aldrich, USA) in PBS for 10 min, and blocked with 1% BSA blocking solution. Primary cilia were stained with the first antibody (acetylated α-tubulin, Santa Cruz Biotechnology, USA) diluted with 1% BSA (1:1000, Sigma-Aldrich, USA) overnight at 4ºC and then in secondary antibody (Human ads-Alexa Fluor® 488, Southern Biotech, USA) diluted with 1% BSA (1:1000) at 4ºC for 1h.

After staining primary cilia, the actin filaments and nuclei were stained with 400X Rhodamine Phalloidins (ThermoFisher, USA) diluted in PBS (1:400) at room temperature (RT) for 1h and Hoechst33342 (ThermoFisher, USA) at room temparture for 20 min, respectively. Washing in PBS three times between each step.

2.2.3 Micro-tensile test

A micro-tensile tester is important for the measurement of mechanical properties of isolated primary cilia in our topic. It was in-house fabricated on an inverted microscope (IX - 81, Olympus, Japan), which is developed from the previous study (Deguchi et al., 2006). The micro-tensile tester includes the cantilevers, the piezo-actuator, and the 3D micro-manipulators (Fig. 2.2). The stiff cantilever is attached to one end of the primary

cilia and connects to the piezo-actuator. The deflected cantilever is used to sense the applied force. The piezo-actuator (PK2FSF1, Thorlabs, USA) is used to apply pulling force to the primary cilia through the stiff cantilever, and two 3D hydraulic micro-manipulators are used to set up the position of both stiff cantilever and force-sensing cantilever before the stretching test.

This section introduces the main components needed for measuring Young's modulus of primary cilia including the technical specifications of the piezo-actuator. The cantilevers' stiffness was measured to classify the soft and stiff cantilevers. The soft or deflected cantilevers were determined as a spring constant smaller than 1 nN/µm, while the stiff ones have a spring constant larger than 3 nN/µm. During the micro-tensile test, the tip of soft and hard cantilevers were thinly coated with an epoxy adhesive (Araldite, Vantico, Japan) to attach to the primary cilium.

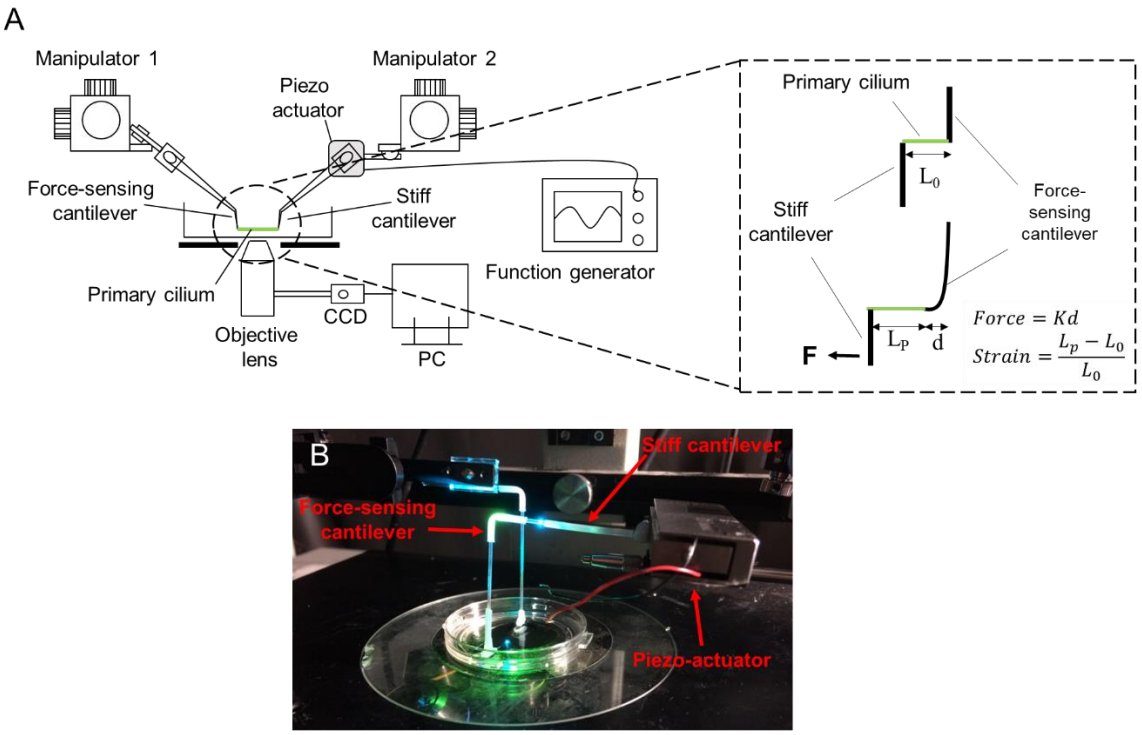

Fig. 2.2: Schematic configuration of micro-tensile test (A) and experimental setup (B).

In order to calculate Young's modulus of the primary cilium, it is simply assumed that primary cilia are homogeneous, isotropic and rounded in cross-section, the Young's modulus $E_{stretching}$ is calculated as Eq. 2.1,

$$E_{stretching} = \frac{4 \times \frac{dF}{d\varepsilon}}{\pi D^2} \qquad (2.1)$$

where F is an applied force, ε strain and D the diameter of primary cilia.

2.2.3.1 Piezo-electric actuator

The PK2FSF1 amplified piezoelectric actuator (Fig. 2.3) consists of a discrete stack in a flexure mount. The flexure increases the travel range through lever amplification and a U-shaped cover provides protection for the discrete PZT stack and wire connections. It offers a maximum displacement of 220 µm ± 15%.

The specification of the actuator is shown in Table 2.1. The voltage-dependent displacement curves of the piezo actuator show a hysteresis curve (Fig. 2.4).

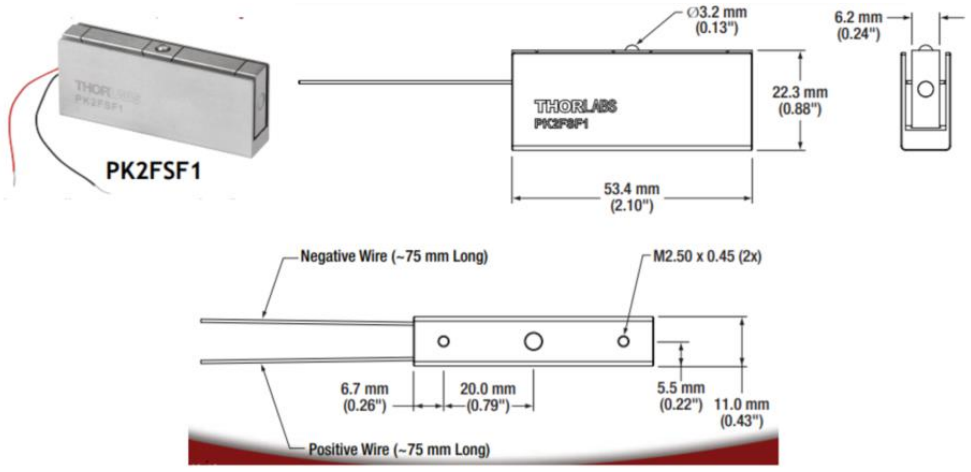

Fig. 2.3: Piezoelectric actuator (SpecSheet of PK2FSF1).

In this study, the piezoelectric actuator was used to produce one single tensile load, so the hysteresis characteristic does not the most concerned parameter. Because of the tiny length of primary cilia (approximately 5 - 10 µm), the required voltage to get 100% strain of primary cilia is much lower than the drive voltage range of this actuator. Moreover, the pulling force in the motion direction is around 5 N, which is enough for measuring the mechanical properties of biomaterial (hundreds pN - tens µN).

Table 2.1: Specification of piezoelectric actuator.

PK2FSF1[a]	
Drive Voltage Range	Maximum: 0 - 75 V
Displacement (Free Stroke) at 75 V	220 µm ± 15%
Maximum Push Force In Motion Direction	100 N (22.5 lbs)
Maximum Pull Force In Motion Direction	5 N (1.1lbs)
Hysteresis	<15% (See Graph on Next Page)
Piezo Stack Used Inside	PK2FSP2
Resonant Frequency	1.0 kHz (No Load)
Impedance at Resonant Frequency	2000 mΩ
Dissipation Factor	<2.0%
Capacitance	9.0 uF ± 15%
Operating Temperature	-25 to 130 °C
Curie Temperature	230 °C
Outer Dimensions	22.3 mm x 11.0 mm x 53.4 mm
Piezo Stack Dimensional Tolerance	± 0.1 mm

a. All specifications are quoted at 25 °C, unless otherwise stated.

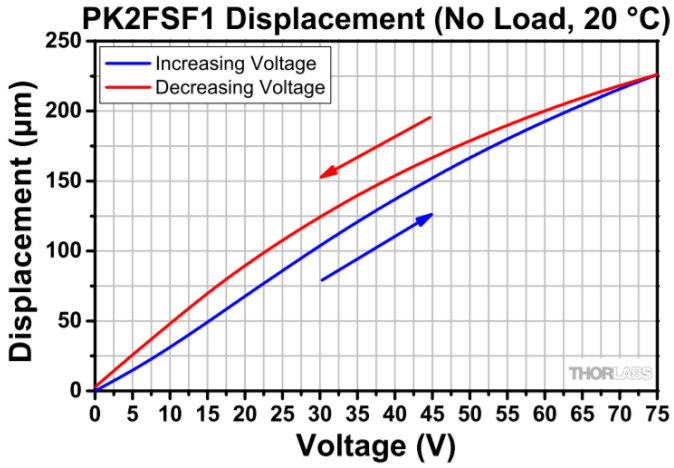

Fig. 2.4: Hysteresis of the actuator's displacement (SpecSheet of PK2FSF1).

Fig. 2.5: Capillary puller and glass tube.

2.2.3.1.1 Cantilever fabrication

A capillary puller (PC - 10, Narishige, Japan) and a glass tube (G - 1, Narishige, Japan) were used (Fig. 2.5). It is said that it is necessary to make a glass needle with a spring constant of several nN/µm in order to measure the load on the primary cilia.

The heater level of the capillary puller was set to 68^0C, four weights were set to one pull, and obstacles were installed so that the weight would stop when it falls down about 1 cm from the ground. The glass rod installed in the device is stretched to the point where the weight comes into contact with the obstacle, the heater is turned off, the glass rod is slightly cooled and the glass rod is re-installed by inserting the pulling area of the glass rod in the first step to the heating section. The obstacle was removed, and the glass rod was cut completely by the weight load. The tip of the glass needle was adjusted with Microforge (MF - 900, Narishige, Japan) to adjust the diameter and the length of the glass needle as needed.

2.2.3.1.2 Stiffness measurement method

The spring constant of the generated glass needle in the previous section was measured. Figure 2.6 (A) shows a schematic diagram of the device used for measuring the glass needle. The spring constant of the glass needle was determined from the equilibrium of the force between the AFM cantilever and the tip of the glass needle using a device in which AFM cantilever (OMCL - TR400PSA, Olympus, Japan) was attached to PDMS of silicone resin. Figure 2.6 (B) shows the generated device process.

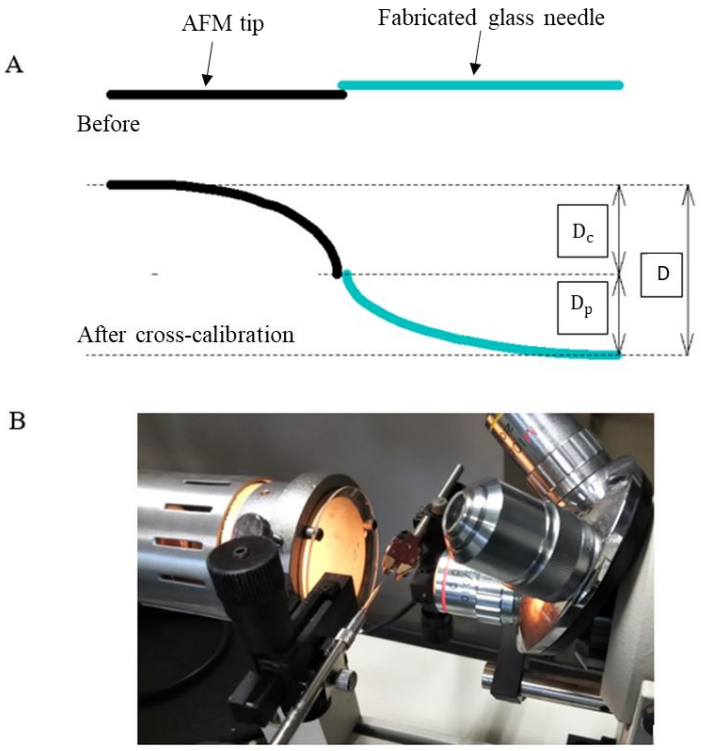

Fig. 2.6: MF - 900 Microforce machine. (A): The schematic of cross-calibration technique. (B): The cantilever making process.

Figure 2.7 (A) shows the state diagram near the tip when measuring the spring constant, and Figure 2.7 (B) shows the device actually used. The spring constant K_c of the glass needle can be calculated from Eq. 2.2.

$$K_p = \frac{D_c}{D_p} K_c \tag{2.2}$$

where, D_p is the displacement of the glass needle, D_c the displacement of the AFM cantilever, and K_c the spring constant of the AFM cantilever.

When observing the deformation of the glass needle tip under a microscope, the deformation of the entire glass needle cannot be observed, so the glass needle displacement D_p is calculated by subtracting the AFM cantilever displacement D_c from the glass needle movement amount D, Equation (2.2) is transformed as in Eq. 2.3,

$$K_p = \frac{D_c}{D - D_c} K_c \tag{2.3}$$

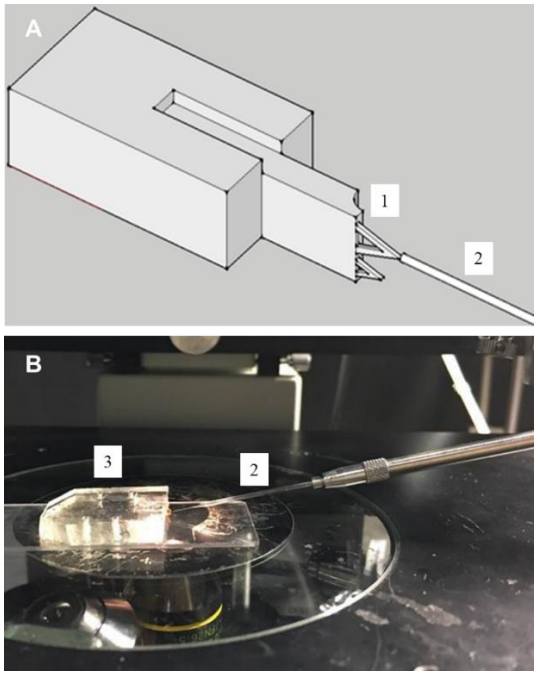

Fig. 2.7: Schematic diagram of spring constant measurement of glass needle. (A): Device schematic diagram. (B): Photograph of the real setup. (1): AFM cantilever, (2): Glass needle, (3): PDMS holder of AFM cantilever.

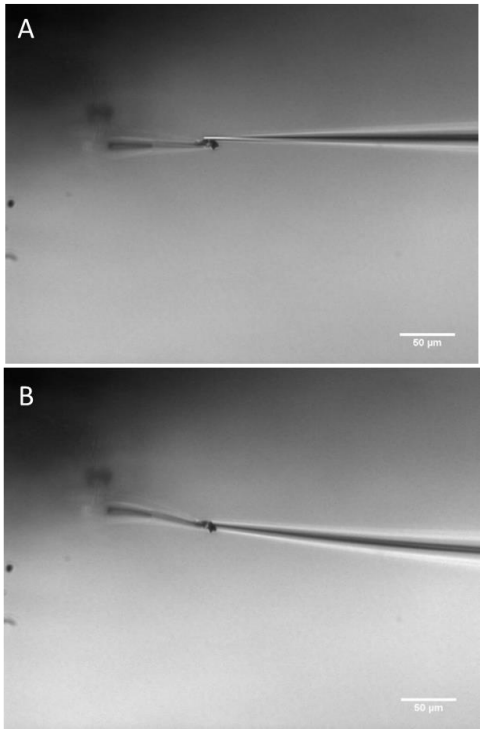

Fig. 2.8: Measuring the spring constant of the glass needle. (A): Before cross-calibration. (B): Cross-calibration process. The scale bar: 50 µm.

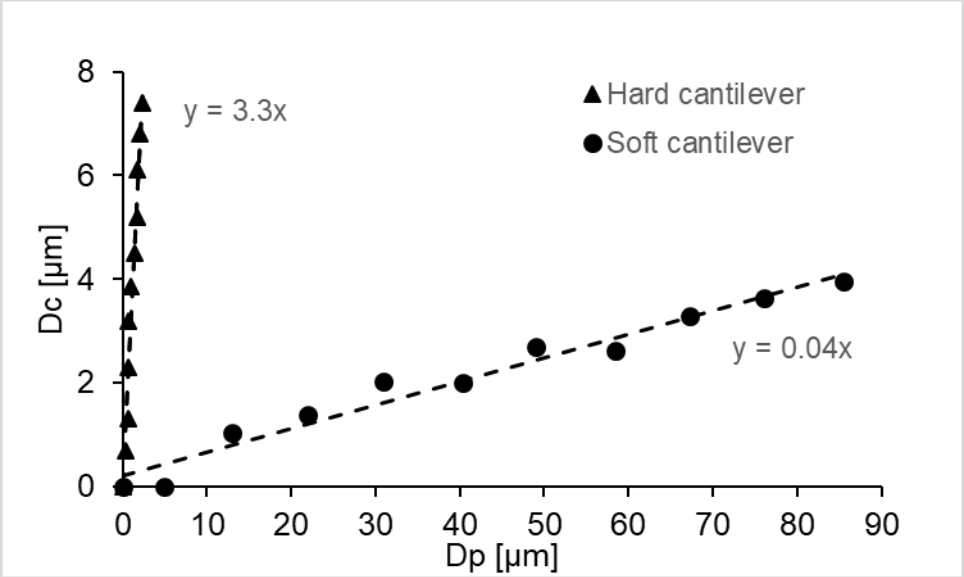

Fig. 2.9: AFM cantilever displacement relative to displacement of soft and hard glass needle.

2.2.3.2 Cantilever stiffness measurement

The spring constant was measured more accurately for the glass needle used in the tensile test. Figure 2.8 shows the displacement D_c of the AFM cantilever measured using the image analysis software ImageJ. For instance, the spring constant of the soft glass needle was calculated by multiplying the estimate of the slope of the approximate straight line by the least-squares method (0.0474) (Fig. 2.9), and the spring constant of the AFM cantilever, 0.02 µN/µm.

2.2.4 Viscoelastic model

Among the viscoelastic models, the Standard Linear Solid (SLS) model successfully describes both creep and stress relaxation, meanwhile, the other types of models such as the Maxwell and Kelvin - Voigt model describe one of those characteristics.

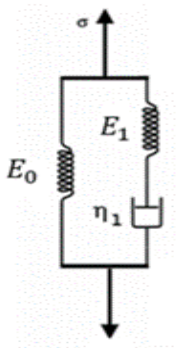

Fig. 2.10: SLS model.

To determine viscoelastic parameters of primary cilia, the SLS model was used to simulate the viscoelasticity of primary cilia (Fig. 2.10). The global fitting of experimental data and model was used

to determine viscoelastic parameters. The transfer function H(s) in the Laplace domain can be written as Eq. 2.4 (Tirella et al., 2014),

$$H(s) = \frac{\bar{\sigma}}{\bar{\varepsilon}} = E_0 + \frac{E_1 \eta_1 s}{E_1 + \eta_1 s} \qquad (2.4)$$

where *s* is the Laplace operator, $\bar{\sigma}$ and $\bar{\varepsilon}$ the stress and strain, respectively, in the Laplace domain, E_0 spring constant in the pure spring arm, E_1 spring constant in the Maxwell arm, η_1 the coefficient of viscosity. Finally, stress $\sigma(t)$ in response to an imposed and constant strain rate ε_p are obtained by inverse Laplace transformation as Eq. 2.5,

$$\sigma(t) = \varepsilon_p \left(\eta_1 - \eta_1 e^{-\frac{E_1 t}{\eta_1}} + E_0 t \right) \qquad (2.5)$$

where *t* is time. In order to derive viscoelastic parameters of primary cilia, the datasets of all stress-time series at different strain rates were globally fitted with the mathematical model using Matlab (R2019b, MathWorks, USA).

2.2.5 Statistical analysis

Results are shown as mean ± SD. Statistical significance was determined using student's t-test. For all tests, $p < 0.05$ was considered significant.

2.3 Results

2.3.1 Visualization of primary cilia.

Figure 2.11 (A) shows a fluorescence image of primary cilia (green), actin filaments (red), and nuclei (blue). The incidence of primary cilia was around 52%. The cells exhibited a relatively rounded shape with dense peripheral bands of actin filaments at the cell peripheries. Figure 2.11 (B) shows primary cilia isolated from cells. Primary cilia were successfully isolated and collected through the ultracentrifuge protocol.

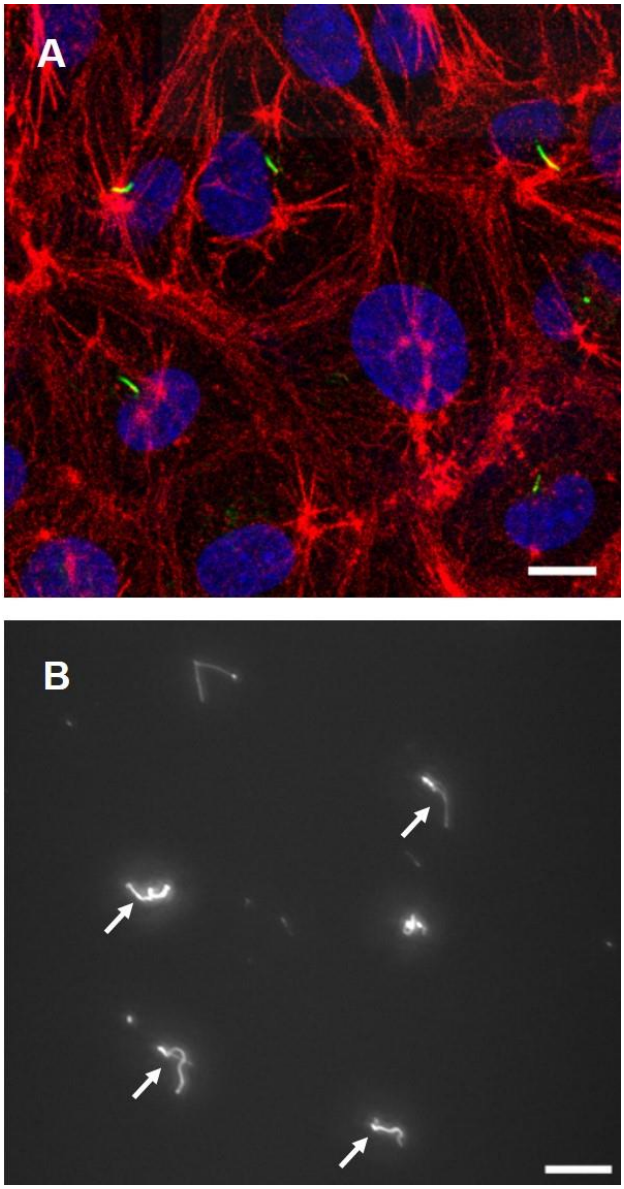

Fig. 2.11: (A): Cell images with primary cilia (green), actin filaments (red), and nuclei (blue). (B): Isolated primary cilia after ultracentrifugation (white arrows). Scale bar: 10 µm.

2.3.2 Young's modulus and viscoelastic properties

As shown in Fig. 2.12, the primary cilium is stretching after applying tensile force and the small displacement of the force-sensing cantilever was indicated.

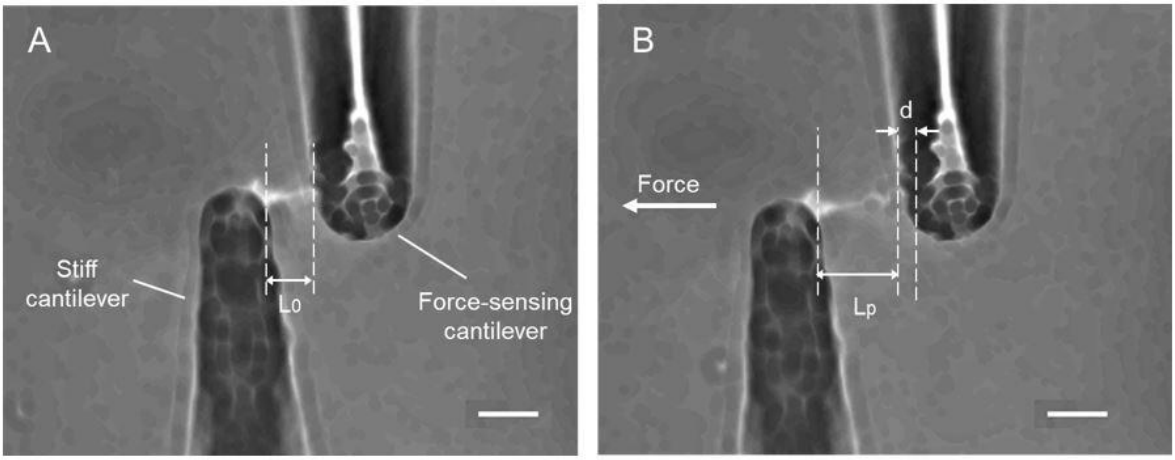

Fig. 2.12: Tensile stretching of primary cilia (A): Before stretching. (B) During stretching, d: the displacement of the force-sensing cantilever, L_0 and L_p: the length of a primary cilium before and after stretching. Scale bar: 10 µm.

The force-strain relationships at the different strain rates of 0.01 s^{-1} - 0.3 s^{-1} are summarized in Figure 2.13 (A). Primary cilia linearly elongated with increasing the applied force within this strain range. The least-squares fitting to the experimental data was applied to determine the global Young's modulus $E_{stretching}$, showing 69.5 ± 12.1 kPa, 94.1 ± 51.4 kPa, 216.7 ± 51.4, and 240.0 ± 90.7 kPa for the strain rates of 0.01, 0.05, 0.1, and 0.3, respectively, as shown in Figure 2.13 (B). The Young's moduli at the strain rates of 0.1 and 0.3 were significantly higher than those at 0.01 and 0.05, indicating the strain rate-dependence of viscoelastic properties of primary cilia.

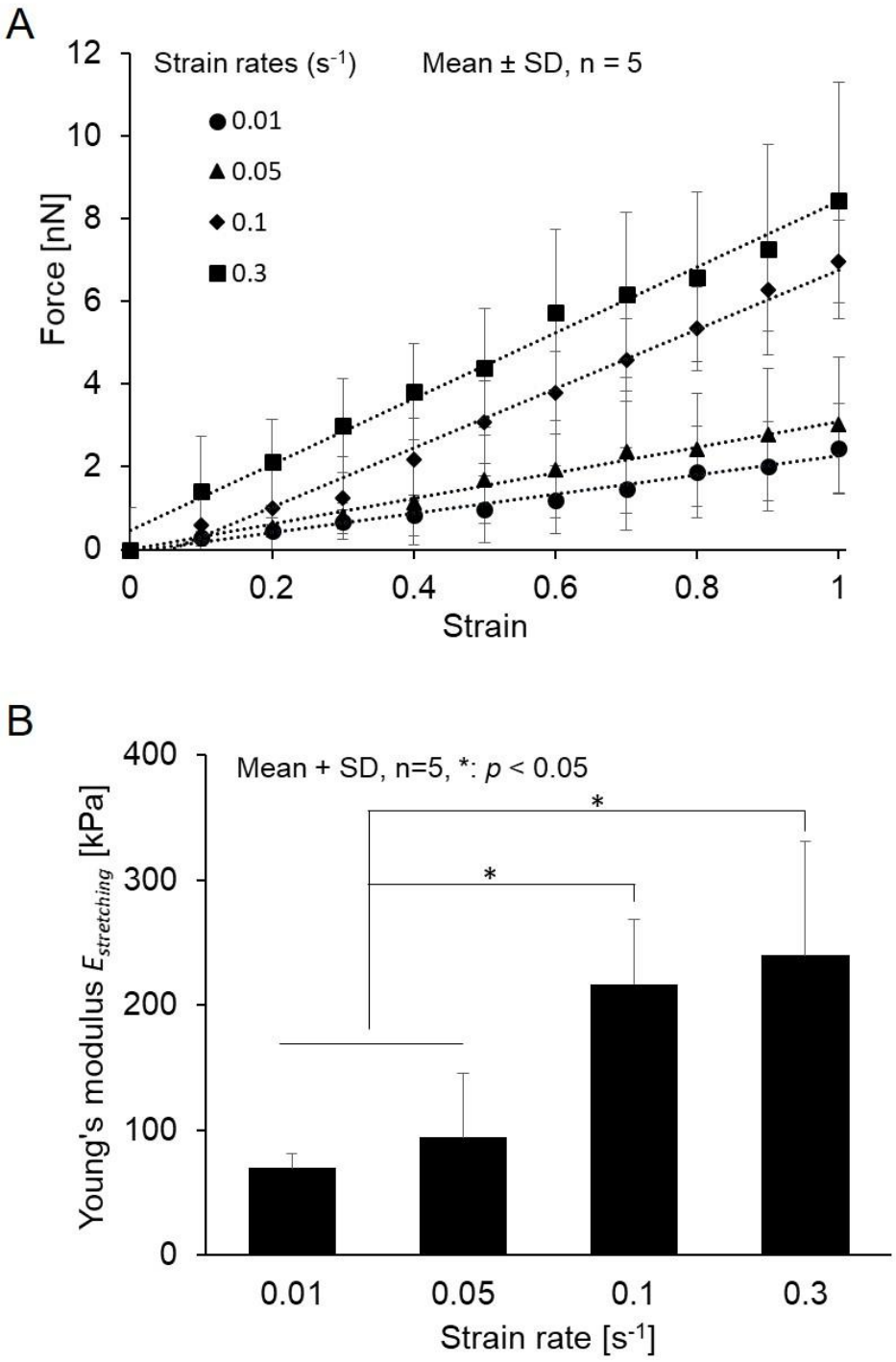

Fig. 2.13: (A): Relationship between force and strain of primary cilia at different strain rates from 0.01 s^{-1} to 0.3 s^{-1} and the least squares fitting. (B): The Young's modulus determined at different strain rates from 0.01 s^{-1} to 0.3 s^{-1}.

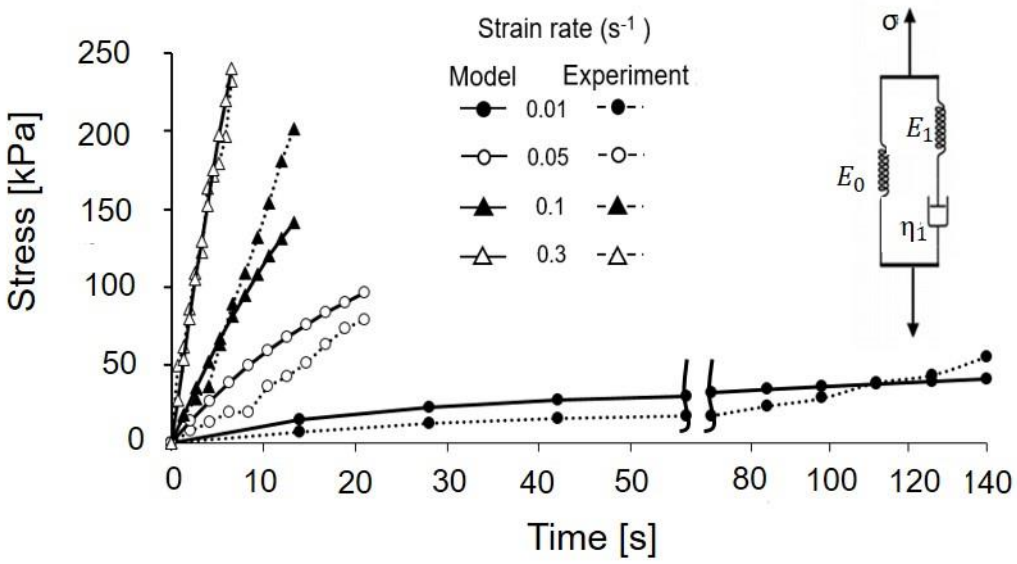

Fig. 2.14: Global fitting the SLS model and experimental datasets.

Figure 2.14 shows the change in stress of isolated primary cilia over time and the global fitting of the Maxwell-type SLS model to the experimental datasets. The instantaneous elastic moduli $E_{inst} = E_0 + E_1$, the equilibrium elastic moduli $E_{inst} = E_0$ and the relaxation time $\tau_1=\eta_1/E_1$ of the SLS model are summarized in Table 2.2 with the coefficient determination R^2=0.86.

Table 2.2: Viscoelastic parameters of primary cilia derived from fitting of experimental data and the Maxwell-type SLS model of primary cilia.

Viscoelastic parameters	Values
$E_{inst} = E_0 + E_1$ [kPa]	143.2 ± 30.0 [kPa]
$E_{eq} = E_0$ [kPa]	11.0 ± 3.0 [kPa]
$\tau_1 = \eta_1/E_1[s]$	19.36 ± 3.7 [s]
R^2	0.86

2.4 Discussion

To date, the flexural rigidity of primary cilia has been extensively studied mainly by application of fluid flow because of many advantages of such experimental approach: quick setup of experimental apparatus, in vivo relevance, etc. However, the flexural rigidity is not a material property of materials but depends on the shape and the size of the cross-section of specimens. Moreover, a mathematical model has to be introduced to determine the flexural rigidity, which could potentially produce the discrepancy between literatures. To our best knowledge, this study is the first report that the Young's modulus of primary cilia could be directly measured. Schwartz et al. (1997) developed the first model of the bending mechanics of kidney epithelial primary cilia, observed bending of primary cilia under various physiological fluid flow rates, and determined the flexural rigidity to be approximately 3.1 x 10^{-23} Nm^2. Later, other groups determined the values to be in the range of 1 - 5 x 10^{-23} Nm^2 (Young et al., 2012) or even significantly higher values of 3.1 x 10^{-22} Nm^2 (Downs et al., 2014). The global Young's modulus $E_{stretching}$ statically obtained at a strain rate of 0.01 s^{-1}, as shown in Fig. 2.13 (B), is 69.5 ± 12.1 kPa. To directly compare our study with the previous studies, the flexural rigidity was converted into Young's modulus under the assumption that primary cilia have a uniform rounded-shaped cross section with a diameter of 205 nm (obtained in this study) by using following equation: $E = EI/I = EI/(\pi a^4/4)$, where E is the Young's modulus, EI the flexural rigidity and a the radius. The comparison is summarized in Table 2.3. Except for Downs's group, the Young's modulus $E_{stretching}$ in this study shows the similar value to the others, although there are some discrepancies between the results and our value is the smallest. As already mentioned in the Introduction section, the previous studies used different mathematical models to determine flexural rigidity. Moreover, as the diameter of 205 nm, which is experimentally determined in this study, is used for conversion, it is quite possible that the actual diameter of primary cilia used in the previous studies would be different from 205 nm. The discrepancies may inherently attributable to these facts. The unique aspect of this study compared to the previous studies is that the Young's modulus of primary cilia is directly measured, in other words, which is not affected by the use of mathematical models and does not need any conversion.

Primary cilia are microtubule-based organelles and the core axoneme is comprised of nine doublet microtubules. Young's modulus (Tuszyński et al., 2005) and flexural rigidity (Gittes et al., 1993; Kikumoto et al., 2006) of microtubules are reported in Table 2.3. The Young's modulus is in the order of GPa, however, Young's modulus of primary cilia obtained in this study is in the order of tens to hundreds kPa.

Table 2.3: Summary of the Young's modulus of primary cilia.

	Author, year (ref)	Flexural rigidity [Nm^2]	Young's modulus [kPa]	Experimental method
Primary cilia	Schwartz et al., 1997	3.1×10^{-23}	356.9 (converted)	Fluid flow
	Young et al., 2003	$1\text{-}5 \times 10^{-23}$	115.1 – 575.7 (converted)	Fluid flow
	Downs et al., 2014	31×10^{-23}	3569 (converted)	Fluid flow
	Battle et al., 2014	2.5×10^{-23}	287.9 (converted)	Optical trap
	Resnick, 2016	1.7×10^{-23}	199.2 (converted)	Optical trap
	Present study	-	143.2	Tensile test
Microtubules	Tuszyński et al., 2005	-	1.32×10^6	Tensile test
	Gittes et al., 1993	2.2×10^{-23}	-	Thermal bending
	Kikumoto et al., 2006	7×10^{-23}	-	Optical trap

This discrepancy in Young's modulus between microtubule-based primary cilia and microtubules can possibly be explained based on the structure. In non-motile cilia such as primary cilia, it is not clear whether there are structural components like the dynein arms to connect the double microtubules together. During the tensile process, the dynein arms pull double microtubules away from each other, and may mainly contribute the mechanical properties of motile cilia. The results here may suggest the alternative components same as dynein arms, which maintain the axoneme's stability and elastic properties for reversible bending of primary cilia. Further investigations could be focused to clarify these components in the structure of primary cilia.

There is no study so far about viscoelasticity of primary cilia. Our global fitting between the experimental data and mathematical model (Fig 2.14), for the first time, provides the viscoelastic parameters of primary cilia. The instantaneous elastic modulus is in the same order as converted Young's modulus in Table 2.2. Regarding the relaxation time, it has the high diversity of values from previous studies. Young et al. (2012) reported the relaxation of the cilium after turning off the application of flow was around 5 s, meanwhile the value of Downs et al. (2014) was around 2 min. This discrepancy may arise from differences in fluid flow conditions. It is unlikely to compare the relaxation time of isolated cilia and cell-attached cilia under fluid flow because of taking into account the rotational relaxation of basal body anchorage. Compared to the relaxation of the microtubule, which was reported to be around 600 s (Lin et al., 2007), the relaxation time of primary cilia is much smaller. It could be explained by the fact that besides the nine doublet microtubules, there are other components inside the cilia structure to couple microtubules together and contribute to the mechanical properties of primary cilia.

In our laboratory, there was one group measured the local Young's modulus of primary cilia using AFM. Despite being conducted in different methods, the global Young's modulus $E_{stretching}$ measured in this study is in agreement with local Young's modulus E_{AFM}. Figure 2.15 shows the distribution of local Young's modulus E_{AFM} along the length of tested cilia. The global Young's modulus $E_{stretching}$ in the static condition (0.01 s^{-1}) is in the same order as the local E_{AFM} values. This agreement between global $E_{stretching}$ and local E_{AFM} showed the confidence of obtained elastic properties of primary cilia.

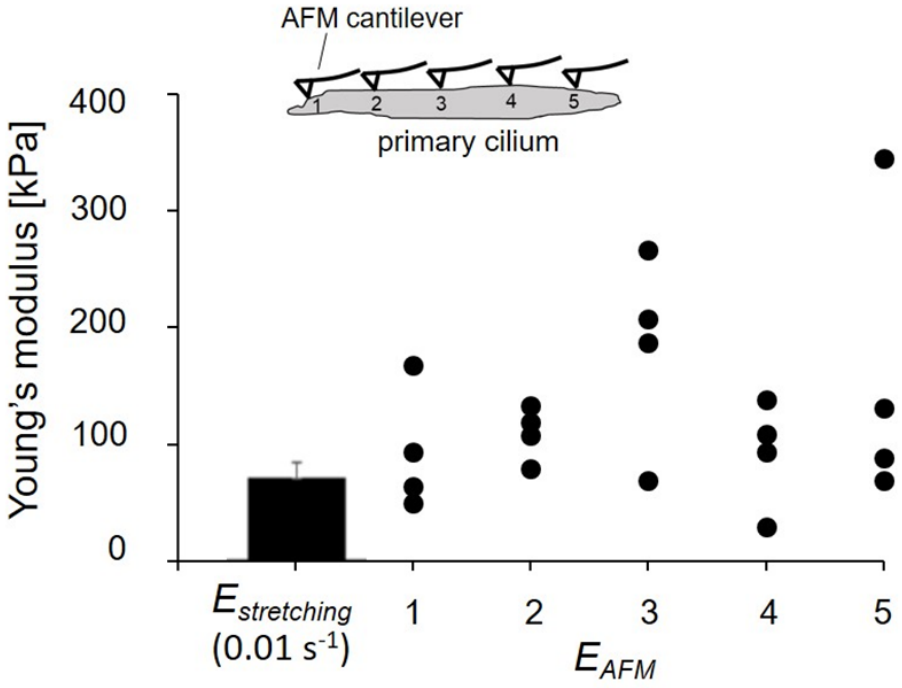

Fig. 2.15: Comparison of global $E_{stretching}$ and local E_{AFM}.

In Fig. 2.15, the SD of Young's modulus $E_{stretching}$ is small, which is partly because $E_{stretching}$ is an averaged modulus across not only the cross-section but also the length. In contrast, the figure clearly indicates the wide range of distribution in local Young's modulus E_{AFM} along the length of primary cilia. The primary cilia structure is non-uniformly along their length and the number of doublet microtubules decreases from the base to the ciliary tip (Gluenz et al., 2010). Different positions of indentation may reach out to different structures of primary cilia, possibly with or without touching doublet microtubules, which could lead to the wide range of E_{AFM} distribution. The measurement of E_{AFM} opens up a new topic for further studies of primary cilia mechanics. For instance, the local distribution of Young's modulus may contribute to building up a more precise mathematical model to predict the bending behaviour of primary cilia. The combination of the micro-tensile test and the AFM tests allows us to obtain a clearer insight into the mechanical properties of primary cilia.

An interesting measured local Young's modulus of primary cilia was obtained by that group is the distribution of E_{AFM} in the radial direction the primary cilia (Fig. 2.16).

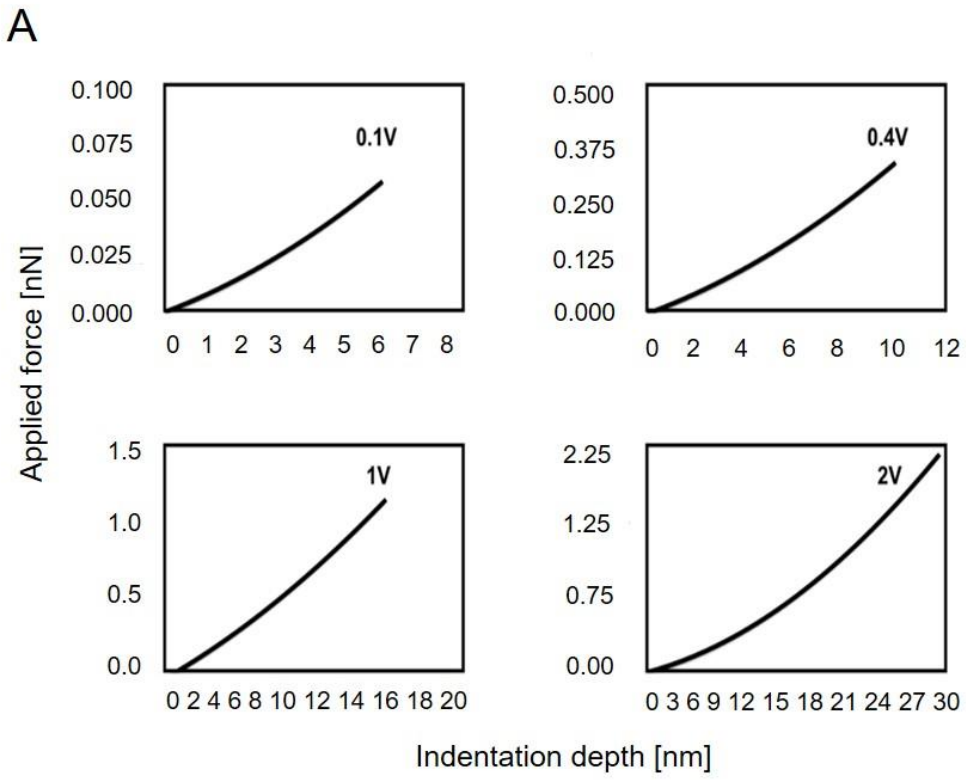

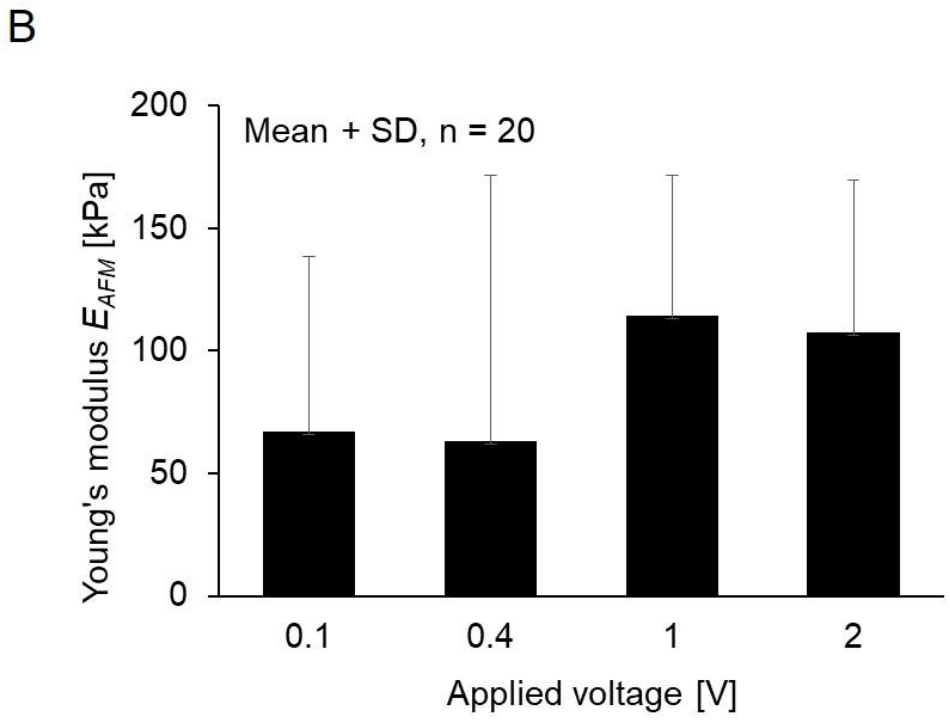

Fig. 2.16: (A): Relationship of applied voltage and indentation depth. (B): The Young's modulus of primary cilia at different applied voltage.

As shown in Fig. 2.16, the local Young's modulus E_{AFM} became higher when the indentation depth increased from 0.4 V to 1 V. It is known from TEM observation that the doublet microtubules distribute evenly surrounding the centerline of ciliary body with a distance of 0.07 μm to the center and double microtubules exist around several 10 nm deep from the cilia surface (Chen et al., 2011). The increase in Young's modulus may be reflected by the presence of the doublet microtubules where the AFM tip more directly comes into contact with the structure. Because of the high Young's modulus of microtubules, it is assumed that the local Young's modulus E_{AFM} was higher when the indenter could reach out the double microtubules.

This study has certain limitations. In the global fitting method, despite the good agreement of Young's modulus of primary cilia with previous converted results (Table 2.3), the R^2 value of 0.86 and the not-good fitting between strain rates groups can be seen. The fast strain rate groups have better fitting than the lower groups. It is possible that the fitting results could be more precisely identified depending on the number of strain rates used, and the range of strain rates employed. The higher number of strain rates and the smaller gap between strain rates may establish better parameters of Young's modulus and relaxation time.

As aforementioned, numerous efforts have so far been made to characterize the bending behavior of primary cilia, however, they seem to lack the validation of material properties such as Young's modulus. It would be beneficial to directly measure Young's modulus from the viewpoint of cell mechanics. A further approach would be needed to shed light on how the global and local Young's moduli could attribute to their structure. For instance, nine doublet microtubules are connected by dynein arms in motile cilia while it is unclear if there are alternative structural components, integrating the nine microtubule in primary cilia such as non-motile cilia. Such an experimental approach based on the microstructure would lead to a better understanding of primary cilia mechanics as well as mechanotransduction.

2.5 Conclusions

In this study, the tensile Young's modulus of primary cilia was for the first time measured with an in-house micro-tensile tester. The results showed the dependence of

the elastic modulus of primary cilia ranging from 69.5 - 240.0 kPa for the strain rates of 0.01, 0.05, 0.1, and 0.3 s^{-1}, which suggested the viscoelastic properties of primary cilia. The viscoelastic mathematical model of primary cilia was built up to perform global fitting with experimental results and then deduce the viscoelastic parameters. The global Young's modulus by the micro-tensile test was also in agreement with the local Young's modulus by AFM test. All of the above results may help to have a better picture of mechanotransduction of primary cilia in further experimental studies and may contribute to build up the appropriate cellular models in numerical studies.

Chapter 3

Remodeling of cellular primary cilia in response to cyclic stretching

3.1 Introduction

The primary cilium is a solid, immotile cilium that presents in almost all eukaryotic cells. It functions by initiating and directing intracellular signaling in response to external mechanical signals. Considering the ability of remodeling in living systems, the endothelial primary cilium is believed to change its structures in the presence of mechanical forces.

Research to date suggests that a variety of ciliary structures occur in the mechanotransduction processes. Espinha et al. (2014) explored that kidney cells exposed to fluid shear had more microtubules at the ciliary base than cells incubated in the control condition, or the increase of microtubule acetylation, which increases binding of microtubule-associated and consequently microtubule stiffness (Geiger et al., 2009). Characteristics of primary cilia, such as axoneme length, can be manipulated to recover or adjust mechano-sensitivity (Marshall et al., 2001). Iomini et al. (2004) also reported that prolonged exposure of high fluid shear stress would induce primary cilia disassembly. Moreover, chondrocytes under compression in 3D agarose model and tendon cells in the presence of loading were also tested to confirm the remodeling of cilia through their length (McGlashan et al., 2010; Donnelly et al., 2010).

The remodeling of primary cilia responses to mechanical signals which directly interact to primary cilia such as fluid flow, or surrounding 3D extracellular environment loading of primary cilia, are well-known investigated (McGlashan et al., 2010; Gardner et al., 2011; Donnelly et al., 2010). However, how primary cilia response to the mechanical signal with indirect interact to the cilia, such as substrate stretching, is still unclear.

The primary cilium is characterized by a 9 + 0 microtubule symmetry and composed of two main parts: the basal body, and the axoneme. The base of primary cilia is microtubule and actin organized centre which connects to the actin cytoskeleton network. The focal adhesion is well-known connected to actin network and changes of substrate loading are transmitted to actin network remodeling through focal adhesions. It is hypothesized that the substrate loading may affect the primary cilia structure through the intermediator of the actin network. Some new evidences indicated the negative regulation

between actin dynamics and cilia. The actin depolymerisation promotes ciliary assembly and elongation, while polymerization or branching of actin is associated with cilia disassembly or inhibited ciliogenesis (Mirvis et al., 2018).

In this study, the responses of endothelial cell's primary cilia in cyclic substrate stretching conditions were firstly investigated. In order to evaluate the effect of actin network changes on the primary cilia remodeling during the substrate stretching, the blebbistatin treatment which inhibits actin myosin was also utilized for cells.

3.2 Materials and methods

3.2.1 Cell preparation

Bovine Aortic Endothelial Cells (BAOEC) cells were cultured on the stretch chamber (STREX, Japan) in Dulbecco's Modified Eagle Medium (DMEM) supplemented with 10% fetal bovine serum, 1% penicillin and 1% streptomycin. Cells were cultured under a humidified atmosphere of 5% CO_2 at 37°C until confluent condition before doing experiments.

3.2.2 Immunofluorescence staining

Immunolabelling of acetylated α-tubulin was performed to visualize primary cilia on cells under fluorescence microscope. After rinsing with PBS, cells were fixed in 4% paraformaldehyde for 10 min at room temperature, treated with 0.2% (vol/vol) Triton X - 100 (Sigma-Aldrich, USA) in PBS for 5 min, and blocked with 1% BSA blocking solution. Cells were stained with the first antibody (acetylated α-tubulin, Santa Cruz Biotechnology, USA) diluted with 1% BSA (1:1000, Sigma-Aldrich, USA) overnight at 4ºC and then in secondary antibody (Human ads-Alexa Fluor® 488, Southern Biotech, USA) diluted with 1% BSA (1:1000) at 4ºC for 1 h. Subsequently, the actin filaments and nuclei were stained with 400X Rhodamine Phalloidins (ThermoFisher, USA) diluted in PBS (1:400) at room temparature for 1 h and Hoechst33342 (ThermoFisher, USA) at room temperature for 20 min. Washing in PBS three times between each step.

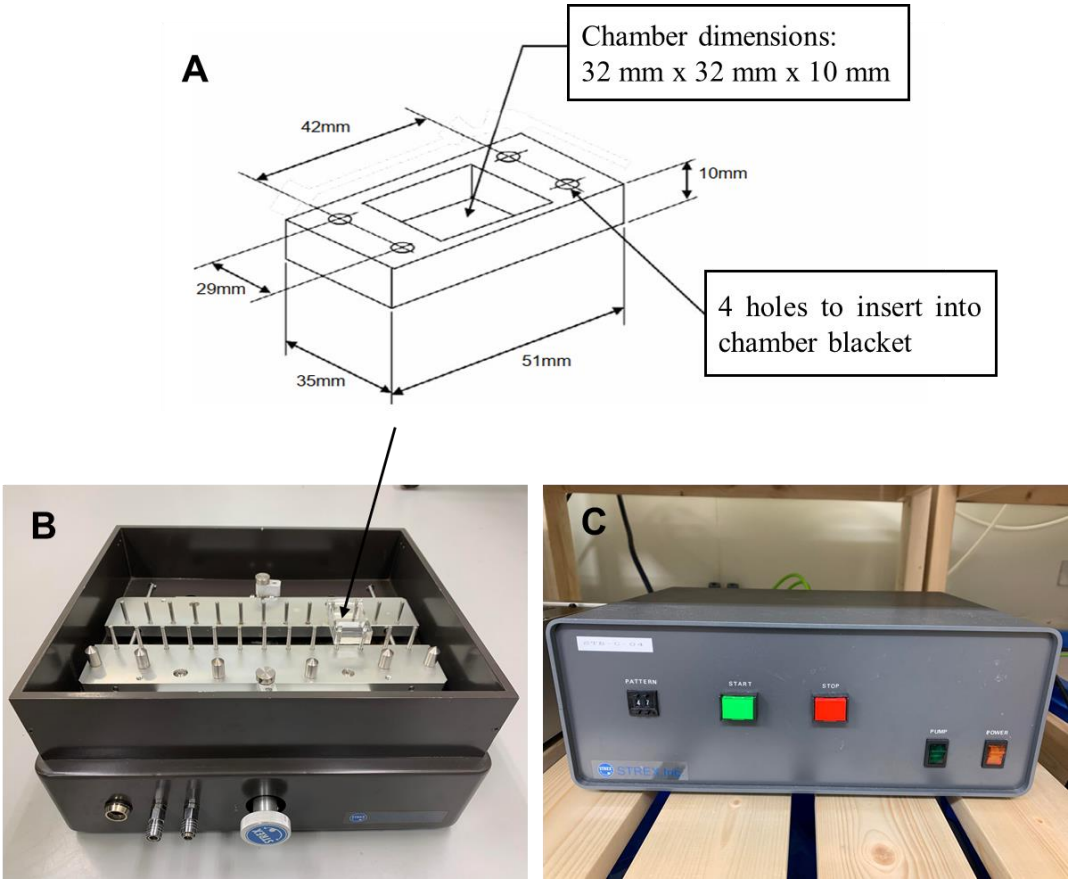

Fig. 3.1: (A): Stretching chamber, (B): Stretching unit, (C): Control unit.

3.2.3 Cyclic stretching experiment

Chambers were autoclaved at 120^0C for 20 min, coated with fibronectin and incubated at 37^0C for at least 4 h. The cyclic loading was applied at 1 Hz at different strain levels (5%, 10%, 20%) for different amount of time (6 h, 12 h, 24 h) using STB - C - 04 (STREX, Japan). Cells were seeded in the stretching chamber (Fig. 3.1 A) until confluence, then the stretching chamber was placed on the stretching unit (Fig. 3.1 B), which is connected and controlled by control unit (Fig. 3.1 C).

3.2.4 Blebbistatin treatment

Confluent cells were incubated in 50 µM active blebbistatin (Calbiochem, Germany) at 37^0C for 30 min and then mounted with blebbistatin-containing medium for the stretching experiments.

3.2.5 Analysis of cilia incidence, cilia length, cell shape index and orientation

For cilia length measurement, a confocal microscope with z-slices capturing was used to obtain fluorescence images. The cilia length is measured from 2 - D images. To quantify the incidence of primary cilia within each condition, random areas selected, each containing 15 - 20 cells were examined using a confocal microscope.

The Cell Shape Index (*CSI*) is a dimensionless quantitative measure of cell morphology ($0 < CSI < 1$), and is calculated as Eq. 3.1,

$$CSI = \frac{4\pi A}{P^2} \tag{3.1}$$

where P is the cell perimeter, A the cell area. These parameters can be obtained by using image processing software ImageJ. The shape of the object will become a line as the *CSI* value approaches 0, while the shape will become a circle as the CSI value approaches 1.

The cell orientation is determined by ImageJ. Cells can be approximated to ellipse by ImageJ, and then the orientation angle of cells is defined by the angle between the direction of the major axis of the approximated ellipse and the horizontal direction.

3.2.6 Statistical analysis

Results are shown as mean ± SD. Statistical significance was determined using student's t-test. For all tests, $p < 0.05$ was considered significant difference.

3.3 Results

Cell morphology in substrate stretching condition was examined. The visualization of cell morphology in control condition and different strain levels was observed in Fig. 3.2. The results showed the cell shape index decreases with the increase of strain levels, which meant cells are more aligned in the response of stretching and a significant change was seen at 20% strain (Fig. 3.3). The alignment angles of cells are in the direction perpendicular to stretching direction (Fig 3.4). As can be seen in Fig. 3.4, in the control condition, cells are randomly oriented in all directions, but over time of stretching at all strain levels (5%, 10% and 20%), cells are oriented perpendicular to stretching direction.

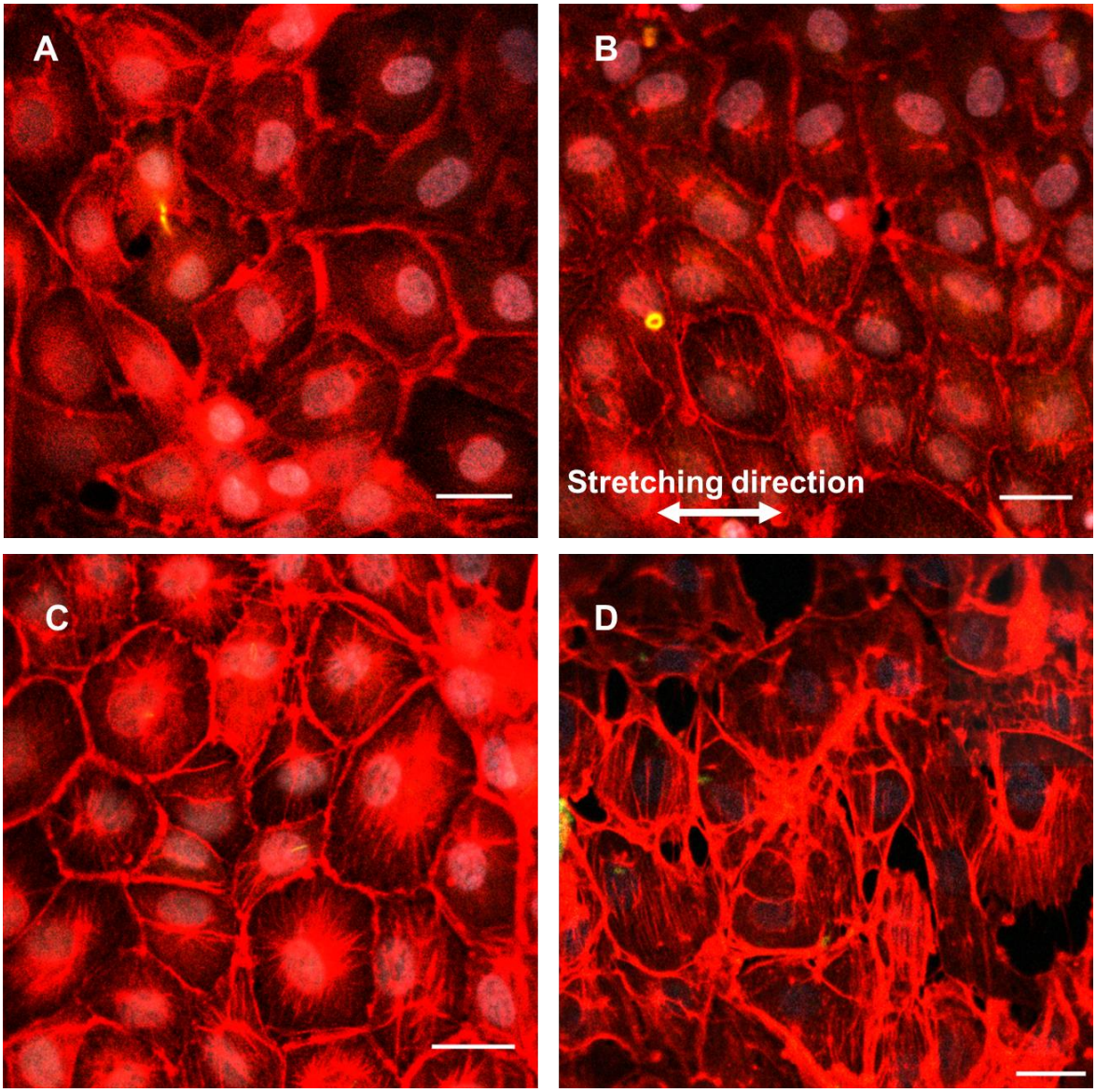

Fig. 3.2: Cell morphology under stretching condition. (A): Control condition. (B - D): 5%, 10% and 20 % strain, respectively. Blue: nuclei, Red: actin. Scale bar: 20 µm.

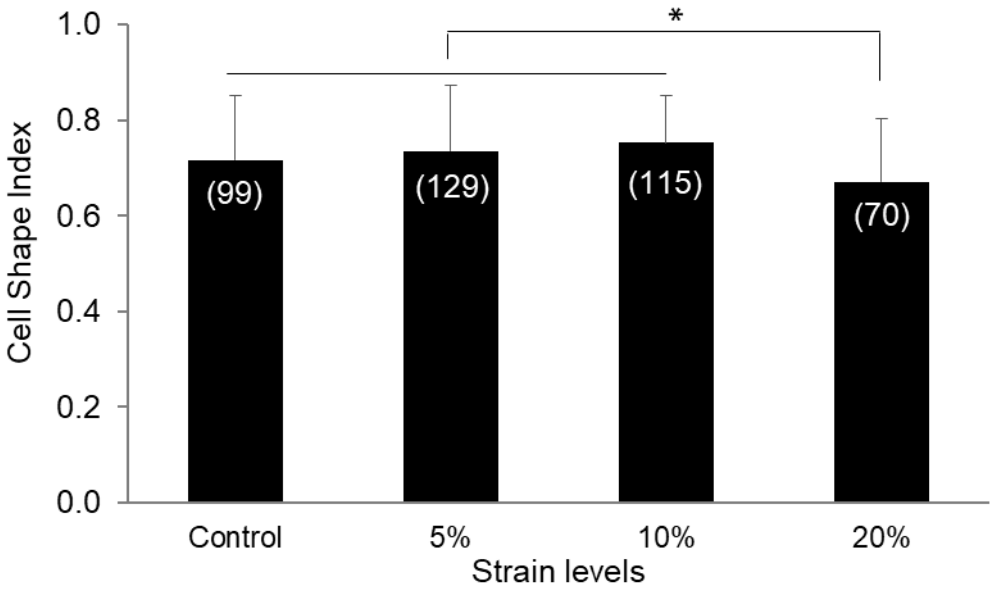

Fig. 3.3: Cell shape index at stretching conditions.

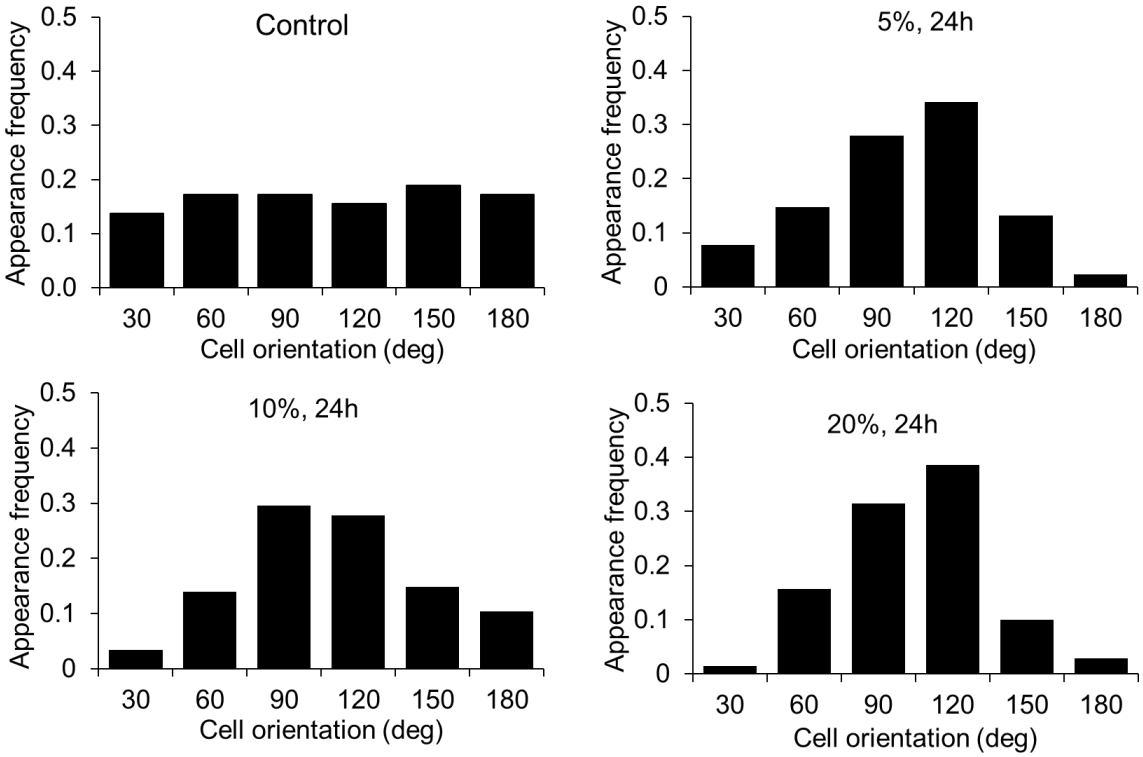

Fig. 3.4: Cell orientation in response to stretching experiments.

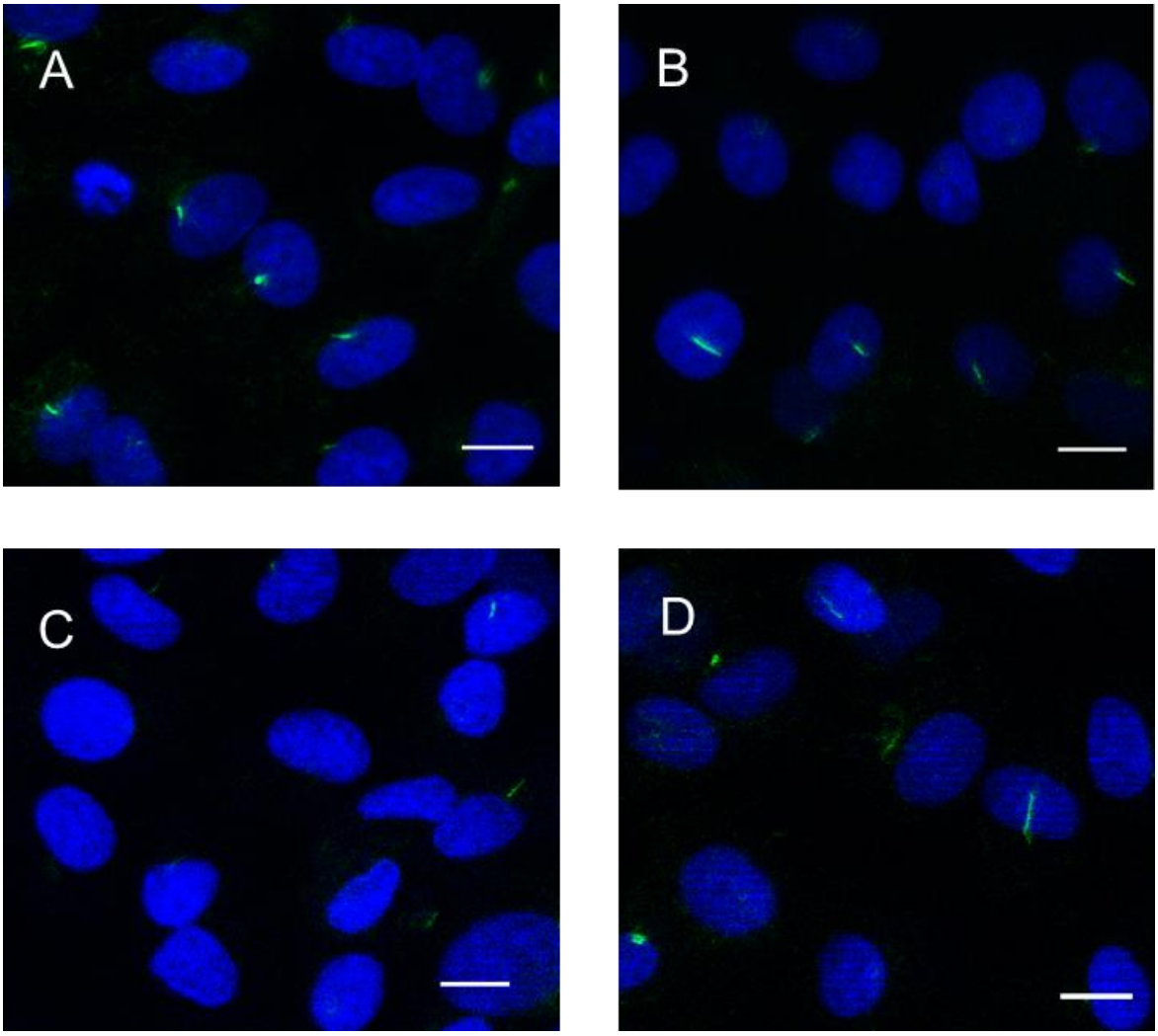

Fig. 3.5: Fluorescence images. (A): Control condition. (B): 5% strain. (C): 10% strain. (D) 20% strain. Blue: nuclei, Green: primary cilia. Scale bar: 10 µm.

After confirming the cell morphology changes, the remodeling of primary cilia in response to the cyclic substrate stretch is investigated. Figure 3.5 shows the representative images of primary cilia under stretching conditions. Generally, primary cilia are longer, and fewer in the presence of substrate stretching.

In Fig. 3.6, endothelial cells subjected to dynamic cyclic loading for 6, 12 and 24 h showed an increase in cilia length. The increasing tendency in the ciliary length over time was demonstrated at all strain levels, from around 2.53 µm in control condition. After 6h of stretching, the ciliary length does not change much, but the bigger increase of ciliary length was seen as the longer stretching time is. Despite no significant increases in the length of

cilia in the same amount of stretching time between strain groups, the higher magnitude of stretching produces slightly longer cilia, except for the case of 5% strain, 24 h.

Following the application of substrate cyclic loading over time at different experimental conditions, cilia incidence showed the decreasing tendency from around 89% in the control condition to the lower percentages as the strain level increases. In each strain level group, the number of ciliated cells falls down with longer time of exposed stretching (Fig. 3.7). Regarding the same of stretching time, the higher strain level reveals a lower number of ciliated cells.

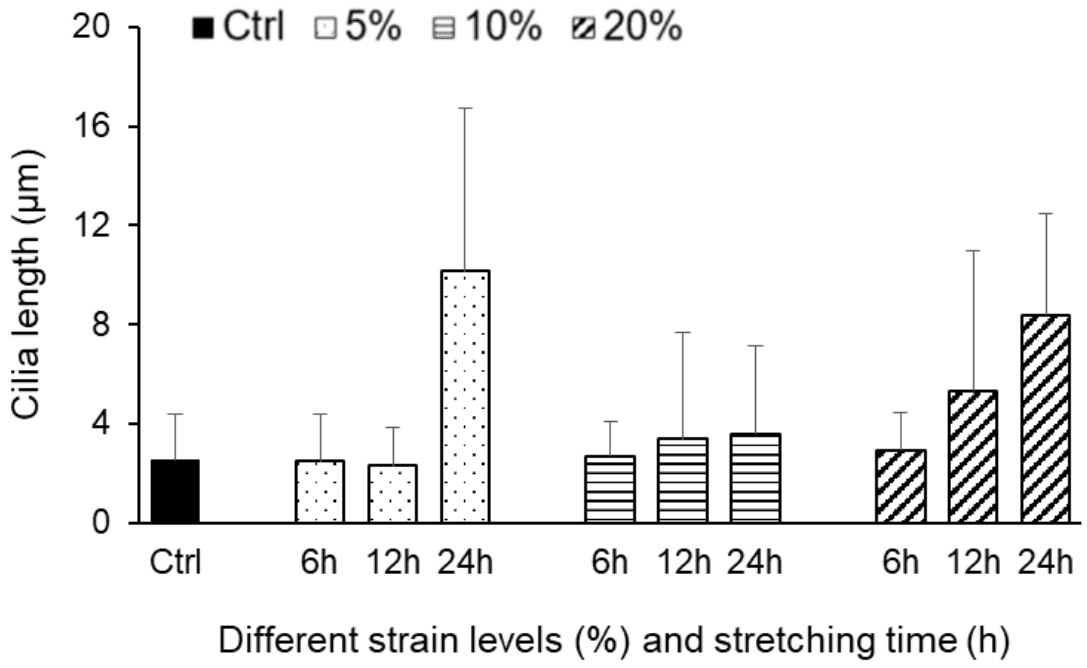

Fig. 3.6: Primary cilia length over time of strain levels.

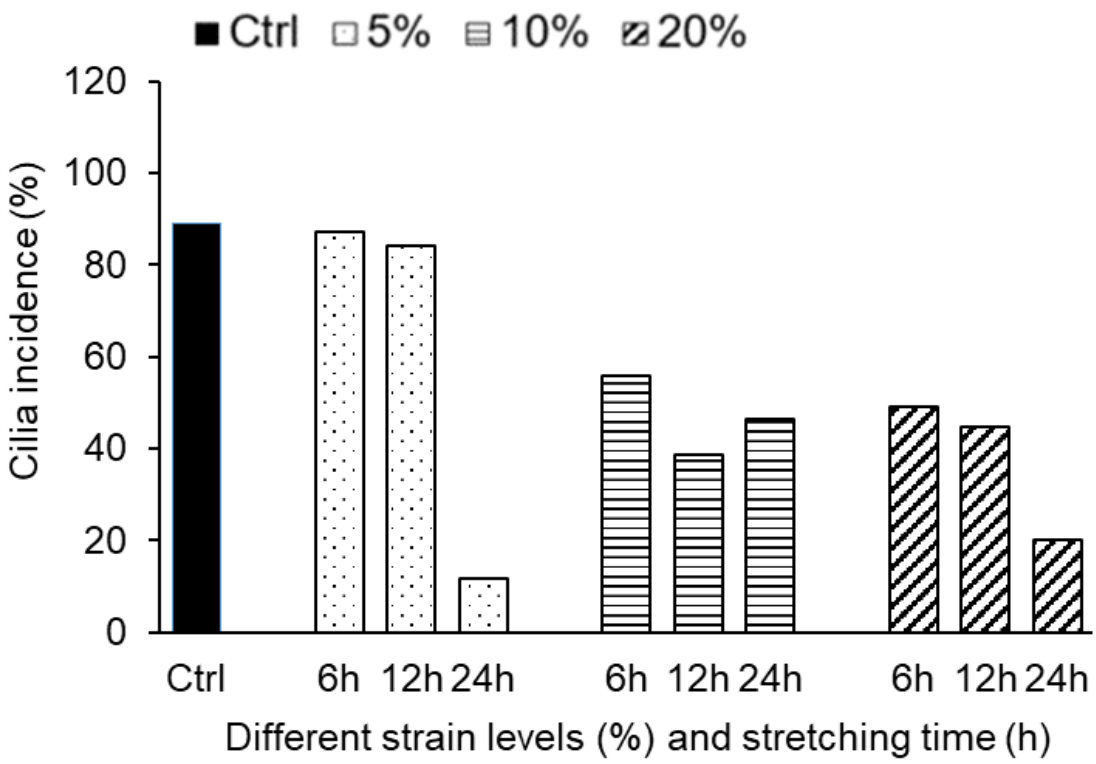

Fig. 3.7: Primary cilia incidence over time of stretching levels.

In the control group, the primary cilia oriented quite randomly, but over the time of cyclic loading, the primary cilia are slightly aligned along the direction of stretching, which is the horizontal direction. In all strain groups, the primary cilia gradually rotated in the horizontal direction after 12 h (Fig. 3.8).

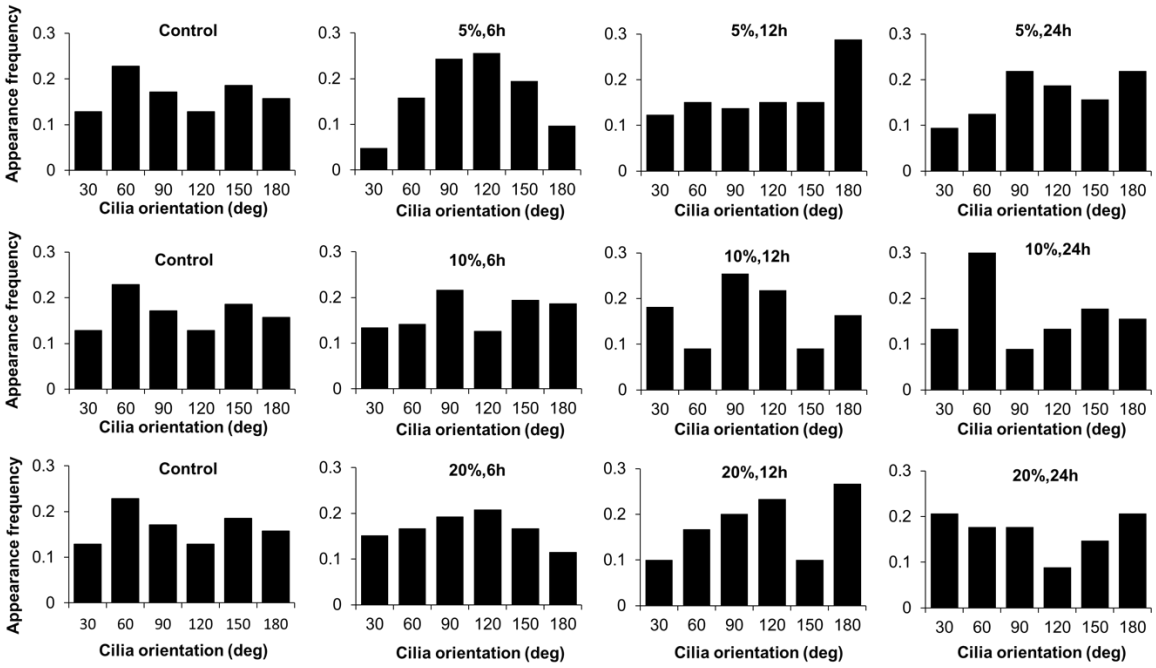

Fig. 3.8: Orientation of primary cilia over time during substrate conditions.

To assess whether the dynamic actin network affects the cilia assembly during cyclic loading, the actin-myosin dynamic was tested by using blebbistatin. Regarding the actin filaments, they are disrupted in blebbistatin condition (Fig. 3.9). At the same condition of stretching (10% strain for 24 h), cells treated with blebbistatin show the shorter cilia (similar as the control condition), compared to no actin-myosin inhibition. The length of primary cilia in blebbistatin condition (2.9 µm) decreases compared to the free blebbistatin condition (6.6 µm) (Fig. 3.10 D). Regarding to cilia incidence, the number of ciliated cells in the blebbistatin condition is slightly higher than the free blebbistatin condition, but there is no significant difference (Fig 3.10 E).

In general, when the actin network was inhibited with blebbistatin, the cilia does not be affected by substrate stretching, and their characteristics (length, incidence) are similar to the control condition.

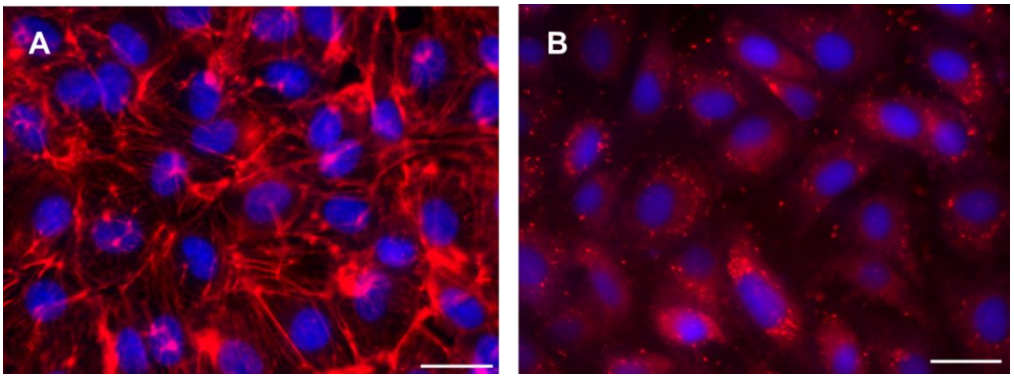

Fig. 3.9: The actin filaments state (A): Control condition. (B): Blebbistatin condition. Blue: nuclei, Red: actin. Scale bar: 20 µm.

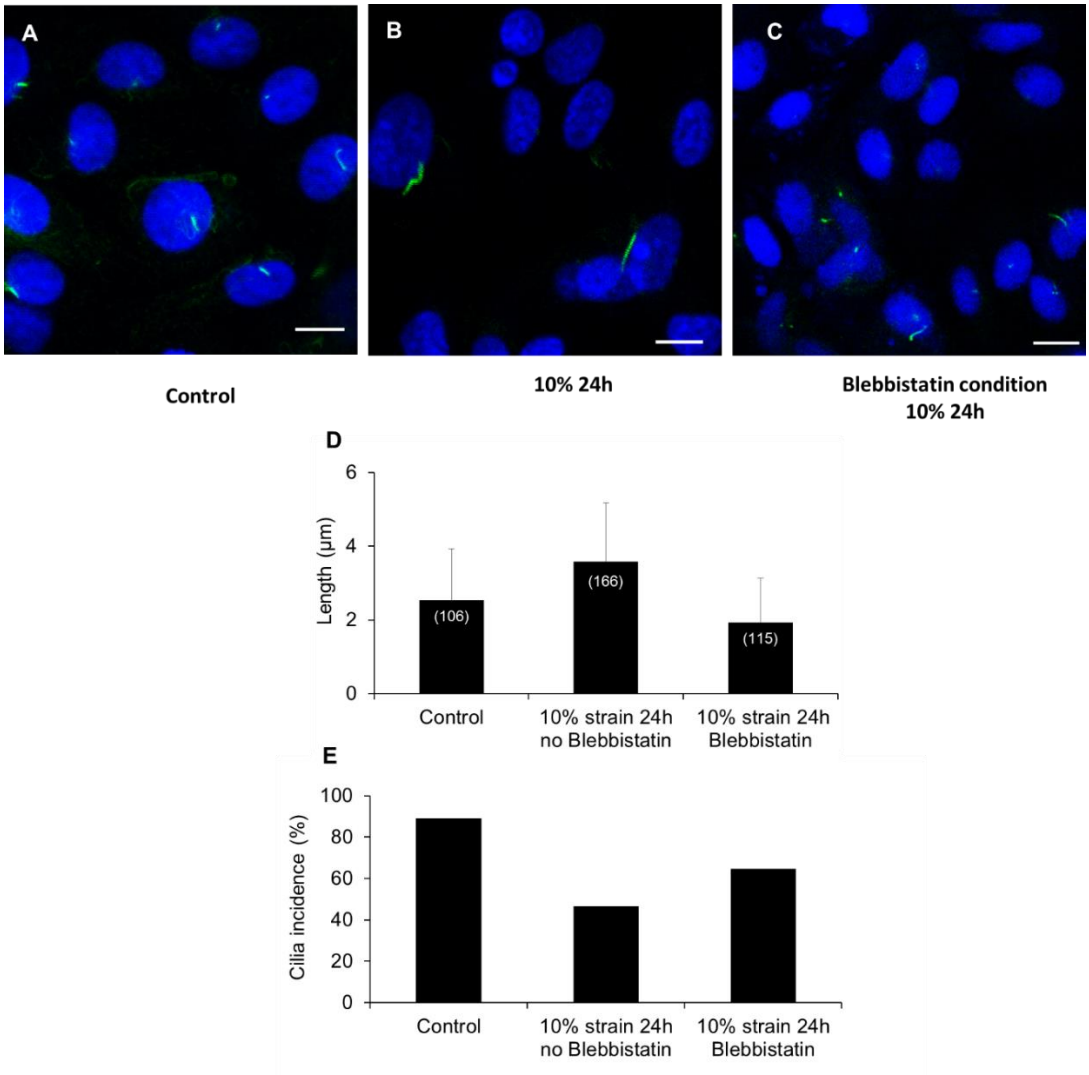

Fig. 3.10: Effect of blebbistatin to primary cilia formation (Blue: nuclei, Green: primary cilia.). (A): Control condition. (B): 10% strain for 24 h. (C): Blebbistatin treatment and 10% strain for 24 h. (D): Cilia length. (E): Cilia incidence. Scale bar: 10 µm.

3.4 Discussion

Figure 3.5 shows representative fluorescence images of primary cilia in the control and experimental condition of substrate stretching. Visually, the primary cilia length increases in the experimental conditions and the analytical results were shown in Fig. 3.6. The wall shear stress on the endothelial layer due to blood flow and circumferential stretch in the vessel wall are simultaneously existing (Lu et al., 2011). The results of primary cilia lengthening in response to mechanical stimuli in this study may suggest that the remodeling of cilia under the presence of cyclic substrate stretching supports the mechanotransduction of cilia to direct stimulation of fluid flow. The longer the cilium, the more sensitive it will be to smaller deflection forces. Schwartz et al. (1997) hypothesised that longer cilia would experience greater membrane strain to increase the opening of stretch-activated ion channels on the ciliary membrane. In addition, longer cilia allow more compartments of proteins and signaling molecules, which enhance signaling transduction. Other groups also showed that the absence and presence of fluid flow result in changes cilia length and enhance the mechanotransduction of cilia (Iomini et al., 2004; Wang et al., 2008; Spasic et al., 2017). Other indirect mechanical stimuli to primary cilia such as cyclic cellular deformation via compressive loading of chondrocyte in a 3D agarose model or the stress-deprived and cyclic tensile loading in tendon cells also produce an immediate and significant increase in the length of primary cilia (Gardner et al., 2011; Lofgren et al., 2015).

The underneath mechanism of how primary cilia remodel in the presence of indirect mechanical signals of substrate stretching is still unclear. The actin network is believed to be the intermediate factor which is able to transmit the cyclic substrate loading to primary cilia. The cyclic loading regulates cytoskeleton network through focal adhesions, meanwhile the basal body of primary cilia are believed as the organized-center of microtubules and actin cytoskeleton. It is well known that the substrate stretching promotes actin development. However, this actin formation could lead to the loss of cilia incidence. Some new evidences indicated in the negative regulation between actin dynamics and cilia formation. The actin depolymerisation promotes ciliary assembly and elongation, while polymerization or branching of actin is associated with cilia disassembly or ciliogenesis inhibition (Smith et al., 2020). The centrosomes, root of

primary cilia, were proved as to be actin-organizing centre (Van der Heiden et al., 2008), which also may suggest the alterations of primary cilia formations during actin network reorganization. Experimental treatments that eliminate the actin network have shown to prevent basal body docking (Farnum et al., 2011, Hierck et al., 2008). Moreover, many actin-associated proteins like actin motor protein and signaling molecules localized within primary cilia and cilia's base.

In contrast to the increase of primary cilia length, the ciliary incidence decreased in the application of mechanical signal (Fig. 3.7). The precise mechanism is unclear regarding the stimulation of substrate stretching. As declaimed above, the actin formation during stretching inhibit the formation of cilia. Regarding to the decrease of ciliated cells in the presence of fluid flow, it was logically explained since longer cilia are exposed to, the greater the drag force are and more likely to be sheared off (Hierck et al., 2008) and endothelial cell primary cilia are flow sensors in regions of low shear (Van der Heiden et al., 2008). Cilia disassembly would be induced by prolonged exposure to high fluid shear stress, since endothelial cells may have other mechanisms, such as glycocalyx, to sense high mechanical forces (Nauli et al., 2011).

Actin network is believed as the mediating factor to transmit the mechanical force from the substrate to primary cilia at the top of cells. In order to test the relationship of dynamic of actin filament and the responses of cilia, the development of actin network is restricted by inhibiting the actin with blebbistatin and the results (Fig. 3.9) showed that the cilia become longer during stretching, but shorten in the presence of blebbistatin. It suggested that the actin myosin activity or the cytoskeleton network transformation during substrate cyclic stretching affects to primary cilia. Many actin myosin are found in the cilia basal body which support ciliary transportation, and the less dynamic of actin network due to actin myosin inhibition may answer why cilia are shorter. Our finding of cytoskeleton filaments at the base of cilia in Chapter 4 may show the mechanical connection between the actin filaments and the primary cilium. By inhibiting the actin network transformation during substrate stretching, the mechanical force from the focal adhesion could not be transmitted to the cilia, which makes the cilia become shorter, compared to the free-blebbistatin condition. The less affection of actin network to

primary cilia in the presence of blebbistatin also makes the number of ciliated cells increased, compared to the free-blebbistatin condition.

Besides the effects to the length of primary cilia, the external forces may also have an effect on the reorientation of primary cilia. As our results, the primary cilia alignment does not show clearly, but a slightly reorientation in the stretching direction is observed. The cilia orientation has shown in some previous studies. Under fluid flow condition, beside one possibility is that the mechanical stress is translated into chemical signals through TRP channels that ultimately change basal body orientation, which results in gradual cilia orientation (Shin et al., 2005). There is another purely mechanical reason to explain the flow-driven orientation of cilia. The shape of power stroke would change during the beating, and this change would translate through the base of the axoneme. Cornelia et al. (2010) demonstrated that axonemal position in 3D space in cartilage is less aligned in non-loaded regions, compared to loaded regions. The connection between cilia reorientation and the mechanical loading of cyclic stretching is not widely studied. Werner et al. (2011) showed that the pool of actin localized subapically, which connects basal body and rootlets, contributes to orient cilia. The planar orientation of cilia was also tested to be driven by complex interactions between basal body and dynamic networks of actin based filaments (Chien et al., 2013).

The results here suggest the cilia remodeling in the substrate stretching conditions may support cellular mechanotransduction function in the fluid flow conditions, but how exactly the support of substrate loading to mechanosensing to fluid flow of cilia is still unclear, and it should be clarified in the further investigations. Among the studies of responses of primary in the surrounding mechanical environment, this is the first study revealed the effect of substrate stretching, which is not directly apply to primary cilia. McGlashan et al. (2010) investigated the cilia responses in the stretching condition of 3D environments. These 3D mechanical loadings can lead to different stimuli to cilia such as the direct stretching from 3D environment, or the cell compression in the dynamic 3D environment leading to changes of cilia. It is impossible to distinguish the stimulation sources apply to cilia. This study specifically focuses on one subject of stimulation, which is the substrate stretching.

3.5 Conclusions

In summary, the results of this study, for the first time, confirmed the remodeling ability of the primary cilia in response to cyclic substrate loading. The length of primary cilia increases from around 3 μm in control condition to 4 - 9 μm in the stretching conditions, meanwhile the presence of ciliated cells decreased from around 80% down to around 20% - 60%; the higher strain level is, the lower of the number of ciliated is. It suggests that the cyclic substrate loading may contribute to cilia remodeling and the mechanotransduction function in response to the direct stimulation of fluid flow. Due to the change in cilia length and cilia incidence in the blebbistatin condition, the suggested mechanism which triggers the remodeling in response to substrate loading is the actin cytoskeleton.

Chapter 4

Investigation of microstructures of cellular primary cilia

4.1 Introduction

The primary cilium is a non-motile cilium protruding from the apical cellular surface (Lim et al., 2015). It is found in multiple types of cells and functions as a mechanosensor to sense changes in surrounding mechanical environment such as fluid flow. The core of primary cilia is the axoneme of nine microtubule doublets extended from triplet microtubule structure at the basal body, which is covered by the cilia membrane. This backbone structure is believed to contribute mainly to the mechanical properties of primary cilia. In primary cilia nine microtubule doublets are arranged radially with no central pairs of microtubules (9 + 0 structure) (Satir, 2017), which distinguishes them from the motile cilia having a 9 + 2 microtubule configuration. Normally, the motile cilia have the molecular motors and dynein arms which contribute to ciliary motion. It is still unclear whether primary cilia have alternative structures to allow the elastic properties of reversible bending in response to mechanical stimuli like fluid flow. Therefore, it is necessary to understand naturally the interaction of components of primary cilia, which may help to understand more clearly their mechanical properties. Together with the axoneme, the backbone of primary cilia, the other ciliary structures and adjacent organelles, such as the ciliary pocket, the cytoplasmic actin and microtubules anchored to the base of primary cilia, the Golgi apparatus, also contribute to the function and mechanical properties of primary cilia

Jensen et al. (2004) is one of the first study group visualizing the ultrastructural component of chondrocyte primary cilium in situ using TEM. Their TEM results revealed the ciliary axoneme and the vesicle particle along the length of proximal axoneme which represents the ICT particles. In 2013, Rogowski et al. (2013) did another TEM study about primary cilia and flagella. They reported the ultrastructures of primary cilia including the longitudinal section of cilia axoneme, the basal body and the subdistal appendages and some IFT particles. From the cross-sectional images, they found that the microtubule doublets are not strictly arranged in the circular pattern, and the number of microtubule doublets changes from the base to tip of cilia. In 2010, Molla-Herman et al. (2010) focused on the importance of ciliary pocket in the cilia function.

One of the main functions of primary cilia is mechanotransduction, which helps cells to sense the mechanical signals and converts them into biological signals inside cells. Calcium expression in intracellular matrix is the most typical signaling pathways of cells thanks to cilia bending. Praetorius and Spring (2001) first identified the relationship between cilium bending and intracellular calcium expression in kidney cells. Cilia were bent under fluid flow and micropipette application; the cellular calcium were observed with fluorescence calcium indicator. This calcium response disappeared in the absence of calcium-free media. Su et al. (2013) developed the targeted genetically encoded calcium indicator (GECI) to observe calcium dynamics in primary cilia and cells under both mechanical and chemical stimuli. In addition, Platelet Derived Growth Factor Receptor (PDGFR) signaling is also regulated through the primary cilium. Schneider et al. (2010) showed that in the presence of PDGFaa in the extracellular matrix during the wound healing, the migration speed and direction of cells are controlled by PDGFR signaling on primary cilia. Most of the signaling proteins received by the primary cilium interact with underneath cellular cascades through Golgi complex, and the close physical distance between these two organelles is needed to well-support these signaling processes. TEM images may help to prove this close physical relation, but so far there is only one study reported about this issue (Poole et al., 1997).

Other adjacent structures of primary cilia, which are the cytoplasmic filaments (actin and microtubules) anchored at the base, may contribute to the elastic bending of cilia in response to fluid flow. This anchor is expected to, at some degree, resist the bending response of the cilium. All the mentioned structures could be clarified by observing the microstructure of primary cilia.

In this work, a primary cilium model was also simulated to provide a appropriated model for further cilia investigations and more information of the cross-linking component inside primary cilia, an important component on deciding the mechanical properties of cilia. Although the primary cilia' structure was discovered by TEM and even constructed in 3D (Sun et al., 2019), the numerical cilia model is not built up yet. In all cilia simulation, the primary cilia were modelled as the homogenous and elastic beam, there is no realistic model with main mechanical components of primary cilia studied so far. The first aim of this numerical study is to build up a cilia model composed of main mechanical components such axoneme of nine microtubule doublets and cross linking component. As discussed in Chapter

2 about the mechanical properties of primary cilia, the microtubule structure has the high Young's modulus (order of GPa), which is much higher than the measured Young's modulus of primary cilia (order of hundred kPa). The second aim of the numerical work after constructing the cilia model is to identify the properties of the cross-linking components, which is also never reported so far.

4.2 Materials and methods

4.2.1 Cell preparation

Madin-Darby Canine Kidney (MDCK) cells were used for experiments. Cell culture medium consists of Dulbecco's Modified Eagle Medium (DMEM) supplemented with 10% fetal bovine serum, 1% penicillin and 1% streptomycin. Cells were cultured under a humidified atmosphere of 5% CO_2 at 37°C up to passage 5 - 10. Cells must be confluent and quiescent, as primary cilia are formed during interphase and reabsorbed during mitosis (Mitchell, 2013). Beyond cell confluence, cells continued to grow for 3 - 5 days to get mature primary cilia and allow them to get their maximal length.

4.2.2 Transmission electron microscopy

The TEM protocol consists of the following steps: fixation, postfixation, dehydration, resin infiltration and embedding, ultrathin sectioning and staining, and visualization. Cells were pre-fixed in 2% Glutaraldehyde in 0.1M phosphate buffer (pH 7.4) overnight at 4^0C and then were post-fixed with 1% osmium tetroxide in 0.1M phosphate buffer (pH 7.4) for 2 h. Cells were washed in 0.1M PB (pH 7.4) three times after each step of pre- and post-fixation. After fixation, cells were dehydrated at 50%, 70%, 90%, 99.5% and 100% ethanol, respectively, for 5 min. Subsequently, the resin infiltration was done at room temperature for 30 min and the samples were embedded in beam capsules, and baked in 60ºC oven for 48 h. Finally the ultrathin sections were cut at 70 nm of thickness by ultra-microtome, collected on grids, stained with uranyl acetate for 10 min and with Pb for 3 min.

4.2.3 Visualization

Sections were studied with a JEM - 2100 transmission electron microscope (Jeol Ltd., Tokyo, Japan) operating at 80 kV, and pictures were analysed using the image analysing software ImageJ.

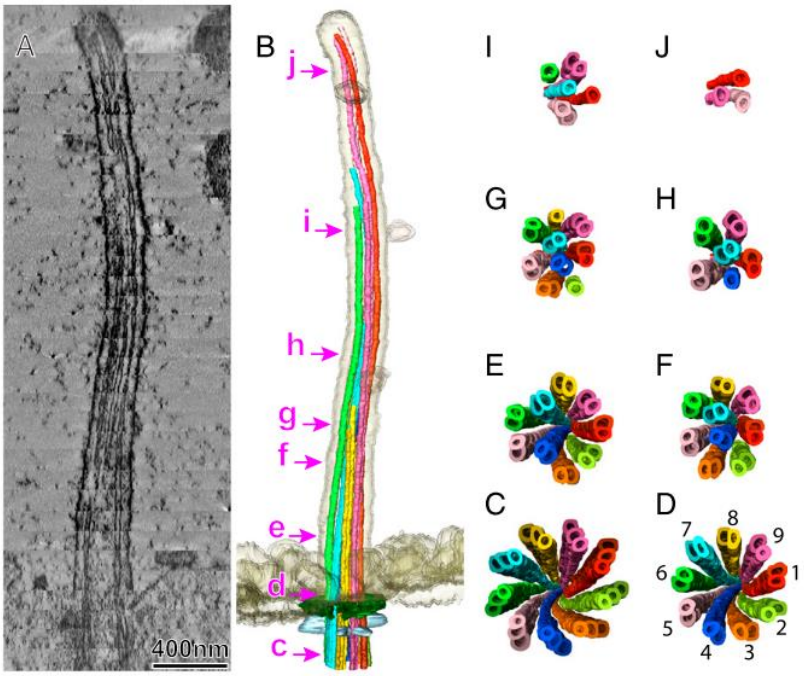

Fig. 4.1: The primary cilium structural map obtained by 3D construction by Sun et al. (2019).

4.2.4 Primary cilium model

Finite Element Modelling (FEM) analysis software (ANSYS Mechanical Multiphysics) was used to simulate the primary cilium model. The model was built up based on the 3D constructed information from Sun et al. (2019) (Fig. 4.1). The primary cilium model includes two structures: the nine microtubule doublets structure and the cross-linking component.

The microtubule doublets structure: the microtubule doublet includes A tubule and B tubule with different diameters (Fig. 4.2). The A tubule has outer diameter of 33 µm and inner diameter of 21 µm, while the numbers of B tubule are 30 µm and 17 µm, respectively. Eight sections (from D to J) along the length of cilia were constructed (Fig. 4.3). At the bottom end (section D), nine doublet microtubules are observed (Fig. 4.4). Along the length of cilia, the number of microtubule doublets reduces, for instance, to 6 microtubule doublets (at section H) and 3 microtubule doublets (at section J). The microtubule doublet structure is not also preserved, and it may transform to single microtubule (at section J, the microtubule doublet of 1, 5 and 9 become single tubule). After the positions of nine microtubule doublet at section were created (Fig. 4.4), an individual microtubule doublet

structure was formed by connecting position of each section to each other. The microtubule in this model is not vertically straight from the proximal to the distal end. The position of one specific doublet microtubule changes at cross-sections, and even the doublet microtubules are twisted.

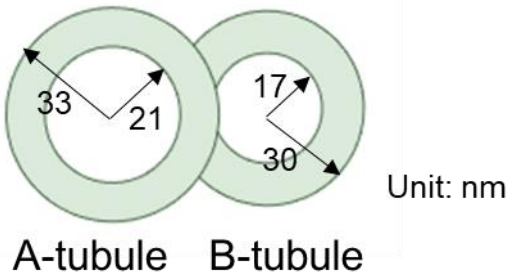

Fig. 4.2: The dimension of doublet microtubule.

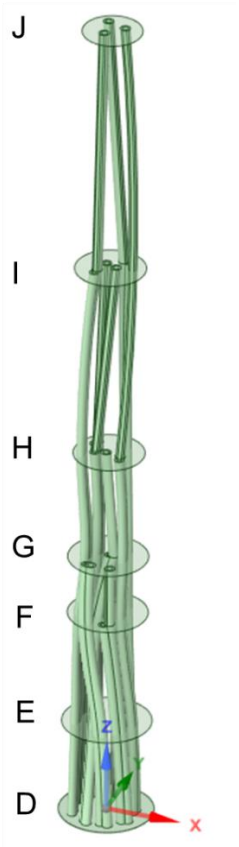

Fig. 4.3: The eight sections along the length of primary cilium model.

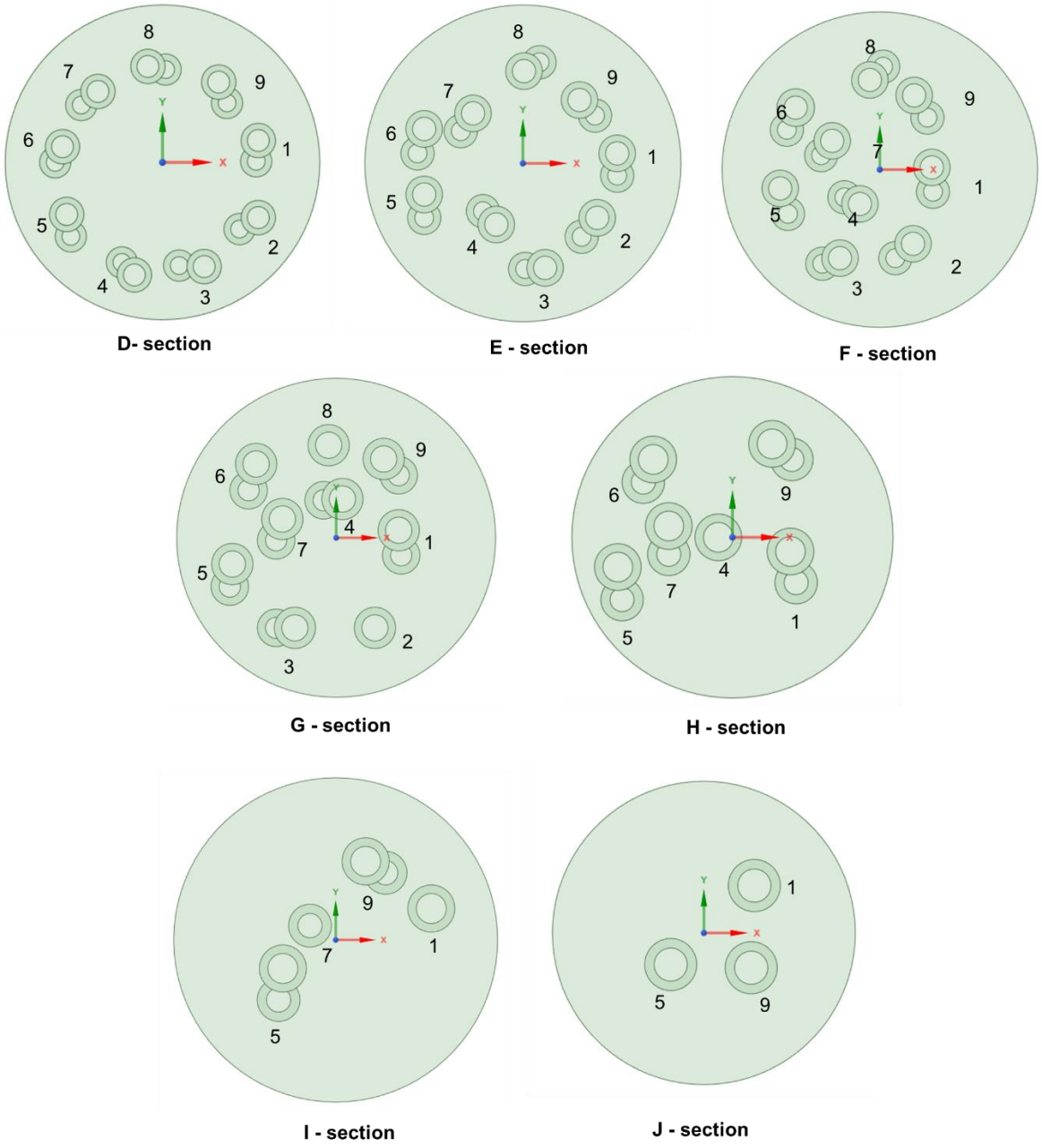

Fig. 4.4: The cross-sections of doublet microtubule of cilium model.

Fig. 4.5: Geometry of primary cilium model.

The cross-linking component: After building up the microtubule doublets, the cilia membrane was created from the boundaries of each section (D to J) to produce a closed package of primary cilium (Fig. 4.5). Sun et al. (2019) discovered the cross-linking components that connect the microtubule doublets to each other and to ciliary membrane. The cross-linking structures are believed to both explain the elastic bending of primary cilia in response to mechanical signals such as fluid flow and the reason why the elastic Young's modulus of the cilia (the order of hundred kPa) is smaller than the Young's modulus of the core structure of microtubule (GPa). These structures are supposed to bind fully along the length of microtubules and to cover the space between microtubules and between microtubule and membrane. At this point of study, to simplify the cilia model, the cross-linking component is assumed to be a structure of subtracting the compacted cilia solid to the nine double microtubule structure (Fig. 4.6).

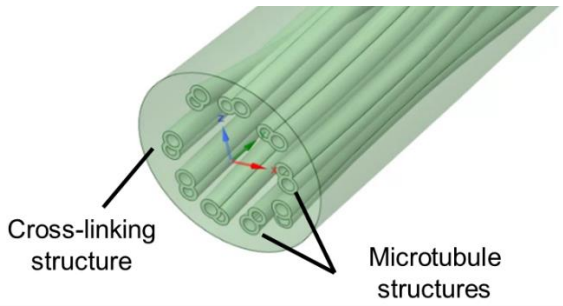

Fig. 4.6: Two main components of the primary cilium model: microtubule structures and cross-linking structure.

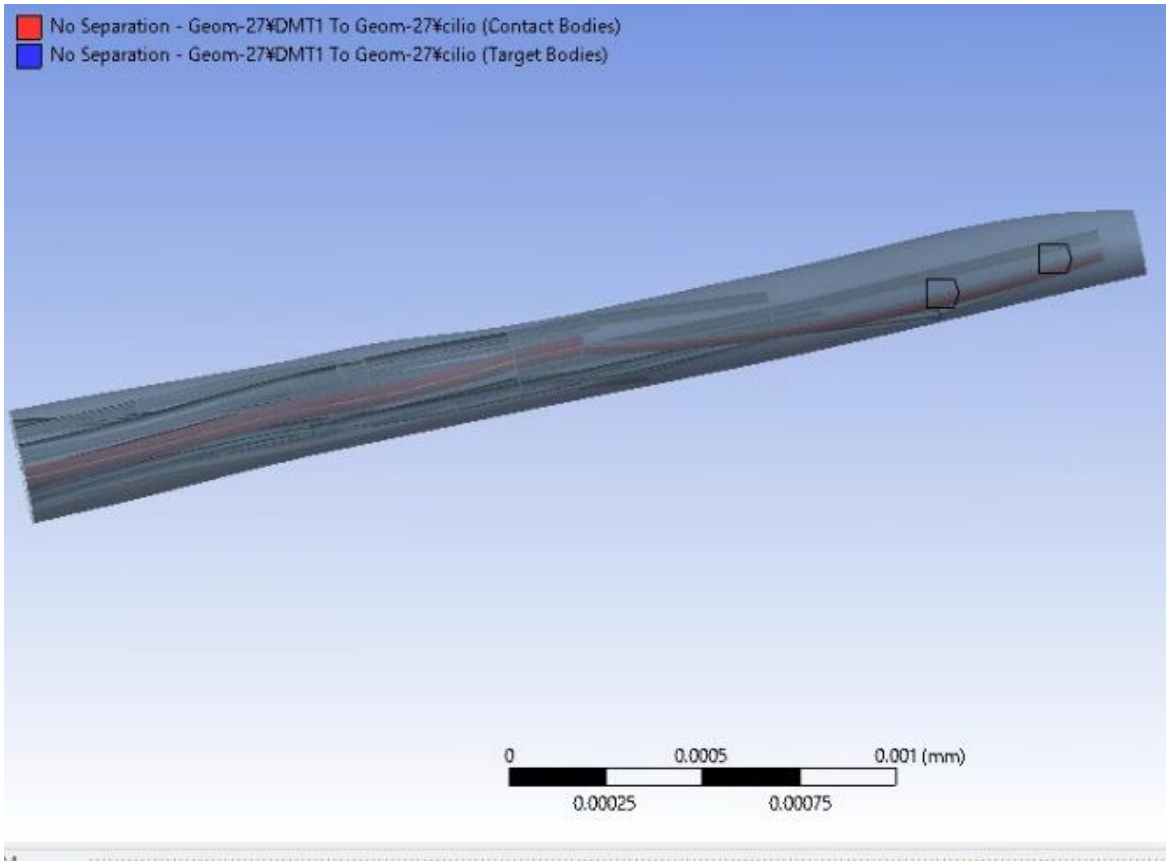

Fig. 4.7: The No separation type of connection between microtubules and connecting structure.

Boundary conditions: As discussed above, the cross-linking structure was supposed to be the elastic component which is the main responsible factor for elastic properties of primary cilia. The connection between nine microtubules and cross-linking structure is No separation type, which means the microtubule and connecting structure can slide one over the other without separation (Fig. 4.7). The meshing study of tetrahydral element type was performed to mesh all components. Overall, the meshing size composed of 1.274.826 nodes and 697.738 elements (Fig. 4.8). A static tensile load of 1 nN was chosen to apply force at one end of the primary cilium. Another end was set as the fix support (Fig. 4.9). For the mechanical properties of nine microtubule structures, the Young's modulus of 1 GPa is assigned (Table 1.3). The mechanical properties of cross-linking component are changed from 0 – 6 kPa to verify the dependence of properties of primary cilia on the properties of cross-linking component.

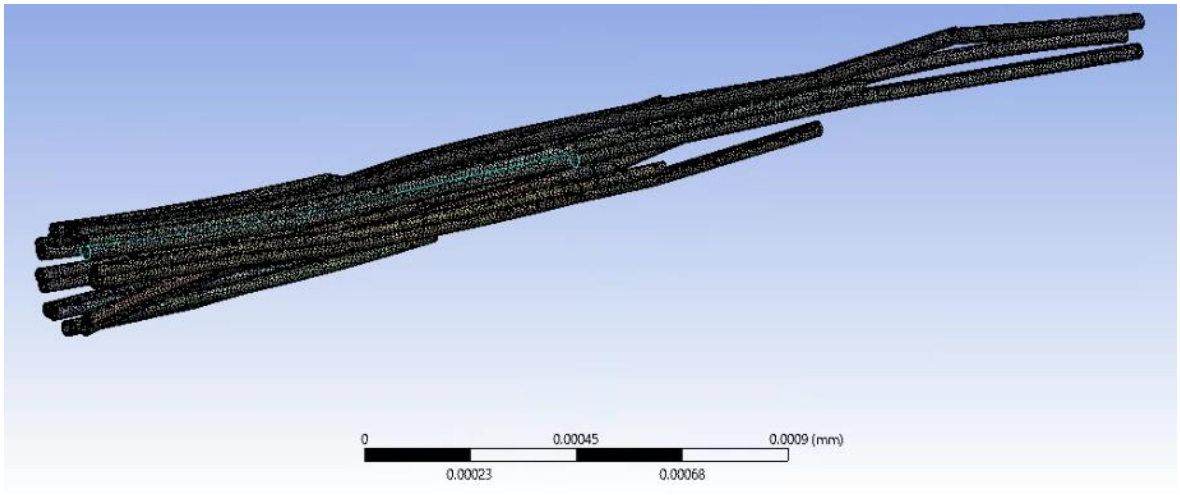

Fig. 4.8: The finite element model of the primary cilium.

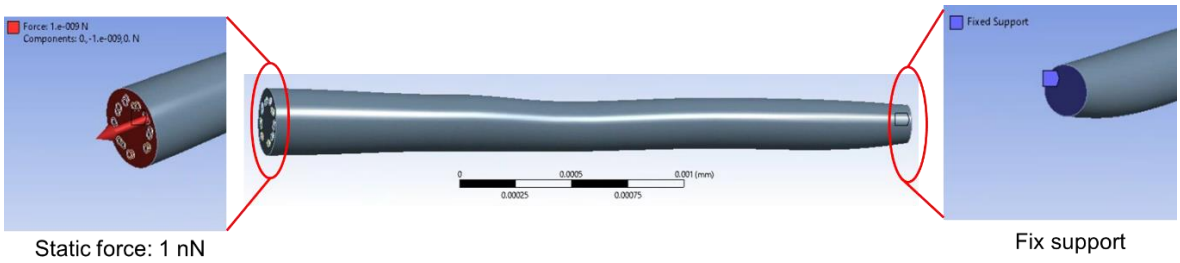

Fig. 4.9: Boundary setting of the primary cilium model.

4.3 Results

4.3.1 Overall structural components of a primary cilium

Looking at the overall picture of the position of primary cilia in relationship with other structures (Fig. 4.10), the diplosomal centriole (basal body) of primary cilium is next to Golgi network, and the axoneme projects to the extracellular matrix. TEM images (Fig. 4.11) confirmed the components of primary cilia which are:

- The displosomal centrioles of primary cilia: including proximal centrioles and distal centriole (the basal body).
- The ciliary body (axoneme).
- The ciliary pocket.
- The basal body constructed by nine triplet microtubules (Fig. 4.11 B).

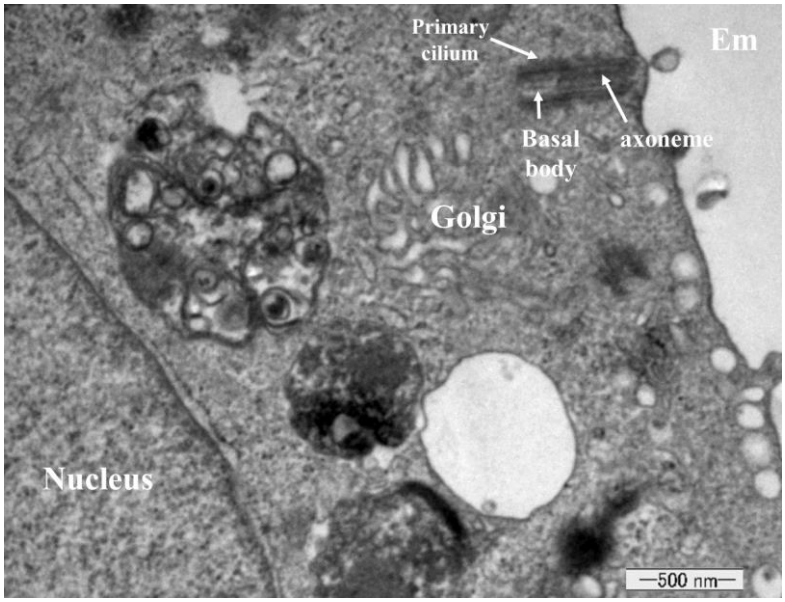

Fig. 4.10: Overall structural relationship of primary cilia with other structure like Golgi, nucleus, extracellular matrix (Em).

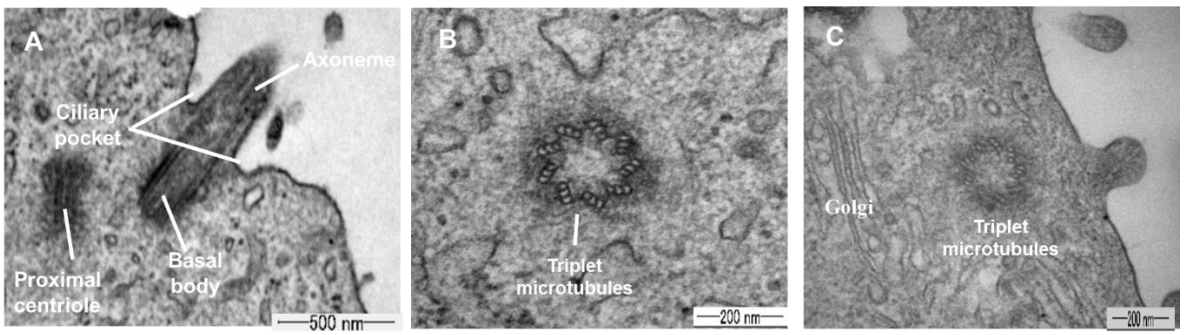

Fig. 4.11: The components of primary cilia.

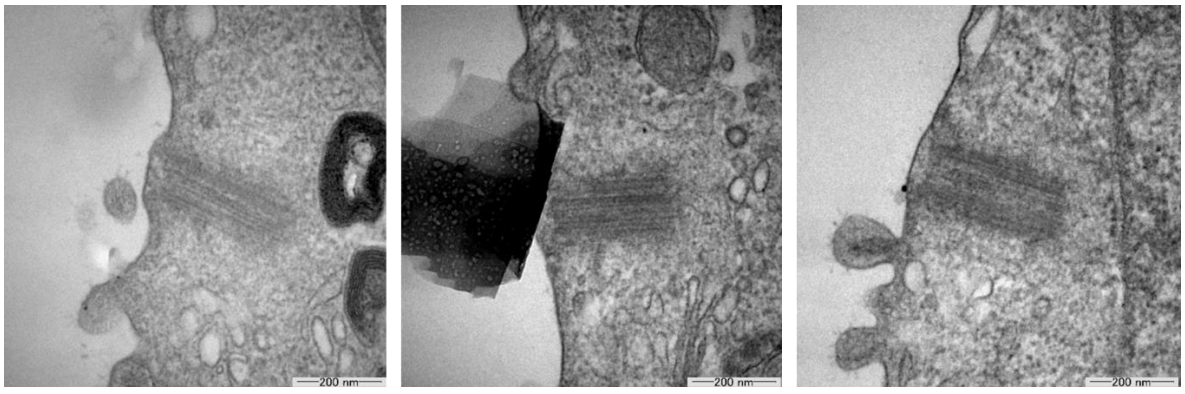

Fig. 4.12: The different basal body of primary cilia.

4.3.2 Basal body

Different basal bodies from different primary cilia were obtained from cutting sections. Various basal body density pictures were also observed (Fig. 4.12); they indicate the high density of microtubules in the basal body parts.

4.3.3 The cytoplasm filaments anchored to basal body

Primary cilia bend in response to mechanical signals such as fluid flow. Mechanically, the cilia are anchored to cells by the connection of their base to cytoplasm filaments such as actin filaments and microtubules. By taking TEM images, this connection can be displayed (Fig. 4.13). This hinge may contribute to the mechanical response of primary cilia to fluid flow.

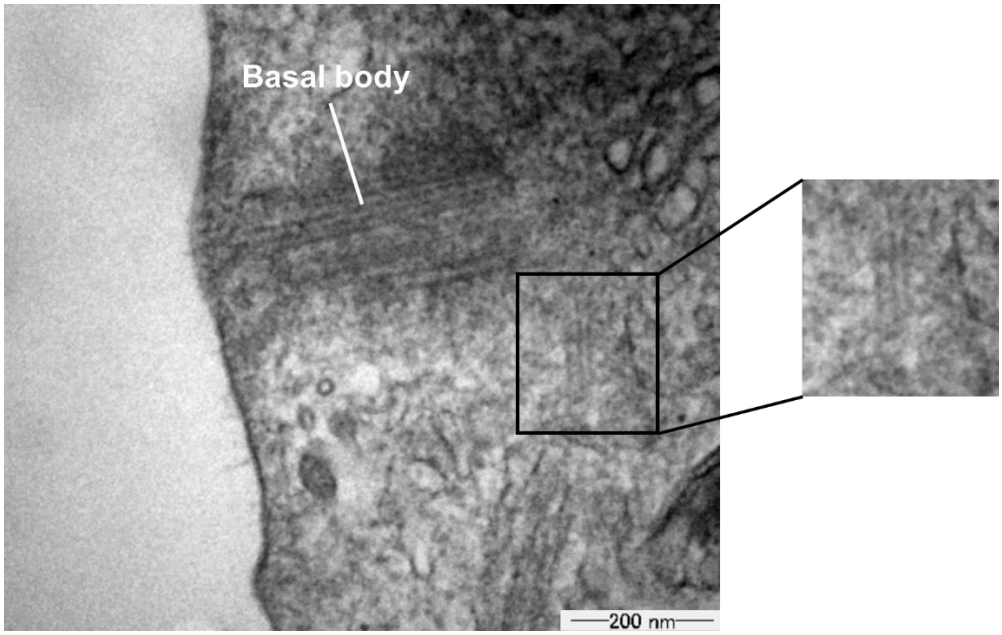

Fig. 4.13: Association of primary cilia and intracellular filaments.

4.3.4 Ciliary axoneme

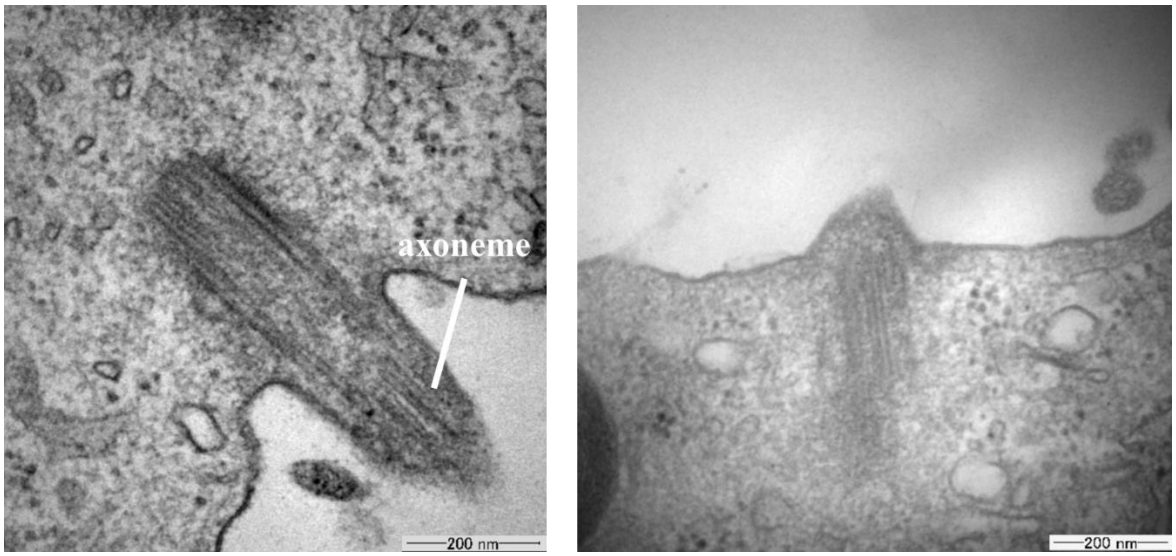

Fig. 4.14: TEM images of primary cilia bending.

Figure 4.14 shows microtubule fibers along the length of an axoneme. Different length of axoneme which protruded to extracellular matrix were obtained. Due to the natural bending of primary cilia, especially in *in vitro* condition, the totally straight axoneme in one cutting section of TEM is hardly obtained.

4.3.5 Simulation results

In the present work, different Young's moduli of cross-linking component were assigned to investigate the effect of cross-linking structure on the mechanical properties of primar cilia. Figure 4.15 depicts that the equivalent Young's modulus of the cilia increases with the increasing of the Young's modulus of cross-linking component. In Chapter 2, the measured Young's modulus of primary cilia varied from around 60 - 200 kPa (equivalent to the red section in Fig. 4.15), which leads to the elastic properties of cross-linking components, being around 100 Pa - 1 kPa.

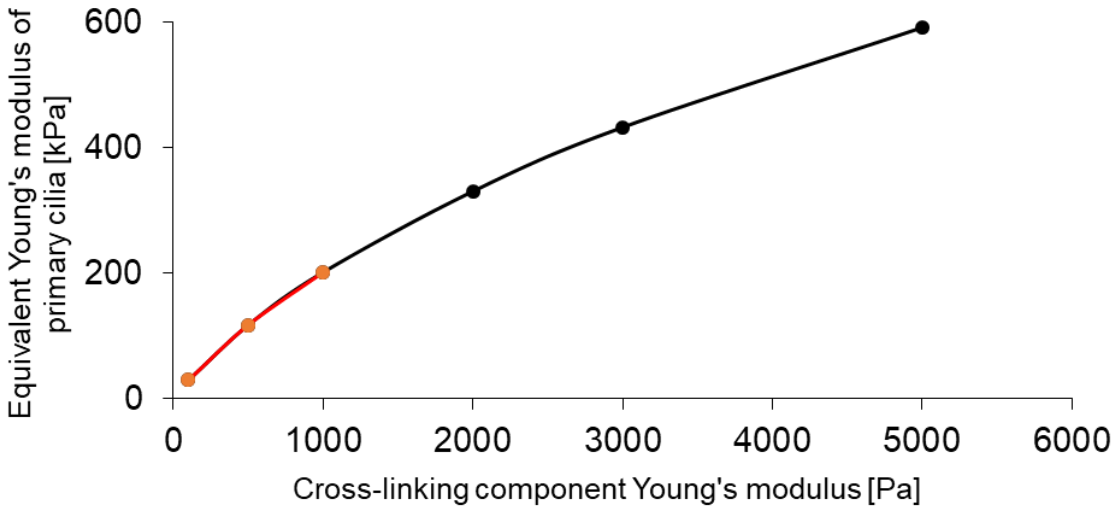

Fig. 4.15: Dependence of equivalent Young's modulus of primary cilia on the Young's modulus of cross-linking component.

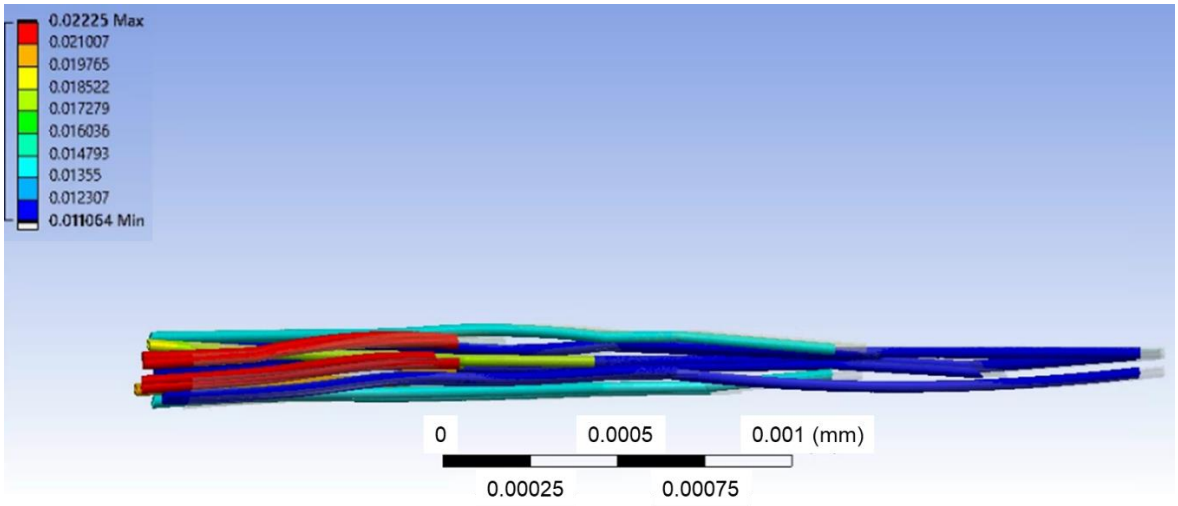

Fig. 4.16: The deformation profile of microtubule structures.

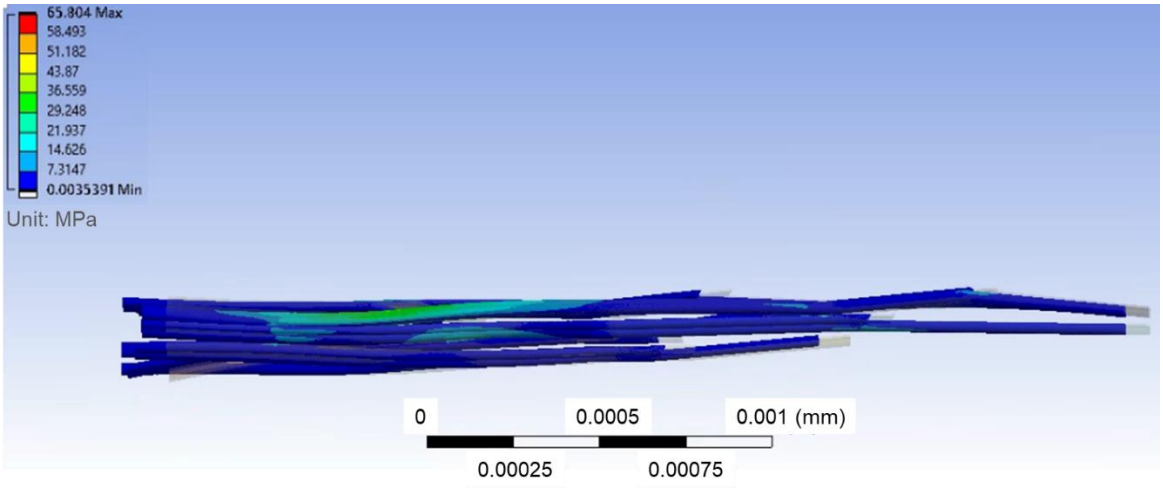

Fig. 4.17: The stress distribution on microtubule structures.

Figure 4.16 shows deformation profile of nine microtubule structure. The short microtubules deformed much more than the longer one. This could be explained by the fact that the shorter microtubule has fewer friction force and experienced the longer sliding distance in the deformed cross-linking environment.

Figure 4.17 shows the stress profile of microtubule structure. The stresses were higher at middle points where the microtubules are closest to each other. Indeed, in this condition, the sliding force is much higher than other positions, where the microtubule is far from each other. The suggestion for the further models is that the cross-linking component should be modelled mainly on the area where microtubules are physical close to each other.

4.4 Discussion

Both the longitudinal section (Fig. 4.10) and the cross-section of the primary cilia (Fig. 4.11 C) reaffirmed that the location of primary cilia is close to the Golgi apparatus. Many researchers studied the involvement of the Golgi and the primary cilium, and argued their functional relationship since there are proteins transportation between these two organelles (Poole et al., 1997; Hsiao et al., 2012; Clement et al., 2013). Golgi apparatus is the intracellular logistic center, which is responsible for transporting and packaging the synthesised proteins from the endoplasmic reticulum into vesicles. Most of ciliary membrane proteins are transmitted to the Golgi and then processed, modified and packaged to be transported to different destination inside the cells.

Follit et al. (2006) reported that the intraflagellar transport 20 (IFT20) which is responsible for the motor transportation along ciliary microtubules, is also localized inside the Golgi apparatus. IFT20 functions to regulate the ciliary membrane proteins transport from the Golgi to the cilia, since the authors observed the dynamic of IFT20 within Golgi apparatus and its movement between the Golgi complex and the cilium. Knockdown of IFT20 expression results in the ciliary assembly and is linked to the reduction of the level of PKD2 in the primary cilia. Lee et al. (2018) demonstrated that the minus end-directed kinesin KIFC1, which accumulates in the Golgi network, is a vesicle motor protein to carry the ciliary membrane proteins secreted from the Golgi. Many other transported proteins between Golgi and cilia were also reported such GTPase, GGA1, Arf4, Arl3b (Kim et al., 2014; Moritz et al., 2001). Because of the key role of Golgi in the ciliogenesis, it provides a potential reason why the Golgi is often physically closed to the basal body. This physical relationship also enhances the efficiency of cellular signaling. Moreover, the mutual functional interactions may be explained for this proximity, which the Golgi proteins need for basal body organization and positioning (Sütterlin et al., 2010).

TEM images are capable of observing the membrane domain at the base of primary cilia, which is named as the ciliary pocket (Fig. 4.11 A). It takes 10 years after discovering of the primary cilium, this ciliary membrane took cautions of researchers. This domain functions mainly as a ciliary vesicular trafficking. The ciliary pocket membrane separates the ciliary membrane from the plasma membrane. The shapes of pocket vary differently not only depending on the cell type, but also within the same cell type. It is regulated by actin polymerization, which controls the adhesion proteins between ciliary pocket and ciliary membrane. The dysregulation of actin polymerization affects the adhesion and therefore the pocket shapes. However, not all cilia in the cell types have the pockets. In some cells, the basal body docks at the apical plasma membrane, where the cilium directly protrudes, and there is no pocket at the base of cilia in this case. The pocket-associated primary cilia are mostly found in the cells where they experience the mechanical stimulation of liquids.

Biologically, the ciliary pocket membrane is enriched in Clathrin-Coated Pits (CCPs) and Vesicles (CCVs), which lead to its function of endocytic gateways allowing the proteins travel between intra and extracellular matrix (Ghossoub et al., 2011). One of the most significant endocytic processes at the ciliary pocket are Shh and TGF-β signaling. The

mechanism and regulation of these two signaling pathways through CCPs and CCVs at the ciliary pockets has been reviewed in details in other articles (Pedersen et al., 2016). Mechanically, it is interesting that the pocket may participate in the position or orientation of primary cilia, due to the association of the pocket and actin polymerization. The changing of actin cytoskeleton might result in changing of pocket region. This may explain the remodeling of primary cilia in response to substrate stretching in the Chapter 3, where actin organization is regulated during the stretching and then reorient in the direction of primary cilia.

Figure 4.12 shows the different basal body of different cilia. One of the factor can be taken into account when considering the mechanical response of primary cilia is the density of microtubule microfilament in the basal body. Higher density of microtubules may produce higher stiffness of basal body, therefore affect the mechanical responses. As can be seen, the higher density (darker configuration) may show the thicker microtubules bundle. Under the exposure of fluid flow, the base of primary cilium experienced the high torque, and the thick microtubule bundle results in higher flexural rigidity for the primary cilia, which helps cells to resist to the higher bending torque. Generally, the architecture of the axoneme provides a strong backbone for elastic bending, but the anchor point and the properties of base is also contribute the cilia's response in flow field.

Mechanically, the primary cilium grows from the basal body and connects to the proximal centriole and the nucleus through the bundle of microtubules and striated rootlets. The microtubules and actin filaments in the cytoplasm are also anchored to the basal body and then spread in all directions. One longitudinal section expressed the existence of these filaments close to the base of primary cilia (Fig. 4.13). This mechanical interaction of intracellular filaments like actin and microtubules with the primary cilium might suggest the transmission of force from the actin cytoskeleton to the primary cilium. This hinge may contribute to mechanical bending of primary cilia in response to mechanical signal or in the orientation and motion of primary cilia associated with the activity of actin cytoskeleton (Resnick, 2015; Battle et al., 2015; Satir et al., 2010). The connection between the actin network and primary cilium has also been screened by changing the actin cytoskeleton stiffness by cytochalasin D, which regulates the primary cilia formation (Kim et al., 2010, Smith et al., 2020; May-Simera et al., 2012; Mirvis et al., 2018; Antoniades et al., 2014).

Resnick (2015) changed mechanical properties of the cilia base and concluded that the physical structures at the base have essential roles in mechanosensing function of primary cilium. Battles et al. (2015) suggested that this hinge is the key aspect of the primary cilium movement, the actin network fluctuations at the base can be translated to the angular movement of axoneme.

Figure 4.14 showed the ciliary axoneme structure. Naturally, the primary cilia bent, it is impossible to find a straight standing primary cilium in the extracellular of liquids such as endothelial cells or kidney cells (MDCK). Moreover, during the preparation steps of TEM experiments *in vitro*, the steps such as resin infiltration or dehydration lead to the bending of cilia, which result in only a portion of a cilium has been observed in one section. Occasionally, all of the ciliary components can be seen (Fig. 4.11 A). In 2004, Jensen et al. (2004), for the first time, presented the electron tomographic reconstructions to build up the 3D structure of cilia axoneme. They observed the vesicles along the length of axoneme between the microtubules structure and ciliary membrane. These vesicles are the IFT proteins which help for transportation of the ciliary proteins from the tip to the base and vice versa. However, this finding could not clarify the microtubule structure inside the axoneme. Sun et al. (2019) developed more deeply accurate 3D structure of primary cilia. Using the serial section electron tomography (SSET) they discovered an interesting feature of the microtubule doublets structure. The 9 + 0 microtubule configuration was not preserved from the base to the tip of the axoneme. The number of microtubule doublets starts from nine at the base, and the number reduces before reaching to the tip. Even the doublet forms are not well preserved, they could transform into singlets of microtubules. Moreover, the peripheral microtubules architecture has the right-hand twist formation. Due to above structural changes, the diameter of primary cilia decreases gradually toward the end tip. The different examples of primary cilia's axoneme in Fig. 4.14 are due to different bending degrees, which produces the different lengths of axoneme protruding from the plasma membrane.

TEM images allow us to map the important structures of primary cilia. The interconnection of these structures helps to understand how these components contribute to the mechanical response of primary cilia and partly understand the mechanotransduction function of primary cilia through Golgi structure. As discussed in Chapter 2, the primary

cilia structure should have the components which connect microtubules together and allow elastic bending of cilia.

Regarding the numerical works of primary cilia, all previous cilia models were assumed to be elastic beams, there was no model with fully mechanical components conducted so far. The simulation in this study, for the first time, modeled the primary cilium including the main components such as axoneme and cross-linking part. Moreover, besides proving the mechanical properties of primary cilia depends mainly on cross-linking components, it also revealed the range of elastic moduli of this component, which is totally new and interesting discovery in this research field. However, these results still have some limitations since the assumption of cross-linking is the subtraction of cilium space to nine microtubule structures. It would be appropriate if there is the cilioplasm in the model as well. The results in Fig. 4.17 suggested that the cross-linking component in the further models could be focused on building up at the locations where microtubules are close to each other. This most realistic cilia model in this study provides a promising model for the further cilia simulation, and could be integrated into cell simulation to understand correctly the mechanics and mechanotransduction of cells.

4.5 Conclusions

TEM demonstrated the main components of primary cilia, including the basal body, the axoneme. Moreover, it showed the ciliary pocket region, one important region that contributes to endocytosis function. The correlated position of the basal body with Golgi structure suggests the close mutual relationship of proteins exchange between these two organelles, which supports the primary cilia function of mechanosensing. In addition, the connection of basal body with filaments such as microtubules and actin networks may explain the mechanical properties of primary cilia in response to extracellular signals such as fluid shear stress. The changing of actin cytoskeleton may also affect the orientation or motion of primary cilia in the cyclic substrate stretching conditions. More deeply studies about the axoneme structure of primary cilia using TEM or some other higher resolution microscopy may be needed to have more understanding of primary cilia. For the first time, the proper primary cilium model with fully mechanical components is revealed; it also found that the cross-linking component takes the main responsibility for

mechanical properties of primary cilia. Moreover, the mechanical properties of cross-linking component, for the first time, have been revealed.

Chapter 5

Conclusions and prospects

5.1 Conclusions

Mechanotransduction is a ubiquitous process among living organisms, which converts surrounding mechanical signals into biological signals, and contributes to the cellular adaptation to surrounding mechanical environment. The primary cilium is an important cellular mechanosensor and supports the mechanotransduction function of cells. The overarching objectives of this dissertation were to provide more information about cilia mechanics such as mechanical properties, mechanical responses, and microstructure components.

Chapter 1 provided the fundamentals of cells and the primary cilium (its structures, the importance in cell life). The prior studies of measurement of mechanical properties of cilia and remodeling function in response to mechanical forces were reviewed. The research purposes were also summarized, together with the technical issues relating to our research, such as micro-tensile test, cyclic substrate stretching.

Chapter 2 introduced an in-house micro-tensile test exclusively to measure mechanical properties of primary cilia. The cantilevers, which were used as force-sensor, were manufactured in our laboratory. The primary cilia were successfully isolated from the cell surface by shear force using centrifugation method. With the fluorescence microscope, we confirmed the isolated primary cilia before applying the stretching method. The microstructure of primary cilia had been observed by TEM images to identify the diameter of the primary cilium. The leading results in this study are the measurement of the elastic modulus of isolated primary cilia. Previous studies, which were mentioned in the literature review, investigated the flexural rigidity of primary cilia, not the material properties, i.e. Young's modulus. As far as we know, this is the first study measuring directly the Young's modulus of isolated cilia. The dependence of elastic modulus at different strain rates has induced the viscoelastic properties of primary cilia and the viscoelastic parameters are also first introduced by fitting experimental and numerical results. The global Young's modulus of primary cilia was revealed and compared to the local Young's modulus investigated by AFM to show confidently the measured values of both methods. The mechanical properties of primary cilia in this study give a better picture of cilia mechanics and contribute numerically and experimentally, to further investigations of primary cilia.

Chapter 3, for the first time, identified the remodeling of primary cilia in response to mechanical signals of cyclic substrate stretching. It was found that cilia may change their morphology and incidence in response to not only the direct exposure of fluid flow but also to the indirect application of substrate stretching. By inhibiting the activity of the actin network during the substrate stretching process, this study also contributes to the affirmation that the actin cytoskeleton affects the ciliogenesis process.

Chapter 4 observed the microstructure of primary cilia, along with the relationship of cilia with other organelles such as Golgi apparatus and cytoplasm filaments (actin and microtubules). It may give more understanding of the mechanotransduction function, and mechanical responses of cilia in response to surrounding mechanical signals. The numerical results, for the first time, provided a primary cilium model with main mechanical components. It showed that the mechanical properties of primary cilia depend on the cross-linking components, and for the first time, the elastic properties of the cross-linking component inside primary cilia are estimated.

5.2 Prospects

The studies presented in this dissertation have advanced our understanding of the mechanical properties of primary cilia and their remodeling function. Although it broadened our understanding of this organelle, many areas need to identify in further studies.

Chapter 2 identified globally the Young's modulus of primary by the micro-tensile tester. However, the microstructure of primary cilia may change along the primary cilium. Recent advances in ultrastructural observation using TEM have revealed the variations of axoneme configuration from the base to the tip of primary cilia, which has the reduction in the number of microtubule doublets to fewer than nine pairs (Gluenz et al., 2010; Sun et al., 2019; Jensen et al., 2004). Moreover, the TEM observation has also revealed that the microtubule doublets exist around a few 10 nm deep from the cilia surface. These changes in structure configuration along the primary cilia suggest the change of mechanical properties along the length of cilia and the need for measurement of local Young's modulus. In our laboratory, the AFM technique was performed to

measure the local Young's modulus of primary cilia, but it needs more results to get a better relation between microstructure and mechanical properties.

In Chapter 3, despite finding the link between the actin network activity and ciliogenesis, further evidence needs to be investigated to clarify the mechanism in detail. This study suggested that the remodeling of cilia in response to substrate stretching may support the mechanotransduction process in sensing the direct stimulation of fluid flow. But it remains unclear and needs to be identified in further studies. Another interesting question is how cilia are oriented. Several studies reported the orientation of cilia is influenced by loading (Donnelly et al., 2010; Farnum et al., 2011), but the underlined mechanism is still unclear and needs to be characterized.

In Chapter 4, regarding the axoneme structure, further works need to do to get the appropriate structure. As measured, Young's modulus of primary cilia is approximately hundreds of kPa, meanwhile, the main component of the axoneme is nine microtubule doublets which have the elastic modulus of GPa. In the motile cilia, there are the dynein arms that connect the microtubules together and are subject to the main elastic force, the primary cilia do not have these structures. The primary cilia axoneme should have alternative components for their elastic recovery in response to mechanical signals. Due to the tiny dimensions of the components, the higher resolution methods should be considered to have a clearer picture of these microstructures of primary cilia. Regarding the primary cilia model, the more refined cilia model could be processed with the more specific location of the cross-linking component, and the addition of cilioplasm into the model.

References

Ambrosi, C. M., J. J. Wille, and FC-P. Yin. "Reorientation response of endothelial cells to cyclic compression: comparison with cyclic stretching." In *Proceedings of the Second Joint 24th Annual Conference and the Annual Fall Meeting of the Biomedical Engineering Society Engineering in Medicine and Biology* 1, (2002): 386-387.

Antoniades, Ioanna, Panayiota Stylianou, and Paris A. Skourides. "Making the connection: ciliary adhesion complexes anchor basal bodies to the actin cytoskeleton." *Developmental cell* 28, no. 1 (2014): 70-80.

Battle, Christopher, Carolyn M. Ott, Dylan T. Burnette, Jennifer Lippincott-Schwartz, and Christoph F. Schmidt. "Intracellular and extracellular forces drive primary cilia movement." *Proceedings of the National Academy of Sciences* 112, no. 5 (2015): 1410-1415.

Binnig, Gerd, Calvin F. Quate, and Ch Gerber. "Atomic force microscope." *Physical Review Letters* 56, no. 9 (1986): 930.

Bloodgood, Robert A. "From central to rudimentary to primary: the history of an underappreciated organelle whose time has come. The primary cilium." *Methods in Cell Biology* 94 (2009): 2-52.

Brown, Jason M., and George B. Witman. "Cilia and diseases." *Bioscience* 64, no. 12 (2014): 1126-1137.

Bustamante, Carlos J., Yann R. Chemla, Shixin Liu, and Michelle D. Wang. "Optical tweezers in single-molecule biophysics." *Nature Reviews Methods Primers* 1, no. 1 (2021): 1-29.

Chen, Duanduan, Dominic Norris, and Yiannis Ventikos. "Ciliary behaviour and mechano-transduction in the embryonic node: computational testing of hypotheses." *Medical Engineering & Physics* 33, no. 7 (2011): 857-867.

Chien, Yuan-Hung, Michael E. Werner, Jennifer Stubbs, Matt S. Joens, Julie Li, Shu Chien, James AJ Fitzpatrick, Brian J. Mitchell, and Chris Kintner. "Bbof1 is required to maintain cilia orientation." *Development* 140, no. 16 (2013): 3468-3477.

Clement, Christian Alexandro, Katrine Dalsgaard Ajbro, Karen Koefoed, Maj Linea Vestergaard, Iben Rønn Veland, Maria Perestrello Ramos Henriques de Jesus, Lotte Bang Pedersen et al. "TGF-β signaling is associated with endocytosis at the pocket region of the primary cilium." *Cell Reports* 3, no. 6 (2013): 1806-1814.

Deepak, Venkatesh. "Primary cilia." *Journal of Oral and Maxillofacial Pathology* 21, no. 1 (2017): 8.

Delling, Markus, Paul G. DeCaen, Julia F. Doerner, Sebastien Febvay, and David E. Clapham. "Primary cilia are specialized calcium signalling organelles." *Nature* 504, no. 7479 (2013): 311-314.

Deguchi, Shinji, Toshiro Ohashi, and Masaaki Sato. "Tensile properties of single stress fibers isolated from cultured vascular smooth muscle cells." *Journal of Biomechanics* 39, no. 14 (2006): 2603-2610.

Donnelly, Eve, Maria‐Grazia Ascenzi, and Cornelia Farnum. "Primary cilia are highly oriented with respect to collagen direction and long axis of extensor tendon." *Journal of Orthopaedic Research* 28, no. 1 (2010): 77-82.

Downs, Matthew E., An M. Nguyen, Florian A. Herzog, David A. Hoey, and Christopher R. Jacobs. "An experimental and computational analysis of primary cilia deflection under fluid flow." *Computer Methods in Biomechanics and Biomedical Engineering* 17, no. 1 (2014): 2-10.

Espinha, Lina C., David A. Hoey, Paulo R. Fernandes, Hélder C. Rodrigues, and Christopher R. Jacobs. "Oscillatory fluid flow influences primary cilia and microtubule mechanics." *Cytoskeleton* 71, no. 7 (2014): 435-445.

Farnum, Cornelia E., and Norman J. Wilsman. "Orientation of primary cilia of articular chondrocytes in three‐dimensional space." *The Anatomical Record: Advances in Integrative Anatomy and Evolutionary Biology* 294, no. 3 (2011): 533-549.

Flaherty, J., Zhe Feng, Zhangli Peng, Y-N. Young, and A. Resnick. "Mechanical Properties of a Primary Cilium from the Stochastic Motions of the Cilium Tip." *bioRxiv* (2018): 292409.

Follit, John A., Richard A. Tuft, Kevin E. Fogarty, and Gregory J. Pazour. "The intraflagellar transport protein IFT20 is associated with the Golgi complex and is required for cilia assembly." *Molecular Biology of the Cell* 17, no. 9 (2006): 3781-3792.

Gardner, Keri, Steven P. Arnoczky, and Michael Lavagnino. "Effect of in vitro stress‐deprivation and cyclic loading on the length of tendon cell cilia in situ." *Journal of Orthopaedic Research* 29, no. 4 (2011): 582-587.

Geiger, R. Christopher, Christopher D. Kaufman, Ai P. Lam, GR Scott Budinger, and David A. Dean. "Tubulin acetylation and histone deacetylase 6 activity in the lung under cyclic load." *American Journal of Respiratory Cell and Molecular Biology* 40, no. 1 (2009): 76-82.

Ghossoub, Rania, Anahi Molla‐Herman, Philippe Bastin, and Alexandre Benmerah. "The ciliary pocket: a once‐forgotten membrane domain at the base of cilia." *Biology of the Cell* 103, no. 3 (2011): 131-144.

Gittes, Frederick, Brian Mickey, Jilda Nettleton, and Jonathon Howard. "Flexural rigidity of microtubules and actin filaments measured from thermal fluctuations in shape." *The Journal of Cell Biology* 120, no. 4 (1993): 923-934.

Gluenz, Eva, Johanna L. Höög, Amy E. Smith, Helen R. Dawe, Michael K. Shaw, and Keith Gull. "Beyond 9+ 0: noncanonical axoneme structures characterize sensory cilia from protists to humans." *The FASEB Journal* 24, no. 9 (2010): 3117-3121.

Hierck, Beerend P., Kim Van der Heiden, Fanneke E. Alkemade, Simone Van de Pas, Johannes V. Van Thienen, Bianca CW Groenendijk, Wilhelmina H. Bax et al. "Primary cilia sensitize endothelial cells for fluid shear stress." *Developmental Dynamics: An Official Publication of the American Association of Anatomists* 237, no. 3 (2008): 725-735.

Hoey, David A., Julia C. Chen, and Christopher R. Jacobs. "The primary cilium as a novel extracellular sensor in bone." *Frontiers in Endocrinology* 3 (2012): 75.

Hooke, Robert. Micrographia or some physiological Descriptions of Minute Bodies. *Royal Society* 1665.

Hsiao, Yi-Chun, Karina Tuz, and Russell J. Ferland. "Trafficking in and to the primary cilium." *Cilia* 1, no. 1 (2012): 1-13.

Huang, Bing Q., Tatyana V. Masyuk, Melissa A. Muff, Pamela S. Tietz, Anatoliy I. Masyuk, and Nicholas F. LaRusso. "Isolation and characterization of cholangiocyte primary cilia." *American Journal of Physiology-Gastrointestinal and Liver Physiology* 291, no. 3 (2006): G500-G509.

Iomini, Carlo, Karla Tejada, Wenjun Mo, Heikki Vaananen, and Gianni Piperno. "Primary cilia of human endothelial cells disassemble under laminar shear stress." *The Journal of Cell Biology* 164, no. 6 (2004): 811-817.

Jaalouk, Diana E., and Jan Lammerding. "Mechanotransduction gone awry." *Nature Reviews Molecular Cell Biology* 10, no. 1 (2009): 63-73.

Jensen, C. G., C. A. Poole, S. R. McGlashan, M. Marko, Z. I. Issa, K. V. Vujcich, and S. S. Bowser. "Ultrastructural, tomographic and confocal imaging of the chondrocyte primary cilium in situ." *Cell Biology International* 28, no. 2 (2004): 101-110.

Kikumoto, Mahito, Masashi Kurachi, Valer Tosa, and Hideo Tashiro. "Flexural rigidity of individual microtubules measured by a buckling force with optical traps." *Biophysical Journal* 90, no. 5 (2006): 1687-1696.

Kim, Hyunho, Hangxue Xu, Qin Yao, Weizhe Li, Qiong Huang, Patricia Outeda, Valeriu Cebotaru et al. "Ciliary membrane proteins traffic through the Golgi via a Rabep1/GGA1/Arl3-dependent mechanism." *Nature Communications* 5, no. 1 (2014): 1-13.

Kim, Joon, Ji Eun Lee, Susanne Heynen-Genel, Eigo Suyama, Keiichiro Ono, KiYoung Lee, Trey Ideker, Pedro Aza-Blanc, and Joseph G. Gleeson. "Functional genomic screen for modulators of ciliogenesis and cilium length." *Nature* 464, no. 7291 (2010): 1048-1051.

Kojima, Hiroaki, Akihiko Ishijima, and Toshio Yanagida. "Direct measurement of stiffness of single actin filaments with and without tropomyosin by in vitro nanomanipulation." *Proceedings of the National Academy of Sciences* 91, no. 26 (1994): 12962-12966.

Kowal, Tia J., and Matthias M. Falk. "Primary cilia found on HeLa and other cancer cells."

Cell Biology International 39, no. 11 (2015): 1341-1347.

Kriegel, Franziska, Niklas Ermann, and Jan Lipfert. "Probing the mechanical properties, conformational changes, and interactions of nucleic acids with magnetic tweezers." *Journal of Structural Biology* 197, no. 1 (2017): 26-36.

Lee, Si‐Hyung, Kwangsic Too, Eun Ji Jung, Hyowon Hong, Jimyung Seo, and Joon Kim. "Export of membrane proteins from the Golgi complex to the primary cilium requires the kinesin motor, KIFC1." *The FASEB Journal* 32, no. 2 (2018): 957-968.

Van Leeuwenhoek, A. "Concerning little animals observed in rain, well, sea and snow water." *Phil. Trans. R. Soc. Lond* 11 (1677): 821-831.

Li, Yongsheng, Yueqin Li, Quanyou Zhang, Lili Wang, Meiqing Guo, Xiaogang Wu, Yuan Guo, Jing Chen, and Weiyi Chen. "Mechanical properties of chondrocytes estimated from different models of micropipette aspiration." *Biophysical Journal* 116, no. 11 (2019): 2181-2194.

Lim, Yi Chung, Sue R. McGlashan, Michael T. Cooling, and David S. Long. "Culture and detection of primary cilia in endothelial cell models." *Cilia* 4, no. 1 (2015): 1-12.

Lin, Yi-Chia, Gijsje H. Koenderink, Frederick C. MacKintosh, and David A. Weitz. "Viscoelastic properties of microtubule networks." *Macromolecules* 40, no. 21 (2007): 7714-7720.

Lofgren, Ian, and Andrew Resnick. "A Model for the Force Exerted on a Primary Cilium by an Optical Trap and the Resulting Deformation." *In Photonics* 2, no. 2 (2015): 604-618.

Lu, Deshun, and Ghassan S. Kassab. "Role of shear stress and stretch in vascular mechanobiology." *Journal of the Royal Society Interface* 8, no. 63 (2011): 1379-1385.

Maeda, Eijiro, Yasufumi Hagiwara, James HC Wang, and Toshiro Ohashi. "A new experimental system for simultaneous application of cyclic tensile strain and fluid shear stress to tenocytes in vitro." *Biomedical Microdevices* 15, no. 6 (2013): 1067-1075.

Marshall, Wallace F., and Joel L. Rosenbaum. "Intraflagellar transport balances continuous turnover of outer doublet microtubules: implications for flagellar length control." *The Journal of Cell Biology* 155, no. 3 (2001): 405-414.

Matsui, Tsubasa S., Shinji Deguchi, Naoya Sakamoto, Toshiro Ohashi, and Masaaki Sato. "A versatile micro-mechanical tester for actin stress fibers isolated from cells." *Biorheology* 46, no. 5 (2009): 401-415.

May-Simera, Helen L., and Matthew W. Kelley. "Cilia, Wnt signaling, and the cytoskeleton." *Cilia* 1, no. 1 (2012): 1-16.

McGlashan, Susan R., Martin M. Knight, Tina T. Chowdhury, Purva Joshi, Cynthia G. Jensen, Sarah Kennedy, and Charles A. Poole. "Mechanical loading modulates chondrocyte primary cilia incidence and length." *Cell Biology International* 34, no. 5 (2010): 441-446.

Mirvis, Mary, Tim Stearns, and W. James Nelson. "Cilium structure, assembly, and disassembly regulated by the cytoskeleton." *Biochemical Journal* 475, no. 14 (2018): 2329-2353.

Mitchell, Kimberly AP. "Isolation of primary cilia by shear force." *Current Protocols in Cell Biology* 59, no. 1 (2013): 3-42.

Molla-Herman, Anahi, Rania Ghossoub, Thierry Blisnick, Alice Meunier, Catherine Serres, Flora Silbermann, Chris Emmerson et al. "The ciliary pocket: an endocytic membrane domain at the base of primary and motile cilia." *Journal of Cell Science* 123, no. 10 (2010): 1785-1795.

Moritz, Orson L., Beatrice M. Tam, Larry L. Hurd, Johan Peränen, Dusanka Deretic, and David S. Papermaster. "Mutant rab8 Impairs docking and fusion of rhodopsin-bearing post-Golgi membranes and causes cell death of transgenic Xenopus rods." *Molecular Biology of the Cell* 12, no. 8 (2001): 2341-2351.

Nauli, Surya M., Xingjian Jin, Wissam A. AbouAlaiwi, Wassim El-Jouni, Xuefeng Su, and Jing Zhou. "Non-motile primary cilia as fluid shear stress mechanosensors." *Methods in Enzymology* 525 (2013): 1-20.

Nauli, Surya M., Xingjian Jin, and Beerend P. Hierck. "The mechanosensory role of primary cilia in vascular hypertension." *International Journal of Vascular Medicine* (2011).

Ohashi, Toshiro, Y. Ishii, Y. Ishikawa, T. Matsumoto, and M. Sato. "Experimental and

numerical analyses of local mechanical properties measured by atomic force microscopy for sheared endothelial cells." *Bio-medical Materials and Engineering* 12, no. 3 (2002): 319-327.

Ohashi, Toshiro, Hironobu Abe, Takeo Matsumoto, and Masaaki Sato. "Pipette aspiration technique for the measurement of nonlinear and anisotropic mechanical properties of blood vessel walls under biaxial stretch." *Journal of Biomechanics* 38, no. 11 (2005): 2248-2256.

Ohashi, Toshiro, Masanori Masuda, Takeo Matsumoto, and Masaaki Sato. "Nonuniform strain of substrate induces local development of stress fibers in endothelial cells under uniaxial cyclic stretching." *Clinical Hemorheology and Microcirculation* 37, no. 1-2 (2007): 37-46.

Pedersen, Lotte B., Johanne B. Mogensen, and Søren T. Christensen. "Endocytic control of cellular signaling at the primary cilium." *Trends in Biochemical Sciences* 41, no. 9 (2016): 784-797.

Plotnikova, Olga V., Elena N. Pugacheva, and Erica A. Golemis. "Primary cilia and the cell cycle." *In Methods in Cell Biology* 94, (2009): 137-160.

Poole, C. Anthony, Cynthia G. Jensen, Judith A. Snyder, C. George Gray, Valentin L. Hermanutz, and Denys N. Wheatley. "Confocal analysis of primary cilia structure and colocalization with the Golgi apparatus in chondrocytes and aortic smooth muscle cells." *Cell Biology International* 21, no. 8 (1997): 483-494.

Praetorius, H. A., and K. R. Spring. "Bending the MDCK cell primary cilium increases intracellular calcium." *The Journal of Membrane Biology* 184, no. 1 (2001): 71-79.

Praetorius, H. A., and K. R. Spring. "Removal of the MDCK cell primary cilium abolishes flow sensing." *The Journal of Membrane Biology* 191, no. 1 (2003): 69-76.

Radmacher, Manfred, Monika Fritz, Claudia M. Kacher, Jason P. Cleveland, and Paul K. Hansma. "Measuring the viscoelastic properties of human platelets with the atomic force microscope." *Biophysical Journal* 70, (1996): 556-567.

Resnick, Andrew. "Mechanical properties of a primary cilium as measured by resonant

oscillation." *Biophysical Journal* 109, no. 1 (2015): 18-25.

Resnick, Andrew. "HIF stabilization weakens primary cilia." *PloS one* 11, no. 11 (2016): e0165907.

Rezaei, Naghmeh, Benjamin PB Downing, Andrew Wieczorek, Clara KY Chan, Robert Lindsay Welch, and Nancy R. Forde. "Using optical tweezers to study mechanical properties of collagen." *In Photonics North* 8007, (2011): 146-155.

Rieder, Conly L., Cynthia G. Jensen, and Lawrence CW Jensen. "The resorption of primary cilia during mitosis in a vertebrate (PtK1) cell line." *Journal of Ultrastructure Research* 68, no. 2 (1979): 173-185.

Rogowski, Michaela, Dirk Scholz, and Stefan Geimer. "Electron microscopy of flagella, primary cilia, and intraflagellar transport in flat-embedded cells." *In Methods in Enzymology* 524, (2013): 243-263.

Rowson, Daniel T., Julia C. Shelton, Hazel RC Screen, and Martin M. Knight. "Mechanical loading induces primary cilia disassembly in tendon cells via TGFβ and HDAC6." *Scientific Reports* 8, no. 1 (2018): 1-12.

Rydholm, Susanna, Gordon Zwartz, Jacob M. Kowalewski, Padideh Kamali-Zare, Thomas Frisk, and Hjalmar Brismar. "Mechanical properties of primary cilia regulate the response to fluid flow." *American Journal of Physiology-Renal Physiology* 298, no. 5 (2010): F1096-F1102.

Satir, Peter, Lotte B. Pedersen, and Søren T. Christensen. "The primary cilium at a glance." *Journal of Cell Science* 123, no. 4 (2010): 499-503.

Satir, Peter. "CILIA: before and after." *Cilia* 6, no. 1 (2017): 1-11.

Schwann T. Mikroscopische Untersuchungen u¨ber die U¨ bereinstimmung in der Struktur und dem Wachstum des Thiere und Pflanzen. W Engelmann*: Leipzig No* 176 (1839).

Schneider, Linda, Michael Cammer, Jonathan Lehman, Sonja K. Nielsen, Charles F. Guerra, Iben R. Veland, Christian Stock et al. "Directional cell migration and chemotaxis in wound healing response to PDGF-AA are coordinated by the primary cilium in fibroblasts." *Cellular Physiology and Biochemistry* 25, no. 2-3 (2010): 279-292.

Schwartz, Eric A., Michelle L. Leonard, Rena Bizios, and Samuel S. Bowser. "Analysis and modeling of the primary cilium bending response to fluid shear." *American Journal of Physiology-Renal Physiology* 272, no. 1 (1997): F132-F138.

Shin, Jung-Bum, Dany Adams, Martin Paukert, Maria Siba, Samuel Sidi, Michael Levin, Peter G. Gillespie, and Stefan Gründer. "Xenopus TRPN1 (NOMPC) localizes to microtubule-based cilia in epithelial cells, including inner-ear hair cells." *Proceedings of the National Academy of Sciences* 102, no. 35 (2005): 12572-12577.

Schleiden M.J. Beitra¨ge zur Phytogenesis. Arch Anat Physiol Wiss Med (J Mu¨ller) (1838) 137–176.

Smith, Claire EL, Alice VR Lake, and Colin A. Johnson. "Primary cilia, ciliogenesis and the actin cytoskeleton: A little less resorption, a little more actin please." *Frontiers in Cell and Developmental Biology* 8 (2020): 622822.

Spasic, Milos, and Christopher R. Jacobs. "Lengthening primary cilia enhances cellular mechanosensitivity." *European Cells & Materials* 33 (2017): 158.

Stavenschi, Elena, Michele A. Corrigan, Gillian P. Johnson, Mathieu Riffault, and David A. Hoey. "Physiological cyclic hydrostatic pressure induces osteogenic lineage commitment of human bone marrow stem cells: a systematic study." *Stem Cell Research & Therapy* 9, no. 1 (2018): 1-13.

Su, Steven, Siew Cheng Phua, Robert DeRose, Shuhei Chiba, Keishi Narita, Peter N. Kalugin, Toshiaki Katada, Kenji Kontani, Sen Takeda, and Takanari Inoue. "Genetically encoded calcium indicator illuminates calcium dynamics in primary cilia." *Nature Methods* 10, no. 11 (2013): 1105-1107.

Sun, Shufeng, Rebecca L. Fisher, Samuel S. Bowser, Brian T. Pentecost, and Haixin Sui. "Three-dimensional architecture of epithelial primary cilia." *Proceedings of the National Academy of Sciences* 116, no. 19 (2019): 9370-9379.

Sütterlin, Christine, and Antonino Colanzi. "The Golgi and the centrosome: building a functional partnership." *Journal of Cell Biology* 188, no. 5 (2010): 621-628.

Tao, N. J., S. M. Lindsay, and S. Lees. "Measuring the microelastic properties of biological

material." *Biophysical Journal* 63, no. 4 (1992): 1165-1169.

Tirella, Annalisa, Giorgio Mattei, and A. R. T. I. Ahluwalia. "Strain rate viscoelastic analysis of soft and highly hydrated biomaterials." *Journal of Biomedical Materials Research Part A* 102, no. 10 (2014): 3352-3360.

Tuszyński, J. A., T. Luchko, S. Portet, and J. M. Dixon. "Anisotropic elastic properties of microtubules." *The European Physical Journal E* 17, no. 1 (2005): 29-35.

Van der Heiden, Kim, Beerend P. Hierck, Rob Krams, Rini de Crom, Caroline Cheng, Martin Baiker, Mathieu JBM Pourquie et al. "Endothelial primary cilia in areas of disturbed flow are at the base of atherosclerosis." *Atherosclerosis* 196, no. 2 (2008): 542-550.

Vaughan, T. J., C. A. Mullen, S. W. Verbruggen, and L. M. McNamara. "Bone cell mechanosensation of fluid flow stimulation: a fluid–structure interaction model characterising the role integrin attachments and primary cilia." *Biomechanics and Modeling in Mechanobiology* 14, no. 4 (2015): 703-718.

Wang, Leanne, Raphael Weidenfeld, Elizabeth Verghese, Sharon D. Ricardo, and James A. Deane. "Alterations in renal cilium length during transient complete ureteral obstruction in the mouse." *Journal of Anatomy* 213, no. 2 (2008): 79-85.

Ware, Stephanie M., Meral Gunay Aygun, and Friedhelm Hildebrandt. "Spectrum of clinical diseases caused by disorders of primary cilia." *Proceedings of the American Thoracic Society* 8, no. 5 (2011): 444-450.

Werner, Michael E., Peter Hwang, Fawn Huisman, Peter Taborek, Clare C. Yu, and Brian J. Mitchell. "Actin and microtubules drive differential aspects of planar cell polarity in multiciliated cells." *Journal of Cell Biology* 195, no. 1 (2011): 19-26.

Wheway, Gabrielle, Liliya Nazlamova, and John T. Hancock. "Signaling through the primary cilium." *Frontiers in Cell and Developmental Biology* 6, (2018): 8.

Young, Y-N., M. Downs, and Christopher R. Jacobs. "Dynamics of the primary cilium in shear flow." *Biophysical Journal* 103, no. 4 (2012): 629-639.

Publication

[1] Tien-Dung Do, Jimuro Katsuyoshi, Haonai Cai, Toshiro Ohashi, “Mechanical Properties of Isolated Primary Cilia Measured by Micro-tensile Test and Atomic Force Microscopy”, Frontiers in Bioengineering and Biotechnology, 11 November 2021. (IF=5.890 as of 2022)

Conference papers

[1] Jimuro Katsuoshi, Tien Dung Do, Ohashi Toshiro, Measurement of mechanical properties of primary cilia in cells by micro-tensile tester, The 9th Symposium on Micro-Nano Science and Technology, 2018.

[2] Tien-Dung Do, Jimuro Katsuyoshi, Toshiro Ohashi, “Mesurement of mechanical properties of isolated primary cilia by micro-tensile tester”, The 42th Annual Meetings of the Japanese Society of Biorheology, 2019.

[3] Tien-Dung DO, Toshiro OHASHI, “Measurement of mechanical properties of primary cilia by micro-tensile test”, VANJ Conference, 2020.

[4] Tien-Dung DO, Toshiro Ohashi, “Mechanical properties and responses of cellular primary cilia”, The 44th Annual Meetings of the Japanese Society of Biorheology, 2021.

[5] Tien-Dung DO, Toshiro OHASHI, “Endothelial primary cilia responses under flow and cyclic substrate stretching conditions”, The 60th Annual Meeting of Hokkaido Branch of Japan Society for Medical and Biological Engineering, 2021.

[6] Tien-Dung DO, Toshiro OHASHI, “Remodelling of endothelial primary cilia in response to flow and cyclic substrate stretching”, The 11th Asian-Pacific Conference on Biomechanics, Kyoto, Japan, 2021.

[7] Tien-Dung DO, Toshiro, OHASHI, “Endothelial Primary cilia remodeling in response to cycilc substrate Stretching”, The 8th International Conference on Flow Dynamics, Sendai, Miyagi, 2021.

Awards

[1] Excellent Young Researcher Award at VANJ (Vietnamese Academic Network in Japan), Conference, Tokyo (28th Nov 2020 online).

[2] Research Encouragement Award at the 60th Hokkaido Branch Meeting, Japanese Society for Medical and Biological Engineering (23rd October 2021, online).

[3] Student Best Presentation Award at 18th International Conference on Flow Dynamics 2021 (29th October 2021, online) for his excellent research presentation.